New techniques for uncertainty realism improvement in Surveillance and Tracking orbit determination processes

A Master of Science Thesis

by Sergi Lopez Jimenez

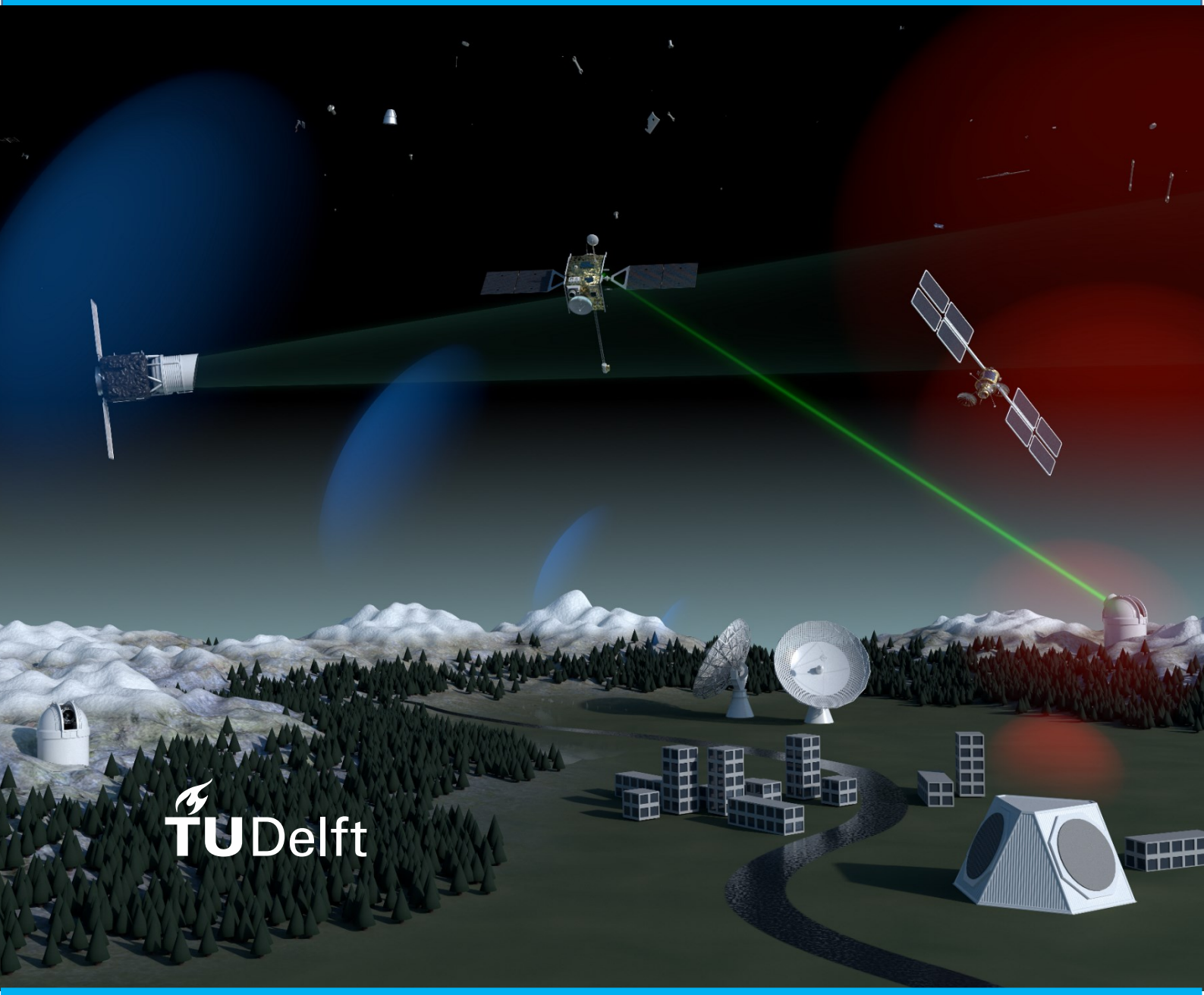

Challenge the future

New techniques for uncertainty realism improvement in Surveillance and Tracking orbit determination processes

By

Sergi López Jiménez

in partial fulfilment of the requirements for the degree of

Master of Science

in Aerospace Engineering

at the Delft University of Technology,

to be defended publicly on Friday January 24, 2020 at 09:30 AM.

Supervisor:	*Dr. Ir. E.J.O. Schrama*
Thesis committee:	*Dr. ir. Wouter van der Wal, TU Delft*
	Dr. Ir. E.J.O. Schrama , TU Delft
	Dr. Alessandra Menicucci, TU Delft
	Dr. ir. Diego Escobar, GMV

Student: *Sergi López Jiménez* *(4734874)*

Cover image: *Photo of ESA's concept of a future surveillance network (2017). © **ESA***

An electronic version of this thesis is available at http://repository.tudelft.nl/.

TU Delft

gmv

This page is intentionally left blank

Preface

This report contains a summary of the work performed at GMV Space and Defence during the Master Thesis Project, part of the Master of Science (MSc) in Aerospace Engineering at the Technische Universiteit Delft, track of Spaceflight, profile Space Exploration. The preparation of the thesis project took place at GMV's headquarters in Tres Cantos, Madrid, from the 26th of April 2019 to the 26th of December 2019.

The work contained in this report is preceded by a detailed Literature Study aimed at laying the foundations of the research presented hereafter. The literature study delves into the motivation by which the work of this thesis is endorsed as well as the potential benefits of the conceptualized approach. In addition, a brief introduction to the Space Situational Awareness framework and particularly to the Space Surveillance and Tracking is given in an effort to get the reader started at the main topics and challenges that both fields of study pose. The research contained in this report represents the continuation of the work done during the Literature Study, hence readers seeking a conceptual insight and an introduction to the topic are encouraged to read the aforementioned document. In addition, potential readers might require a basic knowledge in astrodynamics, orbital mechanics, statistics, linear and differential algebra as well as optimization theory.

This project represents a collaboration between the author, GMV and TU Delft. GMV belongs to the top-tier space engineering technology groups that lead in orbital mechanics, astrodynamics, mission planning and satellite navigation, producing high quality/fidelity software products and being recognized as a worldwide entity on space engineering. TU Delft stands out as one of the most renowned universities around the world by the quality of the education, the passion and competency with which its academic staff educate and inspire students as well as the extensive research output produced.

This project would not have been possible without the close cooperation between these entities, whose shared philosophy of fostering creativity and striving for excellence produces such remarkable and inspiring research projects.

Acknowledgements

The thesis project contained in this report represents the culmination of my academic life, graduating at one of the most renowned universities in the world: TU Delft. So far, it represents my biggest accomplishment, yet full of struggles and challenges along the way that made me endure and enjoy the path. There have been many memorable and rewarding moments that are shared with other people, without whom this work would not have been possible.

First and foremost, my most sincere gratitude to Diego Escobar, Alberto Águeda and Ángel Luis Cerviño for giving me the opportunity to develop such interesting, inspiring and cutting edge research project at GMV's Flight Dynamics and Operations (FDO) division in Madrid. I would strongly recommend any fellow undergraduate from TU Delft to look for internships or Thesis at GMV, as the knowledge and skills learnt during my stay there suppose an MSc on its own. GMV's policy of involving student in real Research and Development projects of the space industry stands as an invaluable learning and working experience.

The degree of precision, correctness and innovation of this work would not have been possible without the guidance and advice of Alejandro Pastor and Diego Escobar, whose critical opinion and dilated experience on the topic were the support I required to succeed in this venture. Furthermore, if anyone has ever taught me good programming practices and the foundations of software engineering those are Alejandro and Diego, so my biggest gratitude goes to them. In addition, I would like to thank all the people from the Space Debris team and the FDO division that have helped me during this period, since they stand out not only for their professionalism but also for their kindness and humanity.

The department of Astrodynamics and Space Mission of the aerospace faculty of TU Delft is a key component to the success of this report due to the outstanding teaching quality and the exceptional academic and administrative staff, who fostered my interest for space engineering and provided me the tools and knowledge required to complete this MSc successfully. Above all, I would like to thank my supervisor Ernst Schrama for the support, critical thinking and guidance that helped me perform my best and deliver such an innovative research work. The subject of Satellite Orbit Determination (taught by Dr. Schrama) lighted the spark that led to this research project. In addition, I would like to thank Ron Noomen, the Space Flight MSc track coordinator, for the amazing subject of Mission Geometry and Orbit Design (which I truly enjoyed), for his advice and wise words when most needed, for his dedication and for being the best student counsellor I could ever find. Finally, I would like to thank Wim Simons for the material provided to complete this project as the final results of this thesis greatly depend on it.

To Alejandro Pastor, Diego Escobar, Alberto Águeda , Srinivas Janardhana Setty and Ernst Schrama my most sincere gratitude for contributing in my first academic publications, especially to Srinivas and Diego who attended the conferences and presented the work on my behalf. Their feedback and help during the drafting of the documents is truly appreciated.

I would like to thank my friends for their support and for standing by my side when I needed them most. To my friends in Sabadell, for being always there and giving me memorable moments during years, they have become part of my family. To my friends from Delft, which I knew through the adventure of going to study abroad, together I gathered the most valuable memories from my stay in the Netherlands. To my friends in Madrid for making this year an incredible one and for making me enjoy the experience even more than I anticipated. To Paula, who brought a sparkle of joy and happiness to my life and whose support was the catalyser that helped me finish this project.

To my parents, who never stopped believing in me and supported me in every step I have taken up to this moment, who represent the role models I have always followed, without them it would have been impossible for me to achieve such incredible things in life. I owe them everything I have accomplished and this work is dedicated to them.

Sergi López Jiménez

Abstract

The future space environment is predicted to grow in number of both operational and inactive man-made objects and the era of constellations is expected to arrive during the following years, with many telecom companies launching constellations of up to 12000 satellites. This situation will inevitably lead to over-population of the most demanded orbits making its exploitation a challenge to the scientific community as well as spacecraft operators.

To allow for a sustainable and efficient exploitation of the orbital resources available, the assessment of the quality of a predicted or estimated orbit state becomes a core aim of modern astrodynamics. It enables the proper functioning of multiple space applications, from Global Navigation Satellite System (GNSS) constellations, optimization of manoeuvres, development of accurate gravitational models, space debris cataloguing build-up and maintenance, etc. A proper definition of state uncertainty entails the characterisation of the probability density function of an object's state, thus defining a region in space within which an orbiting object will be most likely found.

Regular products within the field of Space Surveillance and Tracking (SST) and Space Traffic Management (STM), such as high-risk collisions, upcoming re-entries or fragmentations, rely both on the estimated state and associated uncertainty of detectable Resident Space Objects (RSOs). Orbit Determination (OD) algorithms provide the required estimations, assuming that the uncertainty in the state of the object is properly characterized by its state vector covariance and assuming Gaussian processes.

However, a common problem of OD processes is the misrepresentation of the RSOs uncertainty through the estimated and predicted covariance. Ultimately, this causes a great impact in the quality and accuracy of SST products as the covariance is overly optimistic (too small) and the true uncertainty of the object is not properly captured. One of the causes for the unrealism of the covariance is found in typical OD algorithms, as they fail to consider, or properly characterize, the uncertainty of the dynamical models used to describe the motion of the objects. Representative examples of uncertain dynamic models are the atmospheric drag force or the solar radiation pressure acting on the orbiting RSOs. Because these models provide a deterministic solution to a stochastic phenomenon, an inherent associated uncertainty should be considered when used during an orbit determination and posterior orbit prediction.

The aim of this work is to devise a novel methodology to improve the covariance realism of OD and orbit propagation processes through the classical theory of consider parameters of batch least-squares estimators. The devised methodology uses the theory of consider parameters to add the uncertainty of certain assumed parameters (i.e. consider parameters) to the estimated covariance. When predicting future states and associated uncertainties, the uncertainty of the modelled consider parameters will increase the realism of the predicted covariance through propagation of the corrected estimated covariance. The variances of the consider parameters are estimated using a least-squares process with which the propagated covariance best fits a given observed covariance, previously derived. This original process receives the name of Covariance Determination and is presented throughout this project. The conceived methodology is suitable for any type of measurement or object, although its primary goal is to correct covariance unrealism of non-cooperative targets, i.e. space debris.

Among the wide variety of uncertainty sources affecting covariance realism, the influence and effect of two relevant modelling uncertainties, the atmospheric drag force and the range bias, is discussed during this project. The proposed methodology is applied to a simulated realistic scenario of tracking measurements targeting a simulated RSO to evaluate the consistency of the corrected covariance via Monte Carlo analysis. The impact that perturbations in the aforementioned models trigger to the state estimation and prediction problem is discussed. Furthermore, thorough analyses are presented to illustrate the effect of dynamic and measurement model errors on covariance realism. A practical case with real tracking data is discussed, to assess the uncertainty unrealism in the orbit determination and propagation process of the Sentinel 3A satellite and to demonstrate the capabilities of this novel methodology.

The outcome of this project is a software application integrated as part of the GMV's SST software suite that can deliver efficient and effective covariance realism improvement for a more accurate provision of SST products.

Contents

List of Figures

List of tables

Acronyms

AE	Atmospheric drag model Error
BLSQ	Batch Least Squares Method
CCSDS	Consultative Committee for Space Data Systems
CDF	Cumulative Distribution Function
CKF	Consider Kalman Filter
DLR	Deutsches Zentrum für Luft- und Raumfahrt (German Aerospace Center)
ECEF	Earth Centered Earth Fixed
ECI	Earth Centered Inertial
ECI-J2000	Earth Centered Inertial reference frame with Earth's Mean Equator and Equinox at 12:00 Terrestrial Time on (Julian date) January 1st, 2000.
EME2000	Earth Mean Equator and Equinox of J2000
ERS	European Remote Sensing Satellite
ESA	European Space Agency
ESOC	European Space Operations Center
GCRF	Geocentric Celestial Reference Frame
GEO	Geosynchronous Equatorial Orbit
GTO	Geostationary Transfer Orbit
GNSS	Global Navigation Satellite System
GPS	Global Positioning System
GRACE	Gravity Recovery and Climate Experiment
IAC	International Astronautical Congress
ICSSA	IAA Conference on Space Situational Awareness
IERS	International Earth Rotation Reference Systems
IR	Infra Red
J2000	Julian Date of 2000
CSpOC	Combines Space Operations Center
LEO	Low Earth Orbit
LSQ	Least Squares Method
MC	Monte Carlo
MEO	Medium Earth Orbit

MODEAS	Modular Orbit Determination Error Analysis Software
(NRL)MSISE	(Naval Research Laboratory) Mass Spectrometer and Incoherent Scatter radar
NEO	Near Earth Orbit
NOAA	National Oceanic and Atmospheric Administration
NORAD	North American Aerospace Defense Command
OD	Orbit Determination
OEM	Orbit Ephemeris Message
OPM	Orbit Parameter Message
POD	Precise Orbit Determination
RBE	Range Bias model Error
RMS	Root Mean Squared
RSO	Resident Space Object
SSA	Space Situational Awareness
SST	Space Surveillance and Tracking
TAI	International Atomic Time
TLE	Two Line Element
TNW	Common Cartesian reference frame where T axis is along the velocity vector, W along the orbital angular momentum vector and N completing the system.
TU Delft	Delft University of Technology
USSPACECOM	United States Space Command
WBLS	Weighted Batch Least-Squares

Symbols

Symbols	Description [units]
$\dot{\rho_{Ran}}$	Range-rate [m/s]
C_R	Reflectivity coefficient
C_D	Drag coefficient
W_{Sun}	Solar flux coefficient [$\frac{W \cdot cm}{m^2}$]
ρ_{Ran}	Range [m]
A	Surface area [m^2]
B	Ballistic Coefficient [$\frac{kg}{m^2}$]
c	Speed of light [m/s]
m	Mass [kg]
t	Time [s]
$\boldsymbol{D}$	Drag force [N]
$\boldsymbol{H}$	Design matrix of LSQ algorithm
$\boldsymbol{P}$	Covariance matrix
$\boldsymbol{Q}$	Frame transformation matrix
$\boldsymbol{SRP}$	Solar radiation pressure [N]
$\boldsymbol{W}$	Weighting matrix of LSQ algorithm
$\boldsymbol{c}$	Consider parameters vector
$\boldsymbol{v}$	Velocity [m/s]
$\boldsymbol{r}$	Position [m]
$\boldsymbol{x}$	State vector [m m/s]
$\boldsymbol{y}$	Estimated parameters vector
$\boldsymbol{z}$	Observations
$\boldsymbol{\epsilon}$	Measurement noise
$\boldsymbol{\Phi}$	State transition sensitivity matrix
α	Density [$\frac{kg}{m^3}$]
σ	Standard deviation

1

INTRODUCTION

The upcoming section will detail the concepts that will be discussed during the completion of this research project. The first part of this introductory section will explore the motivation behind this research, giving sound arguments to demonstrate the main current challenges that this research project desires to tackle. In addition, a thorough introduction to the main topics that will be covered during this report is given, having a look at the heritage of the techniques and methods implemented and reviewing state-of-the-art methodologies that seek to accomplish similar results.

1.1 Motivation of the research

ESA's Space Situational Awareness (SSA) program was launched in 2009 with the purpose to guarantee Europe's independent access and exploitation of space, either for scientific or commercial purposes. The ultimate aim of ESA's SSA programme is to detect potential hazards, predict and asses the risk to Earth's population due to space debris from re-entries, in-orbit explosions, in-orbit collisions, potential impacts of NEO (Near Earth Objects) and effects of space weather to the space environment (from [ESA-SSA, 2011]). Europe's access to SSA information has depended on external sources (mainly United States of America defence dept.) until the creation of this programme which will provide Europe with the independence it requires, as detailed in [European-Comission, 2018].

The motivation for the creation of the SSA programme stems from the fact that space services have become essential in modern society. A wide variety of sectors nowadays, ranging from broadcasting to aviation and navigation, greatly depend on space weather. In addition, human life on Earth is at risk due to the existence of NEO objects threatening to impact Earth's surface. But what is more relevant nowadays is the increasing hazard that the Space Debris population poses to the operational satellites orbiting the Earth (see [ESA, Space Situational Awareness - Detecting Space Hazards (brochure), 2017] for further reference). The growth of the space debris population coupled with an easier and cheaper access to space have led to a situation in which Earth orbits are becoming overpopulated.

Nowadays, most of the satellites and orbiting bodies are located at Low Earth Orbits (LEO). Scientific and communications satellites are preferably placed at low-altitude orbits for a wide variety of reasons: limited sensing and power capabilities, less bulky satellites with an easier injection into orbit, use of less powerful/costly launchers, etc (from [Oliver Montenbruck, 2000]). This can be appreciated by looking at Figure 2, where an exponential growth of the number of catalogued objects has been experienced during the past years, being the LEO regime the one that has experienced the most notorious increase.

Not only has the number of objects residing LEO increased but another peculiarity makes this orbital regime the most problematic. More than often, LEO objects (either operational or space debris) happen to share a set of specific orbital parameters. As listed in [Vallado D. A., Fundamentals of astrodynamics and applications, 1997], LEO orbits are used to fulfil many purposes such as communications, weather surveillance, military, earth and ocean resources and scientific research. In order to carry out these missions, a satellite requires a particular set of orbital parameters and, as shown in Figure 1, there are three bands of main relevance: Sun-synchronous orbits ($i = 95 - 105\ deg$), polar ($i = 80 - 90\ deg$) and zero apsidal precession ($i \approx 63{,}43\ deg$). High-inclination orbits will

eventually lead to a considerable spatial density of orbiting bodies at high latitudes (i.e. Polar Regions), decreasing the number of available slots and posing potential threats to actual and future missions.

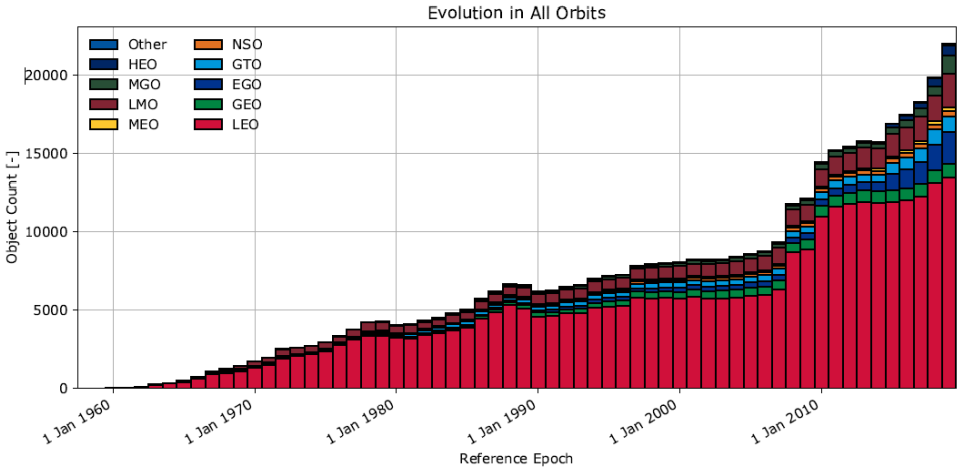

Figure 2 Evolution of number of objects per orbit type, from (ESOC-(ESA), 2019)

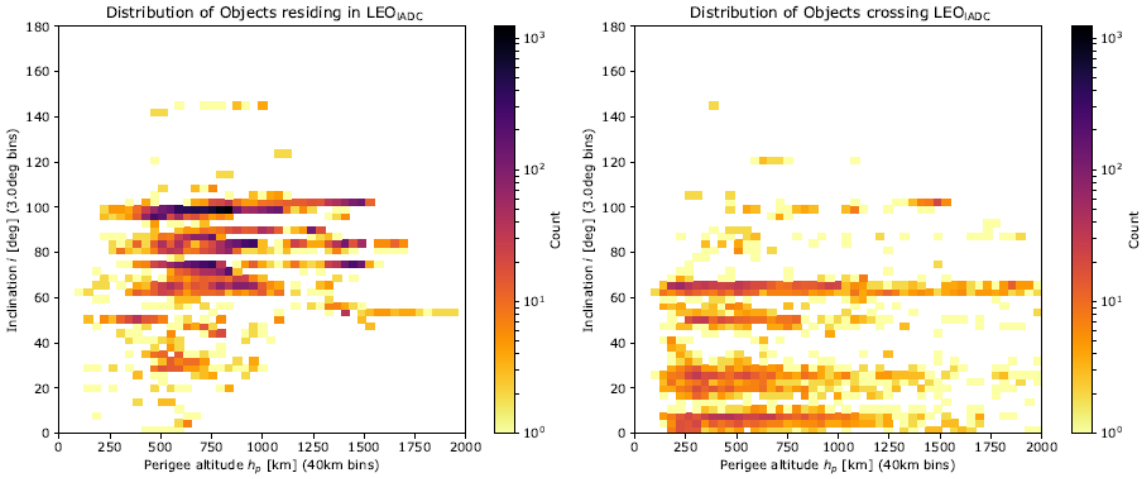

Figure 1 Distribution of objects residing in the LEO regime and distribution of objects crossing the LEO regime, from (ESOC-(ESA), 2019).

Human activity in space has caused the growth of a very large population of resident space objects. More than 20,000 objects are currently catalogued by SST networks with sizes starting around 10 centimetres in LEO and around 1 metre in Geostationary Earth Orbit (GEO), as detailed in [Rossi, 2005]. RSOs comprise fragmentation debris, spacecraft (both operational and not functional), mission-related debris and rocket bodies. Undoubtedly, with such dimensions and depending on the collision conditions, the consequences may be fatal for any operational satellite.

The scope of this research project is within the SST and STM framework and deals with the provision of realistic and accurate products. 2008 became a landmark for SST activities as it marked the first collision between an operational satellite, the Iridium-33 (a telecommunications satellite) and Cosmos 2251, an inactive Russian satellite (see [Kelso, 2019] for further reference), both orbiting the LEO region. The collision took place without STM systems and Satellite Operators to notice the close approach, as the accuracy of the SST products delivered was not sufficient to compute a realistic probability of collision, leading operators to disregard the collision warning (see [Peterson, Sorgeb, McVeyc, Gegenheimerd, & Henninge, 2018] for further reference). Further collisions will take place if the capabilities of SST products are not enhanced, as the future near Earth environment is predicted to grow both in number of space debris and operational satellites. Besides, if the commercial and scientific exploitation of the most sought-after orbital configurations (i.e. LEO Sun-Synchronous, LEO polar) wants to continue being plausible, an upgrade on the current accuracies of SST products should be attained, together with a compliance on space debris mitigation guidelines during mission design.

The central topic of this project becomes the research and validation of a novel methodology to improve the accuracy of SST products, enabling an enhanced provision of services to satellite operators and STM operators. Special emphasis is given to the LEO orbital regime, as it has been shown to be the most troublesome (see [Klinkard, 2006] for further reference). SST services comprise conjunction analysis, sensor tasking and scheduling, catalogue build-up and maintenance and manoeuvre/anomaly characterisation. Unlike orbit estimation with cooperative targets, SST campaigns suffer from data starvation, as the target only reflects incoming radiation or sunlight. Measurements are obtained by SST sensors (optical telescopes, radars, laser ranging stations or space based sensors), whose availability, accuracy and coverage is more limited, resulting in a worse orbit solution when compared to regular OD products (as detailed in [Poore, et al., 2016]).

SST products use the object's covariance as an approximation of the uncertainty of the object's state, since Gaussian statistics deliver a feasible preliminary approximation to the real probability density function under linear regime, i.e. for small uncertainties and short propagation times (see [Yanez, Gupta, Morand, & Dolado, 2019]). The provision of SST services greatly depends on how well modelled is the uncertainty on catalogued objects, in other words the uncertainty realism. Assuming Gaussian processes, the uncertainty of the object's state can be represented by the covariance matrix obtained from a classical OD.

Usually, classical orbit determination processes fail to properly consider all relevant sources of uncertainty, or do not consider them at all. As a result, state vector covariance is not properly determined, leading to an optimistic estimation. A requirement for the correct computation of the covariance matrix relies on the proper knowledge of the measurement standard deviation and in the absence of systematic errors (either in the force or measurement models), as detailed in [Oliver Montenbruck, 2000]. Unlike measurement errors, systematic errors' contribution cannot be removed in orbit determination processes by processing large sets of measurements, as their uncertainty affects the confidence of the used dynamic models. Instead, they affect the estimation and, most importantly, the prediction of a realistic state and associated uncertainty.

The most relevant and unconsidered dynamical model uncertainty is found in the modelling of the atmospheric drag force, affecting the OD processes of LEO objects. In the Literature Study ([Lopez-Jimenez, Literature Study for MSc Thesis - TU Delft, 2019]), a detailed analysis on the uncertainty sources of the atmospheric drag force model is given, where the force model is presented together with the uncertainty that each one of its parameters introduces. The main contributions to the uncertainty of the model are the definition of the atmospheric density, followed by the modelling of the ballistic coefficient of the object (see [Wilkins & Alfriend, 2000] and [Vallado D. A., Fundamentals of astrodynamics and applications, 1997] for further reference).

In addition to dynamical model uncertainties, measurement model uncertainties may play an important role when defining a realistic covariance matrix. Range bias uncertainty greatly depends on the radar system used, therefore a modelling uncertainty should be accounted for each considered radar station. However, during the preceding work of this project, typical station bias standard deviations were found to be below 5% (when compared to their mean). There is no doubt that dynamic model uncertainties are the main influence to the covariance unrealism problem, however uncertainties in the measurement models, for instance those related to measurement correction, might be relevant to the covariance realism problem.

Finally, once the sources for covariance unrealism have been defined, the impact on the aforementioned SST products must be quantified, in order to understand the true dimension of the covariance realism problem. In the Literature Study, a thorough analysis on the effect of an unrealistic covariance to the different services was provided and several conclusions were derived:

- For the conjunction analysis and computation of the collision probability, a common technique is to employ the position covariance to define a Gaussian ellipsoid (i.e. 3D region of confidence) to compute the probability of collision (as explained in [Chan, 2008]). Size, orientation and shape of the true uncertainty region have a great influence over the realistic computation of the collision probability. A deviation in any of the previous parameters can trigger differences in the computation of the probability of collision of several orders of magnitude, being the most important factors the dimension and orientation of the Gaussian ellipsoid.

- For catalogue build-up and maintenance, the use of covariance is key to the processing of large sets of tracks. The most used metric is the Mahalanobis distance (see [Poore, et al., 2016]) which makes direct use of the covariance matrix as a means to establish the statistical distance between two estimated states. Clearly, an unrealistic covariance can lead to the miscorrelation of tracks by generating false positives or false negatives or missing classifiable objects.

- For manoeuvre analysis, a similar analysis applies as for the correlation of tracks. The covariance plays a key role by being the central element of the metrics employed to characterize a manoeuvre or an orbital anomaly (see [Lopez-Jimenez, Literature Study for MSc Thesis - TU Delft, 2019]).

The previous section has defined the framework of the coming research, more concretely, SST and STM activities targeted to the urging problem of space debris, has motivated, using numerous references, the need for an improvement of the accuracy of SST products, has outlined the main causes for covariance unrealism and has summarized the effects that covariance unrealism has in the accuracy of SST products.

Next section will address the central topic of the Master Thesis, covariance unrealism, together with the heritage that previous research has produced. A relevant exposition of state-of-the-art methods to correct covariance unrealism is provided, emphasising concepts or techniques that will be used in the development of the methodology to be presented in this Master Thesis.

1.2 Covariance realism heritage

The present section will explore the field of covariance realism, providing the reader with a clear introduction into the different areas of this particular field of study and reviewing the heritage that previous research has developed. The section is organized so as to first provide an introduction to covariance theory, define the conditions under which the covariance can be considered a feasible approximation of the orbital uncertainty. Last, this section explores the different metrics developed to measure the realism of covariance matrices and give an overview of the different techniques employed by the scientific community to correct for covariance unrealism (either in the orbit determination or propagation of the object's state).

1.2.1 Covariance as an approximation of orbital uncertainty

Batch Least-Squares (BLS) orbit determination algorithms base their mathematical formulation in the estimation of certain parameters, typically a state and additional dynamic parameters, which minimize the weighted squared sum of the residuals between the observations and the estimated trajectory. The estimation assumes that measurements are uncorrelated, unbiased and normally distributed, i.e. affected by Gaussian white noise. In addition, a weighting matrix must be defined, according to typical measurement standard deviation, to allow for data fusion and proper processing of different types of measurement. Considering all of the above, the variance of the estimation coincides with the covariance matrix of the estimated parameters (state and dynamic variables), defined from [Oliver Montenbruck, 2000]) as follows:

$$\boldsymbol{P_x} = (\boldsymbol{H_x^T W H_x})^{-\mathbf{1}} \tag{1.1}$$

Where $\boldsymbol{Hx}$ is the matrix of partials of the measurements with respect the state vector and $\boldsymbol{W}$ is the weighting matrix containing the standard deviation of the measurements. The classical formulation of the covariance matrix is affected by the tracking geometry, the number and type of the measurements, its distribution and the quality (i.e. measurement noise). For the present work, the estimated parameter space will comprise state (position and velocity) and additional dynamic parameters (drag coefficient and/or solar radiation pressure coefficient) leading to a squared 7x7 or 8x8 covariance matrix.

A statistical interpretation of the covariance matrix can be found in many relevant literature references (for instance in [Vallado D. A., Fundamentals of astrodynamics and applications, 1997]). The diagonal elements of the covariance matrix (i.e. variances or squared standard deviations) provide a statistical measure of the confidence of the estimation, in other words the closeness of the fit to the processed observations. Covariance is also indicative of the observability of the estimated parameters given the processed observations, as some parameters are estimated more accurately if certain observations are processed (for instance, range measurements are more sensitive to variations in the radial and along-track component, range-rate to variations in the along-track direction). The off-diagonal terms contain the correlation between estimated parameters and express the variability of one parameter with respect another.

Since the previous formulation only accounts for the expected measurement standard deviation, the covariance becomes a good representation of the uncertainty of the state vector if measurement weights are properly defined and if errors, either in the dynamics or measurement models, are not present. However, real OD and propagation processes are affected by such errors as the knowledge of the measurement model and the dynamics of the object

is limited. Hence, covariance is unrealistic and does not represent the uncertainty of the object's state estimation and prediction. The motivation for achieving a covariance realism improvement is further elaborated in [Lopez-Jimenez, Literature Study for MSc Thesis - TU Delft, 2019] and the previous section, however a formal definition of the field of study of covariance realism is sought in this section.

In modern literature, both covariance consistency and covariance realism may be used to describe the same field of study: the proper characterization of the uncertainty in the estimation of an object's state (i.e. an OD process). This is usually done by measuring how well the covariance represents orbital differences between an estimated and reference/truth orbit. During the previous section, it has been made clear that covariance is being relied upon more and more as SST activities develop but it serves no purpose if its representation of the orbital uncertainty is not accurate or if it requires considering very restrictive assumptions.

Before deepening into covariance realism, a careful consideration must be noted. Covariance realism and uncertainty realism are different concepts. The latter implies the first, however uncertainty realism describes the proper characterisation of the probability density function of the state estimation even when the phenomena governing the distribution are not Gaussian. Assuming linear regime and processes affected by Gaussian noise, both concepts coincide. It is common practice to represent the uncertainty of the orbital state with the covariance matrix derived from an OD process (from [Oliver Montenbruck, 2000], [Vallado D. A., Fundamentals of astrodynamics and applications, 1997] and [Tapley, Schutz, & Born, 2004]), provided that measurement residuals are zero mean normally distributed random variables and that the aforementioned assumptions hold.

However, when the previous assumptions fail, either due to a long propagation period of the satellite state or due to large orbital uncertainties, linear regime and Gaussianity cannot be assumed (from [Hill, Alfriend, & Sabol, 2008], [Chris Sabol, 2010] and [Akella, Junkins, & Alfriend, 1996]). Studies show that there are two causes for the error distribution of the orbit state to become non-normal: state representation and linearization of dynamics. In [Folcik, Lue, & Vatsky, 2011], it is shown that degradation of Gaussianity in the representation of orbital uncertainty during propagation is achieved quicker when using a linear geometric reference frame (i.e. Cartesian space) rather than element-based (osculating or averaged orbital elements). This is confirmed by [Aristoff & Poore, Non-linear uncertainty propagation in orbital elements and transformation to Cartesian space without loss of realism, 2014], yet an important remark is made: linearized dynamics and Cartesian frame are adequate if orbital differences are up to the order of hundreds of meters.

On the other hand, when a Gaussian distribution is not feasible by any means, other studies explore the possibility to characterize non-gaussian orbital state uncertainty with different Probability Density Functions (PDF) such as Gaussian Mixtures or Gauss von Mises distributions among others (from [Horwood & Poore, 2012] and [Poore, et al., 2016]). For the sake of simplicity, and because the ranges of orbital uncertainties that will be treated during this research are comprised between meter to kilometre magnitudes, linear propagation and Cartesian representation are assumed. This strong hypothesis is justified by means of normality tests.

1.2.2 Metrics for covariance realism

During the past, unrealistic covariance have aroused little concern, as the focus was directed to perfecting state estimation, but, as more SST products rely on covariance and due to the urgent need of a provision of accurate solutions, numerous studies have been developed (from [Poore, et al., 2016]). For a covariance to be considered consistent or realistic, a series of conditions must be fulfilled (from [Vallado & Seago, Covariance realism, 2009]):

- The mean error of the orbital state prediction should be close to 0, i.e. unbiased from the true state.
- The distribution of the predicted orbital state should tend be normal, i.e. follow a Gaussian distribution
- The dispersion or spread of the error in the predicted state should be consistent with the predicted covariance.

The first conditions are relatively easy to test and can be achieved by inspecting the mean value of the orbital differences distribution. The second condition becomes harsher to test, as multivariate analysis of normality is a complex process. A common assumption is to test for univariate normality for all the components of the covariance matrix and assume multivariate normality of the whole function (from [Thode, 2011]). From [Vallado & Seago, Covariance realism, 2009], normality tests for the orbital differences are proposed and assessed but two tests stand out among others for their power and proven robustness: Shapiro-Wilk normality test ([Shapiro & Wilk, 1965]) and Michael's Dsp test ([Royston, 1993] and [Michael, 1983]). Especially, Michael's Dsp normality test allows for the definition of bound regions to test for the normality of the sample.

Finally, a commonly accepted metric for testing the dispersion of the resulting orbital differences is the Mahalanobis distance, and assuming a normal distribution covariance its definition is the nominal one (a generalized

Mahalanobis distance is also available to test for different probability density functions rather than normal, from [Horwood, Aristoff, Singh, Poore, & Hejduk, 2014]). The Mahalanobis distance (see [Mahalanobis, 1936]) represents a measure of the statistical distance between a given orbital perturbation and the resulting distribution of orbital states, standing out as one of the most common metrics for covariance and uncertainty unrealism, widely employed in numerous references ([Drummond, Jr., & Waugh, 2006], [Folcik, Lue, & Vatsky, 2011] and [Drummond, Ogle, & Waugh, 2007]). The Mahalanobis test for covariance realism can also be interpreted in the literature as a test for covariance containment and represents the ultimate metric to test for covariance realism.

Further elaboration on the mathematical description and implementation of the described covariance realism metrics is provided in section 2.6.

1.2.3 Covariance realism techniques

Nowadays, a set of different techniques have been developed with the aim to correct for covariance unrealism. In [Poore, et al., 2016], a broad and more detailed review of the different methods can be found, however, for the sake of simplicity, only three categories addressed for well-known estimators such as the sequential Kalman filter or the Batch Least Squares method will be dealt in this section. These methodologies fall into three different categories: scaling methods, process noise methods and consider analysis methods.

1.2.3.1 Scaling techniques

In [Laurens, Seimandi, Couetdic, & Dolado, 2017], an example of the simplest methods for covariance realism improvement is presented, where an improvement of covariance realism is sought with a scale factor and artificial augmentation techniques of the covariance. Many organisms such as CSpOC (Combined Space Operations Center) use this technique (from [Schiemenz, Utzmann, & Kayal, 2019]) in which a scaling factor is normally used to increase the volume of a Gaussian ellipsoid based on a series of statistical measures (i.e. Mahalanobis distance among others). The method is suitable both for Kalman and batch least-squares estimators.

1.2.3.2 Process noise

Process noise methods are based in the addition of a process noise covariance matrix in the propagation of the covariance as a means of taking into account uncertainties in the modelling of the system's dynamics. The process noise matrix is a covariance matrix composed by the acceleration errors characterised as white noise. Process noise is commonly applied to sequential estimators (i.e. Kalman Filters) to avoid filter saturation and to increase the realism of the propagated covariance matrix. Recent applications have been developed aiming to derive a realistic process noise matrix to include in batch estimators. From [Vallado D. A., Fundamentals of astrodynamics and applications, 1997], the derivation and posterior tuning of a physically representative acceleration error model for the process noise is a complex procedure but allows to characterise and quantify the impact of different uncertainties in the modelling of the dynamics.

From [Duncan & Long, 2006], a method for performing a more accurate propagation of the estimated covariance is devised, based on the derivation of a process noise matrix and posterior tuning. The methodology incorporates a process noise matrix to the propagation of the covariance and, provided that the process noise is accurately modelled and calibrated, its propagation will resemble that of an observed "true" covariance evolution. The modelled process noise covariance matrix becomes a 7x7 matrix, with a 6x6 element covariance expressed in a local frame plus an extra element that accounts for the uncertainty in the estimation of dynamic parameters (such as C_D). From [Duncan & Long, 2006], a method for building an observed covariance from the aggregation of orbital differences among different OD with respect to a "true" state is presented. The presented methodology is reproduced in later sections as will be considered for the calibration of the Covariance Determination methodology.

In [Schiemenz, Utzmann, & Kayal, 2019], a more complex mathematical process is exposed for the definition of a process noise matrix that considers the propagation error due to uncertainty in the density model. The process noise matrix is then implemented as part of the estimation problem of a batch least-squares or for a covariance propagation. Again, the modelling of the process noise becomes a critical design step in which a dynamical noise is expected to be modelled. The derived process noise covariance accounts for the propagation of density uncertainties to state vector uncertainties, detailing an analytical procedure to derive the different correlations included in the process noise matrix. A similar approach to that of the consider parameters is followed in which a classical Weighted Batch Least-Squares (WBLS) formulation is extended to incorporate extra parameters in the estimation process. Although the similarities of the methodology with a consider analysis, the method does not implement a differentiation between a consider space and an estimation space. The novelty of the paper is based in the continuation of the paper presented by [Emmert, Warren, Segerman, Byers, & Picone, 2017] and the extension of the uncertainty coefficients developed, not only for the correlation of atmospheric uncertainties in the along-track position but other position components.

1.2.3.3 Consider parameters techniques

There are numerous references that highlight the extended use of consider parameters (i.e. consider analysis) among SST industry stakeholders for improving the realism of the covariance derived from an OD ([Poore, et al., 2016], [Duncan & Long, 2006], [Schiemenz, Utzmann, & Kayal, 2019] or [Wiegel & Patyuchenko, 2011]). From the references, organisations such as the CSpOC, Numerica Corp. or DLR make use of consider parameters or pseudo-consider parameters to increase covariance realism, mainly modelling the uncertainty of the atmospheric model by considering a ballistic coefficient parameter variance, coupled with the estimation of empirical accelerations. Other parameters that are normally modelled comprise uncertainties in measurement biases and noise, uncertainties in tropospheric corrections, uncertainties in tracking station locations or uncertainties in the definition of Earth and Sun gravitational parameters, among others.

In [Wiegel & Patyuchenko, 2011], the implementation of the consider parameters theory on a batch least-squares estimator is detailed, giving the Modular Orbit Determination Error Analysis Software (MODEAS), analogous to the implementation presented in this work based in [Oliver Montenbruck, 2000] and [Tapley, Schutz, & Born, 2004]. In [Yang, Yue, & Dempster, 2016], the formulation of a Consider Kalman Filter (CKF) is provided, where the estimation space is reduced considering some non-estimated parameters that have an impact in the computed covariance through the process noise and initial covariance matrix. Despite all the references available and the application of consider analysis for both batch and sequential estimators, no information is provided on the how the assumed weights of the consider parameters are computed, which is of the utmost relevance as the corrections to the covariance matrix depend on them.

1.2.3.4 Conclusions on existing techniques

Three different categories have been discussed because of the relevant techniques described to tackle the problem of covariance realism. The Covariance Determination methodology presented in the following report lies its foundations in the theoretical background of the consider parameters technique presented by [Oliver Montenbruck, 2000] and [Tapley, Schutz, & Born, 2004]. Different consider parameters will be modelled, as a means of defining a process noise matrix in the consider space that will impact both the estimation and propagation of the covariance matrix.

From the methods presented above, some features will be adapted to the concept of Covariance Determination while others remain common:

- All covariance realism techniques make use of empirical data to calibrate the process noise matrix or scaling factors, as a means of achieving a realistic correction of the covariance realism.
- The derivation of the observed covariance is done similar to the description included in [Duncan & Long, 2006]. The observed covariance will be ingested by the algorithm to perform the calibration of the consider parameters.

The use of the consider analysis theory allows for an alternative formulation of the process noise matrix, which has inherent benefits compared to the techniques presented above:

- Scaling techniques lack physical insight and only rely on statistical analysis of empirical data to provide corrections. It is difficult to generalize or extrapolate any result since the scaling factors are not linked to any physical process (i.e. the dynamics of the problem are not characterized).
- Process noise techniques require extensive analytical derivations of the acceleration error terms that affect the uncertainty of each component of the covariance matrix. Modelling a single contribution leads to a complex matrix formulation.

Finally, the benefits of the Covariance Determination methodology are summarized as follows:

- Modelled consider parameters are tightly correlated to uncertain physical processes affecting the motion of the object. Therefore, empirical insight in the uncertainty of such models is easily derived with applications to future orbit predictions and covariance realism upgrades.
- The consider analysis presents advantages with respect other techniques. Although relevant references mention its extended use, no methodology has been found that defines a process to empirically determine the contributions of consider parameters. The purpose of the conceived methodology is to propose a robust solution to the aforementioned problem.
- The consider parameters uncertainty matrix will have a simple and solid approach, without requiring extensive analytical derivations as shown in [Schiemenz, Utzmann, & Kayal, 2019], allowing for the

modelling of several uncertainty contributions through different parameters within a single consider covariance matrix.

- The covariance realism improvement introduced by the consider parameters is relevant not only during orbit propagation (like process noise techniques) but also during the orbit estimation process.

For the present study, uncertainty in the dynamic models has been assumed as white noise, however as pointed by [Siminski J. , 2016] and [Schiemenz, Utzmann, & Kayal, 2019], other noise models such as random walk or Brownian motion could be considered.

The present section has addressed the topic of covariance realism and the heritage that previous research on the topic has produced. The theoretical background and relevant metrics to test for covariance realism have been reviewed from different relevant references. In addition, from the spectrum of different techniques developed as of today, three categories have been exposed in more detail outlining the main characteristics and features that will be considered during the development of the novel methodology of Covariance Determination. The main strong points of this novel methodology are the use of both dynamics and statistics in the correction of covariance unrealism, where a model calibration is achieved by ingesting empirical data whereas an analytical derivation of the consider parameters matrix allows to obtain physical insights of the dynamics.

1.3 Proposal of research

During the previous sections, a detailed exposition of the motivation, state-of-the-art and relevant techniques for covariance realism improvement have been detailed. The present section establishes the proposal of research by clearly stating the aim and the research questions to be answered during the completion of this report.

1.3.1 Aim

The aim of the research to be conducted in the present Thesis can be summarized by the following statement: *"Conceptualize, develop, implement and validate a novel methodology to achieve a covariance realism improvement during state estimation and orbit prediction using the theory of the consider parameters in batch least-squares estimators".*

1.3.2 Research questions

The following section aims to establish solid research questions to define an investigation roadmap. The questions to be answered are the following:

1. To what extent do dynamic and measurement modelling inaccuracies impact the state estimation and prediction problem, i.e. the provision of an accurate state and a realistic covariance?
2. How can dynamic and measurement modelling uncertainties be characterized in the theory of the consider parameters using a Weighted Batch Least-Squares estimator?
3. To what extent does the Covariance Determination methodology improve the covariance realism of regular orbit determination and propagation products?
4. To what extent does the proposed validation methodology reflect the fitness and power of the Covariance Determination methodology?
5. To what extent are the present results of the study on covariance realism improvement of a satellite tracking campaign of the Sentinel 3A satellite representative of the inaccuracies of real dynamic and measurement models?
    a) Can the results obtained be used for further covariance realism upgrades?
    b) Is the methodology robust and useful in a real working environment?

1.4 Structure of report

The present thesis report is structured in five different chapters: introduction, methodology, results, discussion and conclusions. The Introduction provides an extensive review of the motivation behind the present research project, the relevant scientific heritage of the central topic and the research questions to be answered. The Methodology chapter goes over the specific details to reproduce the Covariance Determination methodology and the validation methodology proposed. The Results chapter gives an objective exposition of the different test cases executed as

well as the result of the tracking campaign of the Sentinel 3A satellite together with the results on estimated consider parameters. The Discussion chapter provides insightful examination of the results presented in the previous chapter. Finally, the Conclusions and recommendations chapter summarizes the most relevant findings and features of the proposed methodology and provides a series of further recommendations to continue the research on the topic of covariance realism. Additional annexes are included in the end of the project report containing relevant information about the developed software, measurement and dynamic models used and the batch least-squares algorithm. Next chapter will detail the complete methodology to reproduce the Covariance Determination algorithm.

2

METHODOLOGY

The following chapter provides all the relevant details concerning the formulation and implementation of the novel methodology of Covariance Determination.

The first part introduces some basic concepts that are used and implemented during the devised methodology, such as commonly employed reference frames and terminology. Next, the theory of the consider parameters is introduced and reviewed so as to give enough insight to the reader on the peculiarities of its formulation. Finally, the covariance determination algorithm is presented, illustrating the application of the consider parameters theory to a classical batch least-squares orbit determination, with the purpose to improve covariance realism.

The second part details the consider parameters that are modelled in order to correct for covariance unrealism. In addition, a methodology for the generation of a covariance evolution over time is presented.

The third part defines the validation chain devised to verify the implementation of the methodology giving extensive proof through the computation of several Monte Carlo (MC) analysis, of the covariance realism improvement achieved. In addition, covariance realism metrics are introduced and thoroughly revised.

2.1 Introductory knowledge

The purpose of this section is to clarify the relevant terminology that will be used hereafter as well as the definition of the reference frames, gravitational and dynamical models.

2.1.1 Relevant Terminology

The relevant terminology described in the following section applies to the whole report and will be used during the description of the covariance determination methodology as well as the discussion of the results. The relevant terms used are:

- Measurement: Result of a physical process by which a sensor captures incoming radiation from a target (either emitted by the sensor itself, by the target or a reflection of a secondary emitter) obtaining a numerical value that represents a physical magnitude. Examples of different measurements are: range, range-range, azimuth and elevation, right ascension, declination. A definition of common SST measurement models can be found in [ESA, Mathematical Models and Algorithms, 2009].

- Observation: set of measurements related to a certain epoch, belonging to a particular object and obtained by a certain sensor.

- Orbit Determination (OD) : process by which the orbital state (state vector as well as dynamical parameters such as drag or solar radiation pressure coefficient) is estimated at a certain epoch, named the estimation epoch, using observations obtained from sensors, typically telescopes and/or radars in SST.

- Estimated parameters (orbital state): set of orbital parameters, defined at a certain epoch, obtained through an orbit determination process providing a trajectory which represents the best fit to the available observations (minimum residuals). Orbital parameters comprise: position, velocity, dynamical parameters, etc. and are considered as Gaussian random variables.

- Estimated/determined orbit: time evolving orbital state of an object obtained as a product of an orbit determination process over a time interval with available observations.

- Predicted/propagated orbit: time evolving orbital state of an object obtained through a propagation process (either analytical, semi-analytical or numerical) over a time interval without available observations.

- Covariance: Measure of the joint variability of N random Gaussian variables. Covariance is used to quantify uncertainty and provide an estimate of accuracy in orbit determination processes under normality assumptions. The covariance matrix is diagonal if all variable are independent, semi-definite positive and symmetric. For the upcoming research, covariance matrix is computed using the normal equations of an orbit determination process, as shown in Equation (1 .1).

- A-posteriori covariance: covariance of the estimated orbital state resulting from an orbit determination process. Depending on whether the covariance matrix takes into account consider parameters or not:

    - Noise only Covariance: if no consider parameters have been included in the orbit determination, the covariance matrix only accounts for the measurement noise.

    - Consider covariance: if consider parameters are included in the orbit determination process, the consider covariance also accounts for the uncertainty of the aforementioned parameters in the computation of the final covariance, producing a larger covariance with respect to the noise-only one.

- Propagated covariance: time evolving characterization of the orbit uncertainty (position and velocity) obtained after propagation of the a-posteriori covariance.

- Consider parameters: Non-estimated parameters that are added to the orbit determination process. Its contribution has no effect on the estimated orbital state but its uncertainty is added to the a-posteriori covariance (noise-only) in order to improve covariance realism. Likewise estimated parameters, consider parameters are considered Gaussian random variables.

- Variance of consider parameters: Uncertainty of the consider parameters, characterized as a Gaussian distribution.

- Observed covariance: Uncertainty characterization over time of the object's orbital state generated from a statistical comparison of estimated and propagated orbits.

- Covariance determination: process in which the variance of the consider parameters is estimated by obtaining a best fit of the propagated covariance to the observed covariance. The fitting process is analogous to an orbit determination process that uses a batch least-squares estimation method.

- Mahalanobis distance: from [Mahalanobis, 1936], measure of the statistical distance between a certain orbital state with respect to a distribution of orbital states.

2.1.2 Relevant reference frames

The following section will define the relevant reference frames used for the representation of the covariance and to carry out orbital and covariance propagation.

2.1.2.1 TNW reference frame

The chosen reference frame to express the covariance evolution over time is a well-known local frame named TNW Local orbital frame ([CCSDS, Navigation data: definitions and conventions (green book), 2010]). Local frames are defined using the object's position and velocity at a certain epoch and are normally employed for attitude estimation and attitude control purposes. However, local frames are also helpful to characterize orbital uncertainty, since orbital differences are best expressed from a local centre of coordinates and axis aligned with the main orbital perturbations. Especially for LEO objects, the use of a local frame becomes highly useful as one of the greatest non-conservative perturbations is the atmospheric drag, which acts antiparallel to the object's velocity (and is aligned with the local along-track direction). Looking at the Clohessy-Wiltshire equations (see [Wakker, 2015]

p.213), there is no doubt that a local frame can provide a better understanding on the evolution of orbital differences if linear dynamics apply.

Local TNW reference frame is defined as Tangential, Normal and W denoting the orbital plane (i.e. direction of angular momentum). The origin of the reference frame is located in the centre of mass of the object. The tangential direction is defined as the normalized velocity vector, the W direction (omega) is defined as the normalized angular momentum direction and N completes the trihedron by computing the cross-product over W and T. Equation (2 .1) and Figure 3 give the mathematical formulation as well as the graphical representation of the TNW frame.

$$\boldsymbol{Q_{TNW}} = [\boldsymbol{t} \quad \boldsymbol{n} \quad \boldsymbol{w}] = \left[\frac{\boldsymbol{v}}{||\boldsymbol{v}||} \quad \boldsymbol{w} \times \boldsymbol{t} \quad \frac{\boldsymbol{\omega}}{||\boldsymbol{\omega}||}\right] \tag{2 .1}$$

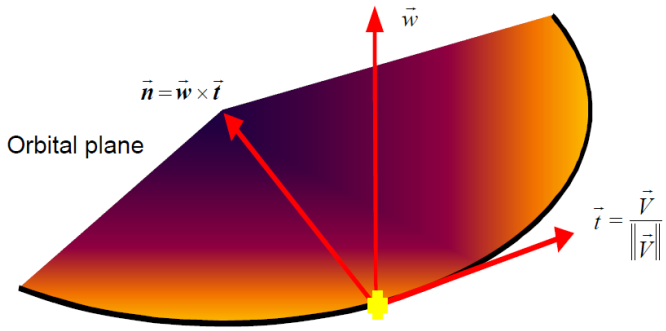

Figure 3 Graphical representation of TNW local reference frame, from (CCSDS, Navigation data: definitions

Finally, the following formula will be used when computing covariance frame changes from J2000 to TNW and vice-versa, from [Vallado D. A., Fundamentals of astrodynamics and applications, 1997]:

$$\boldsymbol{P_{TNW}} = \boldsymbol{Q_{TNW}^T P_{J2000} Q_{TNW}} \tag{2 .2}$$

Since the frame transformation matrix $\boldsymbol{Q_{TNW}}$ is orthogonal, the counter transformation is achieved by inversing the previous matrix and, because of the inherent properties of the transformation, its transpose equals its inverse:

$$\boldsymbol{P_{J2000}} = \boldsymbol{Q_{TNW} P_{TNW} Q_{TNW}^T} \tag{2 .3}$$

2.1.2.2 J2000 reference frame

J2000 reference frame, EME2000 or GCRF, is an Earth-centered quasi-inertial frame with its origin located at the centre of mass of the Earth. The x axis is defined by the mean equinox at 12:00 terrestrial time on January the 1st 2000, the $\boldsymbol{z}$ axis is defined by the equatorial plane direction and the $\boldsymbol{y}$ axis defined by the cross product of the aforementioned axis, completing the trihedron (from [Wakker, 2015]).

Quasi-inertial reference frames are commonly used to express satellite state as the effect of apparent forces is removed and the modelling of satellite dynamics becomes easier and straightforward. For this reason, the propagation process as well as the orbit determination process are performed using the J-2000 reference frame.

2.1.3 Relevant orbital perturbations

In the following section, the relevant orbital perturbations that will affect the motion of any LEO space object and that introduce a considerable uncertainty in the computation of the orbit determination will be detailed. Aside from geopotential orbital perturbations, which have been measured precisely (and whose error may be chosen by the user due to the truncation of the geopotential model), non-conservative stochastic dynamic perturbations are of main relevance to the problem of covariance realism. Looking at [Oliver Montenbruck, 2000] p. 55, considering the

LEO regime, atmospheric drag and solar radiation pressure are the most critical orbital perturbations to bear in mind.

2.1.3.1 Atmospheric Drag

Atmospheric drag plays a crucial role when modelling the dynamics of orbiting bodies interacting with the atmosphere, being the dominant non-conservative perturbation for satellites with a perigee altitude from 120 km up to 600 km (from [Lafontaine & Hughes, 1982], some studies show that the threshold could be set at 1000 km although other studies are more conservative setting the threshold at 600 km, as shown in [Heiner Klinkard, 1998]). The standard definition of the atmospheric drag acceleration can be found in many references, for instance [Wakker, 2015]:

$$\boldsymbol{D} = -\frac{\frac{1}{2}C_D \alpha A}{m}|\boldsymbol{v}|\boldsymbol{v} \tag{2.4}$$

The parameters that define the atmospheric drag force are the following:

- α: Atmospheric density parameter.
- C_D: The coefficient of drag.
- A: The object's cross-sectional area
- m: The mass of the body
- $\boldsymbol{v}$: Relative velocity of the body with respect to the surrounding medium.

It is common to collapse certain of the aforementioned parameters in a certain coefficient, also known as the ballistic parameter:

$$B = \frac{m}{C_D A} \tag{2.5}$$

In [Lopez-Jimenez, Literature Study for MSc Thesis - TU Delft, 2019], a thorough explanation on the different sources of uncertainty that the modelling of each parameter introduces to the computation of the atmospheric drag acceleration is given. As introduced in section 1.1, the modelling of the atmospheric density is the source of error with the most substantial impact on the atmospheric drag force and hence on the uncertainty realism of the a-priori covariance (noise-only).

Several atmospheric models exist nowadays and despite the quality and the large availability of measures used to derive them, like the Jacchia-Bowman 2006/2008 or the NRLMSISE-00, they cannot reproduce the stochastic nature of the atmosphere, providing fairly accurate predictions of the density. From [Vallado & Finkleman, A critical assessment of satellite drag and atmospheric density modeling, 2014] and [Bruinsma, Sanchez-Ortiz, Olmedo, & Guijarro, 2012], a careful review of the different atmospheric models available is done and several important conclusions are derived: there is not a single best atmospheric model but rather different models that are demonstrated to be more accurate than others depending on the orbital altitude, solar and geomagnetic conditions of the environment. For this reason, the selected model to be employed during the research of this project will be the NLRMSISE-00, as from [Bruinsma, Sanchez-Ortiz, Olmedo, & Guijarro, 2012], it provides a better performance for orbits above the 500 km attitude range. Below that range, the Jacchia-Bowman 2006/20008 stands out as the most accurate atmospheric model.

Another remarkable conclusion from [Vallado & Finkleman, A critical assessment of satellite drag and atmospheric density modeling, 2014] is that the uncertainty in the modelling of the atmospheric density does not only depend on the chosen atmospheric model but rather correlates with the implementation of the model by the researcher or actual values for solar and geomagnetic activity, among others. In order to quantify such uncertainty, a review of typical values used or assumed in the industry is done. In [Bowman, et al., 2008], a review of the JB-2008 model is provided with some figures about the improvement of density standard deviation errors, however the conclusion is that typical density standard deviations in LEO orbits are of the order of 9-10%. Other studies suggest that typical assumed uncertainties values for atmospheric models range from 10% to 20% ([Vallado & Finkleman, A critical assessment of satellite drag and atmospheric density modeling, 2014], [Kuang, Desai, Sibthorpe, & Pi, 2014]). In Appendix A, a careful review of the NLRMSISE-00 model is provided together with the most relevant proxies employed and the different sources of uncertainty concerning the definition of each parameter.

Errors in the modelling of the atmospheric density are paramount to the proper characterisation of typical errors in the atmospheric drag force model. However, the assumption of other relevant time-varying parameters may also yield important contributions to the uncertainty of the drag force model. The uncertainty of the ballistic coefficient modelling is the second main source of uncertainty as it depends on a wide variety of phenomena, basically stemming from the definition of a representative C_D and cross-sectional area. Typical variability of the C_D is found to be from 1.5 to 3 depending on the interaction of the satellite's surfaces with the different flow regimes found in the atmosphere's strata, from [Oliver Montenbruck, 2000]. In addition, spacecraft cross-sectional area can be known for attitude controlled satellites, however for space debris it can lead to changes of up to 10 times the initially estimated value (from [Poore, et al., 2016]). Therefore, the definition of a representative ballistic coefficient is difficult and subject to strong variations as the object moves through the atmosphere.

Rather than modelling the ballistic coefficient, a common practice is to estimate it through an orbit determination as it may be a useful mitigation mechanism to capture errors in the definition of a correct area-to-mass ratio or average errors in the atmospheric density models. However, its estimation is not sufficient to determine the stochastic nature of the atmosphere or the unknown motion of the object as it orbits through the atmosphere (from [Wilkins & Alfriend, 2000], [Oliver Montenbruck, 2000] and [Kuang, Desai, Sibthorpe, & Pi, 2014]). Moreover, because the estimation of the drag coefficient only adjusts the dynamical model to the observed dynamics (through the measurements), the estimated variance of the drag coefficient provides a measure of the goodness of the fit but not a measure of the real uncertainty of the atmospheric drag model.

There is no doubt that the process of modelling the atmospheric drag acceleration of an object entails a great uncertainty, with many different uncertainty sources stemming from the very definition of its key parameters: atmospheric density and ballistic coefficient. If unconsidered, the computed covariance of an orbit determination process may be a poor estimation of the true uncertainty of the object's state.

2.1.3.2 Solar radiation pressure

Solar radiation pressure is the force exerted by the photons of the Sun impacting the satellite and being absorbed or reflected. Its most notorious effects have a direct impact in the change of eccentricity and longitude of the perigee. Its effect is bigger in bodies with a high area-to-mass ratio (for example satellites with low weight and big solar panels).

Solar radiation pressure represents a nearly constant impact on the dynamics of Earth orbiting bodies. From the previous section, there is no doubt that the atmospheric drag acceleration plays a crucial role when modelling the dynamics of orbiting bodies at orbits below the 600 km of altitude. However, for satellites orbiting above 600 km of altitude (depending on solar activity) solar radiation becomes the predominant non-conservative perturbing force. For instance, from [Heiner Klinkard, 1998], the case of the ERS-1 is presented where radiation pressure is shown to deliver orbital perturbations 4 times bigger than atmospheric drag perturbations. In addition, direct solar radiation has been shown to deliver forces of at least one order of magnitude higher than other radiation pressure forces (like Earth's albedo, Earth's IR and the object's IR emission). For this reason, only solar radiation pressure will be considered for its impact to uncertainty realism. From [Wakker, 2015], the analytical definition of the solar radiation pressure acceleration is:

$$\boldsymbol{SRP} = -\frac{C_R W_{SUN} A}{mc}\boldsymbol{e_s} \tag{2.6}$$

Each of the parameters of the solar radiation pressure definition are a source of uncertainty and are defined as follows:

- M: mass of the body
- A: cross-sectional area of the body affected by sunlight.
- C_R: satellite/body reflectivity.
- c: is the speed of light
- $\boldsymbol{e_s}$ unit vector defined between the body and the Sun.
- W_{SUN}: energy flux of the Sun incident on the object.

The sources of uncertainty that each of the previous parameters introduce to the modelling of the solar radiation pressure can be found in [Lopez-Jimenez, Literature Study for MSc Thesis - TU Delft, 2019]. The parameter with the highest impact on the variation of the solar radiation pressure model is found to be the cross-sectional area of the body exposed to the radiation. While the other parameters can be characterized and predicted with a sufficient level of accuracy (or do not exhibit large variations) the cross-sectional area of the object can change up to an

order of magnitude, depending on the object's configuration and attitude (from [Vallado D. A., An analysis of state vector propagation using differing flight dynamics programs, 2005]).

An important remark has to be made, and that is the relative impact on the orbit uncertainty coming from both orbital perturbation models (solar radiation pressure uncertainty and atmospheric drag uncertainty). A study on the sensitivity of orbital differences assuming variability for both models is carried out in [Vallado D. A., An analysis of state vector propagation using differing flight dynamics programs, 2005] showing that although the solar radiation pressure can be a more relevant orbital perturbation, its modelling uncertainty (or model variability) displays a lesser effect than that of the atmospheric drag modelling. This translates into the fact that for LEO objects, the uncertainty on the modelling of the atmospheric drag force has a greater impact on the overall covariance unrealism and therefore represents the critical modelling uncertainty to treat, on a first approximation to the improvement of covariance realism in LEO orbits (see also [Poore, et al., 2016], p.33 and [Siminski J. , 2016]).

Next section is going to deal with the theoretical background of the consider parameters theory, giving a thorough definition of the main concepts and the important modifications that apply to a regular batch least-squares orbit determination algorithm.

2.2 Consider parameters theory on Batch Least-Squares

Classical orbit determination algorithms represent a compromise between dynamics and statistical estimation. The achievable accuracy depends on how well the dynamic models and measurement models describe the motion of the orbiting body. There are many different sources of error in the assumption or definition of the previous models that can be summarized in the following way (from [Tapley, Schutz, & Born, 2004]):

- Errors in the mathematical description or modelling of the measurement
- Errors in the definition of the numerical values assigned to non-estimated measurement and dynamic model parameters.

The field of covariance analysis has the aim to study the sensitivity of the uncertainty representation (i.e. the covariance) to the unconsidered error sources. This translates into the realism of the achievable accuracy of the estimation or, in other words, into the covariance realism problem. In the end, the unconsidered error sources described before can be classified as non-estimated parameters (either from measurement of dynamical models) with a certain uncertainty that is normally not included when computing the covariance matrix of the estimation problem.

The theory of the consider parameters assumes that the covariance computed in the estimation process of the object's state is not representative of the true uncertainty of the object when model errors are present and not considered. In [Oliver Montenbruck, 2000] and [Tapley, Schutz, & Born, 2004], consider parameters are assumed as random variables with a Gaussian PDF. The consider parameters are assumed to have zero mean and certain variance:

$$c \sim N(0, \sigma_c^2) \tag{2.7}$$

Unlike measurement noise, uncertainties of measurement and dynamics models cannot be averaged out by processing large batches of information, as they affect the estimation process in a systematic fashion. Thus, by implementing certain consider parameters, the consider covariance becomes less sensitive to large batches of observations and turns out to be a more realistic representation of uncertainty (as seen in [Scheeres, 1993]).

The classical weighted batch-least squares theory suffers some modification due to the inclusion of the consider parameters. Additional terms are added to a standard non-linear batch least squares algorithm to represent the consider parameters (from [Oliver Montenbruck, 2000] p.266):

$$\boldsymbol{z} = \boldsymbol{h}(\boldsymbol{y}_o, \boldsymbol{c}) + \boldsymbol{\epsilon} \tag{2.8}$$

Where the observations $\boldsymbol{z}$ are expressed as a function of the estimated parameters $\boldsymbol{y}_o$ plus the consider parameters $\boldsymbol{c}$. The derivation process is similar to a regular BLS algorithm, where the cost function minimizes the residuals between the observed measurements and the modelled ones:

$$J = min\,|\big(\boldsymbol{z} - \boldsymbol{h}(\boldsymbol{y}_o, \boldsymbol{c})\big)^T \big(\boldsymbol{z} - \boldsymbol{h}(\boldsymbol{y}_o, \boldsymbol{c})\big)| \tag{2 .9}$$

A linearization of Equation (2 .8) is performed, as in any standard batch least-squares orbit determination algorithm:

$$\Delta \boldsymbol{z} = \boldsymbol{H}_y\big(\boldsymbol{y}_0 - \boldsymbol{y}_0^{ref}\big) + \boldsymbol{H}_c\boldsymbol{c} + \boldsymbol{\epsilon} \tag{2 .10}$$

Where $\Delta\boldsymbol{z}$ is the difference between the observed and modelled measurements (linearizing at point $\boldsymbol{y}_0^{ref}$), $\boldsymbol{H}_y$ is the matrix of partials of the observations with respect to the estimated parameters correction $\boldsymbol{y}_0 - \boldsymbol{y}_0^{ref}$, $\boldsymbol{H}_c$ is the matrix of partials of the observations with respect the consider parameters. As a consequence of the assumption that consider parameters have a zero mean and that its variance are uncorrelated with measurement noise, the solution of the state estimation of the OD is identical to that of an original OD process, as its expectancy becomes null:

$$E\big(\boldsymbol{y}_{\boldsymbol{0}}^{lsq}\big) = \boldsymbol{y}_0 + \big(\boldsymbol{H}_y^T\boldsymbol{W}\boldsymbol{H}_y\big)^{-1}\boldsymbol{H}_y^T\boldsymbol{W}\big(\boldsymbol{H}_c E(\boldsymbol{c}) + E(\boldsymbol{\epsilon})\big) = \boldsymbol{y}_0 \tag{2 .11}$$

However, the formulation of the covariance matrix of the estimated parameters differs by some amount due to the uncertainty introduced by the consider parameters' variance, leading to the consider covariance:

$$\boldsymbol{P}_c = \boldsymbol{P} + \big(\boldsymbol{P}\boldsymbol{H}_y^T\boldsymbol{W}\big)(\boldsymbol{H}_c\boldsymbol{C}\boldsymbol{H}_c^T)\big(\boldsymbol{P}\boldsymbol{H}_y^T\boldsymbol{W}\big)^T \tag{2 .12}$$

Being $\boldsymbol{P}$ the estimated a-posteriori covariance from a regular OD (also known as noise-only covariance), without consider parameters, $\boldsymbol{W}$ the weighting matrix, and $\boldsymbol{C}$ a diagonal matrix containing the variance of the estimated parameters. The dimensions of the involved matrices are gathered below for clarification:

- $\boldsymbol{P}$, $\boldsymbol{P_c} \in \mathbb{R}^{n_y} \times \mathbb{R}^{n_y}$
- $\boldsymbol{H_y} \in \mathbb{R}^{n_z} \times \mathbb{R}^{n_y}$
- $\boldsymbol{H_c} \in \mathbb{R}^{n_z} \times \mathbb{R}^{n_c}$
- $\boldsymbol{W} \in \mathbb{R}^{n_z} \times \mathbb{R}^{n_z}$
- $\boldsymbol{C} \in \mathbb{R}^{n_c} \times \mathbb{R}^{n_c}$

Where n_y is the number of estimated parameters, n_z is the number of measurements and n_c the number of consider parameters of the orbit determination process. Note that matrix $\boldsymbol{W}$ has been considered as the inverse of the measurement covariance matrix. From Equation (2 .12), there is an additional contribution to the estimated covariance and this contribution depends directly on the value of the variance of the consider parameters. Note that consider parameters are assumed to be random variables with a certain variance, hence the $\boldsymbol{C}$ matrix is defined as:

$$\boldsymbol{C} = \begin{bmatrix} \sigma_{c,1}^2 & 0 & 0 \\ 0 & \ddots & 0 \\ 0 & 0 & \sigma_{c,n}^2 \end{bmatrix} \tag{2 .13}$$

As it will be assumed that the consider parameters are uncorrelated, the consider parameters matrix will be diagonal. A definition of the $\boldsymbol{H}_y$ matrix is widely known whereas the definition of the $\boldsymbol{H}_c$ matrix might be less known and is of the utmost relevance to the consider parameters theory. Both matrices define the partials of the measurements with respect to the estimated parameters and consider parameters respectively. The formulation of the $\boldsymbol{H}_c$ is the following:

$$\boldsymbol{H}_c = \left(\frac{\partial \boldsymbol{h}(\boldsymbol{y}_0, \boldsymbol{c})}{\partial \boldsymbol{c}}\right)_{\boldsymbol{y_0}=\boldsymbol{y_0^{ref}}} = \left(\frac{\partial \boldsymbol{z}}{\partial \boldsymbol{x}}\frac{\partial \boldsymbol{x}}{\partial \boldsymbol{c}}\right)_{\boldsymbol{y}_0=\boldsymbol{y}_0^{ref}} \tag{2 .14}$$

It is important to note that depending on the nature of the consider parameters, the evaluation of the previous expression will be done via two separate methods. If the consider parameter has a direct influence in the observations (for instance, a station calibration bias affecting directly the measurement model) the computation of the partial derivatives is a straightforward procedure.

However, if the consider parameter has indirect implications to the measures, through the dynamic models, its derivation is similar to computing the partials of the measurements with respected the estimated parameters. From Equation (2 .14), the first part of the partial derivatives, $\partial \boldsymbol{z}/\partial \boldsymbol{x}$, is commonly known from any BLS algorithm. However, the second partial derivate, i.e. the sensitivity matrix of the state vector with respect the consider parameters, needs to be defined. Analogous to the state sensitivity transition matrix, the sensitivity matrix is evaluated using the variational equations:

$$\frac{d}{dt}\left(\frac{\partial \boldsymbol{x}}{\partial \boldsymbol{c}}\right) = \frac{\partial \boldsymbol{f}\left(t, \boldsymbol{x}(t)\right)}{\partial \boldsymbol{x}(t)} \cdot \frac{\partial \boldsymbol{x}(\boldsymbol{t})}{\partial \boldsymbol{c}} + \frac{\partial \boldsymbol{f}\left(t, \boldsymbol{x}(t)\right)}{\partial \boldsymbol{c}} \tag{2 .15}$$

An equivalent expression for the equation would be:

$$\dot{\boldsymbol{S}}(t) = \boldsymbol{F} \cdot \boldsymbol{S}(t) + \begin{pmatrix} 0_{3\times n_c} \\ \dfrac{\partial \boldsymbol{a}(\boldsymbol{r}, \boldsymbol{v}, t, \boldsymbol{p})}{\partial \boldsymbol{c}} \\ 0_{n_p \times n_c} \end{pmatrix} \tag{2 .16}$$

Where $\boldsymbol{S}(t)$ represents $\partial \boldsymbol{x}/\partial \boldsymbol{c}$, $\boldsymbol{F}$ represents the matrix of the partial derivatives of the first derivative of the state vector with respect the state vector, $\dot{\boldsymbol{S}}(t)$ represents the derivate of $\boldsymbol{S}(t)$ and an additional term is added with the partial of the equations of motion with respect to the consider parameters. Since the consider parameters will affect the dynamic models that characterize the object's motion, its contribution will be seen in the acceleration terms. Equation (2 .16) is solved by numerical integration via Runge-Kutta or multi-step methods (preferred).

Finally, for an easier implementation of the aforementioned equations on the Covariance Determination algorithm, some modifications are introduced in the formulation of Equation (2 .12). The correction terms of the equation can be aggregated leading to a simpler formulation of the consider covariance, where a new matrix named $\boldsymbol{K}$ matrix is defined (i.e. sensitivity matrix of the consider parameters with respect to the estimated state):

$$\boldsymbol{K}^T = \boldsymbol{P}\left(\boldsymbol{H}_y^T \boldsymbol{W} \boldsymbol{H}_c\right); \;\; \boldsymbol{K} \in \mathbb{R}^{n_c} \times \mathbb{R}^{n_y} \tag{2 .17}$$

$$\boldsymbol{P}_c = \boldsymbol{P} + \boldsymbol{K}^T \boldsymbol{C} \boldsymbol{K}$$

The $\boldsymbol{K}$ matrix is performing a change from the consider parameters space to the state space by pre and post multiplying the variance of the consider parameters $\boldsymbol{C}$. In [Scheeres, 1993], some properties of the sensitivity matrix (i.e. $\boldsymbol{K}$ matrix) are provided:

- The noise-only covariance matrix decreases as more measurement are considered. However, due to the formulation of the sensitivity matrix, the consider covariance does not decrease by adopting more measurements (and it may even increase).
- The consider covariance is invariant to a scaling of the weighting matrix $\boldsymbol{W}$, due to the formulation of the sensitivity matrix**.** If only one data type is being used, the consider parameters contribution will be independent of the measurement noise. However, for proper definition of the consider parameters contribution, measurement weights should be precisely tuned.
- A measurement model consider parameter (range bias error, station coordinates error, etc.) will have a constant impact on the consider covariance and generally has no terms that increase with time.
- A dynamic model consider parameter (atmospheric drag model error, solar radiation pressure model error) will have a time-dependent impact on the consider covariance, normally increasing with time.

Finally, it is worth mentioning that for the Covariance Determination algorithm, the $\boldsymbol{K}$ matrix will represent an input to the method whereas the $\boldsymbol{C}$ matrix will become the estimation parameters.

This section has detailed the theoretical background of the theory of covariance analysis and consider covariance together with the extensive review of the mathematical procedure required to adapt a classical Batch least-squares algorithm to the theory of consider parameters. An important remark can be made about the consider parameters theory: the formulation, as exposed previously, enables a covariance correction without a degradation on the orbital integrity. The relevance of this statement is of crucial importance to the problem. Next section is going to deal with the mathematical definition of the covariance determination algorithm and its implications on the covariance realism correction.

2.3 Covariance determination algorithm

The following section will define the novel methodology introduced in this research Thesis named Covariance Determination. The chosen terminology arises from the fact that the method devised follows a similar approach to that of an OD process, being conceptualized with great parallelism to it. The initial solution, namely the noise-only covariance (obtained as a product of an OD), is corrected using the consider parameter variances. These variances are estimated in a statistical process using a weighted BLS estimator algorithm.

To introduce the reader to the many parallelisms of the Covariance Determination methodology with an OD process,the following table is included:

Table 1 Orbit determination vs Covariance Determination comparison

	Covariance Determination	**Orbit Determination**
Observations	Observed covariance	SST sensor measurements
Estimated parameters	Consider parameter variance	State vector and/or dynamic parameters
State vector	Consider covariance independent terms	Position and velocity terms

The observations comprise batches of observed covariance matrices that capture the evolution of the uncertainty as it evolves far from the initial state. The parameters to estimate become the variances of the consider parameters, through the consider covariance formulation. The process is structured in two main steps which will be detailed in the coming section, but for a general overview of the processing chain of the Covariance Determination algorithm, see the following figure:

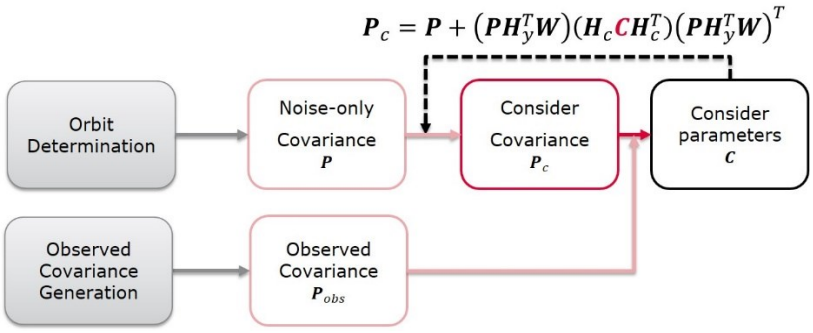

Figure 4 Algorithm of the Covariance Determination methodology

In Figure 5, a conceptual representation of the evolution of a covariance element in the in-track direction of both observed, consider and noise-only matrix is provided. Note that all the represented sigma tend to grow rapidly due to the propagation effect as uncertainty grows when no measurements are available. The base concept of the covariance algorithm is to provide a fitting to the evolution of the observed covariance by starting from the noise-only a-priori covariance, which evidently is not able to capture the real uncertainty of the orbit's state as time

evolves. The algorithm will provide, through the estimation of the consider parameters' variance, a correct representation of the orbital state uncertainty.

There is no doubt that within the propagation region two different behaviours can be appreciated, the first being a periodical fluctuation of the covariance over its means value (osculating covariance) whereas a secular effect is also observed (due to the propagation of the uncertainty). During the first part of the propagation period, the osculating terms prevail over the secular terms, as not enough time has elapsed for the propagation to produce a sufficient impact on the propagation of the uncertainty. In the end, as covariance is propagated further from the estimated state (OD region) the secular component prevails over the osculating.

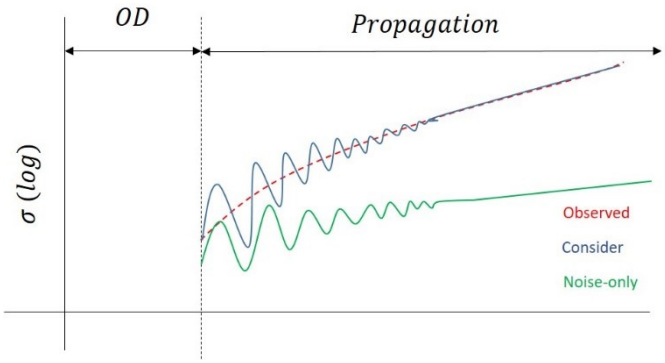

Figure 5 Visual representation of a covariance fitting

The Covariance Determination methodology has an effect on the covariance matrix during the orbit estimation and prediction, however its most important contribution in improving the realism of covariance is during the propagation of the orbit. Therefore, this technique is better suited for improving covariance realism of orbit propagation processes.

The complete workflow consists of two different parts (see Figure 4), the first one being a pre-processing and the second one involving the estimation of the consider parameters variance through an iterative batch least-squares process. In the next sections, a detailed explanation on the processes involved in each step will be given, shedding light on the peculiarities of the Covariance Determination algorithm.

2.3.1 Pre-processing

The pre-processing step of the Covariance Determination algorithm entails the generation of the a-priori unrealistic noise-only covariance, the generation of the observations, namely the observed covariance, and the generation of the so-called $\boldsymbol{K}$ matrix, whose definition is found in Equation (2 .16).

The pre-processing of the Covariance Determination algorithm cannot be accomplished without the previous computation of an OD over a time span with available SST measurements as the methodology not only requires the a-priori covariance but also the required partial derivatives to define the $\boldsymbol{K}$ matrix.

2.3.1.1 Generation of the noise-only covariance matrix

The generation of the noise-only covariance follows from the orbital state estimation performed using an OD algorithm. In order to produce a consistent solution, a careful definition of the environmental conditions for the proper processing of the observations must be performed, which includes:

- Proper definition of the measurement and dynamic models at use during the OD process or a-posteriori propagation. It is of the utmost relevance that both models represent with a high degree of fidelity the dynamics of the tracked object in order to provide a consistent estimation and orbit prediction.
- Measurement availability will condition the attainable orbit accuracy. If not enough orbital tracks are available at separated epochs, the orbital estimation becomes highly sensitive to variations of other parameters, measurement noise, or errors in the dynamic models. By considering a sufficient amount of orbital tracks, the robustness of the solution is ensured (more observations can be considered to construct the normal equations matrix and leave an ill-conditioned situation). From [Pastor, 2017], it is concluded that the condition number of the normal equations matrix decreases as more observations are considered during an OD process (which gives a measure of the sensitivity of the estimation). In addition, other factors play an important role in the achievable accuracy like the observations geometry.

- Measurement weighting defines the confidence or quality of the processed measurements. Proper measurement weighting ensures that more accurate measurements (i.e. range for radar station) have a greater impact on the final solution than low quality observations. Variations in the weighting will affect the computation of the orbital state and the noise-only covariance.

Finally, the geopotential, dynamical and tidal models implemented in the orbit determination process of GMV's software are listed in Table 2. Furthermore, the measurement models employed in GMV's SST software suite can be found in [ESA, Mathematical Models and Algorithms, 2009].

Table 2 Processing strategy of GMV's SST software used at GMV

Full dynamical model	
Gravity field (Static)	EIGEN.GRGS.RL03.v2 (up to 120x120)
Gravity field (time-varying)	Drift/ annual /semi-annual piece wise linear terms up to 50x50
Third body perturbations	Sun & Moon
Polar motion and UT1	IERS C04 08
Pole Model	IERS 2010 conventions
Precession/ Nutation	IERS 2010 conventions
Solid Tides	Applicable (IERS 2010 conventions)
Atmospheric Model	MSISe-90; Fit performed for ballistic coefficient
Solar Radiation Pressure	Box-wing (S1) Constant area (S2); Fit performed for coefficient of reflectivity
Ocean Tide model	EOT11a (up to 50x50)
Earth Pole Tide	IERS 2010
Ocean Pole Tide	IERS 2010
Geodetic surface	ERS-1
Reference frame	J2000 ECI

2.3.1.2 Generation of K matrix

From the orbit determination process that provides the estimated state and the noise-only covariance, the required partial derivatives necessary to compute the $\boldsymbol{K}$ matrix are obtained as well. Looking at Equation (2 .16), there are several terms that need to be computed:

- $\boldsymbol{P}$**:** noise-only covariance computed after the orbit determination process.
- $\boldsymbol{H_y}$**:** partial derivatives of the measurements with respect to estimated parameters of the orbit determination process, also known as Jacobian matrix.
- $\boldsymbol{H_c}$**:** partial derivatives of the measurements with respect to consider parameters of the orbit determination process, as defined in Equation (2 .14) (2 .15) and (2 .16).
- $\boldsymbol{W}$: weighting matrix of the measurement of the orbit determination process.

There is no doubt that once the final solution of the orbit determination process is attained, the aforementioned terms remain constant and can be properly defined. During the pre-processing of the Covariance Determination algorithm, the $\boldsymbol{K}$ matrix is computed being a constant value through the whole process, as the partial derivatives mentioned above are referred to the estimation epoch.

Once all the required inputs are defined, the application of the central algorithm of the Covariance Determination algorithm will follow. Next section will provide an insightful explanation on the devised novel methodology.

2.3.2 Iterative Batch Least-Squares for the Covariance Determination algorithm

The central iterative part of the Covariance Determination algorithm will be explained in detail during the following section, once the different inputs of the method have been defined.

The basic idea of applying a least-squares estimation to the Covariance Determination algorithm is to determine the variances of the consider parameters for which the square root of the residuals between the modelled and empirical observed covariance matrices is minimized (i.e. define the values of the variances of the consider parameters that provide the best fit of the consider covariance to the observed covariance). Let the estimated vector of the consider parameters be:

$$\boldsymbol{y}_0 \leftarrow \boldsymbol{diag}(\boldsymbol{C}) \tag{2 .18}$$

As presented in Equation (2 .13), the covariance matrix of the consider parameters that produces the correction (Equation (2 .12)) is diagonal as the consider parameters are considered to be uncorrelated. Let the measurement vector be defined as:

$$\boldsymbol{z} \leftarrow \begin{pmatrix} \boldsymbol{P}_{\boldsymbol{obs}}^{\boldsymbol{0}} \\ \vdots \\ \boldsymbol{P}_{\boldsymbol{obs}}^{\boldsymbol{n}} \end{pmatrix} \tag{2 .19}$$

Where $\boldsymbol{P}_{\boldsymbol{obs}}^{\boldsymbol{i}}$ are the components of an observed covariance measured at a time t_i. The components of the observed covariance are ordered following a lower triangular line-by-line sequence, as shown in the following equation:

$$\boldsymbol{P}_{obs}^{i} = \begin{pmatrix} P_{r_{TT}}^{i} \\ P_{r_{TN}}^{i} \\ P_{r_{NN}}^{i} \\ \vdots \\ P_{v_{WN}}^{i} \\ P_{v_{WW}}^{i} \end{pmatrix}_{obs} \in \mathbb{R}^{21} \tag{2 .20}$$

The observed covariance components comprise the position and velocity terms of a covariance matrix, i.e. a vector of 21 terms is defined. The rest of the terms of a covariance matrix are not relevant to the fitting of the consider parameters as they are expected to be small if compared to position and velocity terms. Recall from Section 2.1.2.1, that expressing covariance in the TNW frame entails several benefits and for this reason the definition of the observed covariance is done in a local frame.

For the Covariance Determination algorithm, the assumed stated vector (as an analogy to the orbit determination algorithm) is defined as the lower triangular consider covariance terms ordered following a line-by-line sequence, as shown in the following equation:

$$\boldsymbol{x} \leftarrow \boldsymbol{P}_c(t_0, \boldsymbol{y}_0) = \begin{pmatrix} P_{r_{TT}}^{0} \\ P_{r_{TN}}^{0} \\ P_{r_{NN}}^{0} \\ \vdots \\ P_{v_{WN}}^{0} \\ P_{v_{WW}}^{0} \end{pmatrix}_{c} \in \mathbb{R}^{21} \tag{2 .21}$$

For the sake of simplicity, the state vector has been defined as the consider covariance at reference epoch t_0. Note that the state vector (i.e. independent elements of the consider covariance) is also defined in the TNW frame. For the model, a linear covariance propagation is sufficient to obtain the modelled observations (i.e. modelled observed covariance matrices) at the epoch of the measurements:

$$\boldsymbol{P}_c(t, \boldsymbol{y}_0) = \boldsymbol{\Phi}(t, t_0)\boldsymbol{P}_c(t_0, \boldsymbol{y}_0)\boldsymbol{\Phi}^T(t, t_0) \tag{2 .22}$$

The observations are described by:

$$\boldsymbol{z}_i(t_i) = \boldsymbol{P}_c(t_i, \boldsymbol{y}_0) + \boldsymbol{\epsilon}_i \tag{2 .23}$$

Or in a more compact formulation:

$$\boldsymbol{z} = \boldsymbol{h}(\boldsymbol{y}_0, t_i) + \boldsymbol{\epsilon} \tag{2.24}$$

The $\boldsymbol{h}$ vector denotes the model value as a function of time and the consider parameters variance $\mathbf{y}_0$. The solution of the previous system of equations is difficult as the $\boldsymbol{h}$ function is affected by non-linear effects and a linearization at a reference point $\mathbf{y}_0^{ref}$ is applied to allow for the resolution of the system (analogous to the resolution of an OD). Skipping the derivations of the linearization, the resulting system is the following:

$$\Delta \boldsymbol{z} = \boldsymbol{H}_y^* \left(\boldsymbol{y}_0 - \boldsymbol{y}_0^{ref}\right) + \boldsymbol{\epsilon} \tag{2.25}$$

The Jacobian matrix is defined as in a regular least-squares OD process:

$$\boldsymbol{H}_y^* = \left(\frac{\partial \boldsymbol{h}}{\partial \boldsymbol{y}_0}\right)_{\boldsymbol{y}_0^{ref}} = \frac{\partial \boldsymbol{z}}{\partial \boldsymbol{y}_0} = \frac{\partial \boldsymbol{z}}{\partial \boldsymbol{x}} \frac{\partial \boldsymbol{x}}{\partial \boldsymbol{y_0}} \tag{2.26}$$

The first term of the Jacobian matrix becomes the identity matrix, due to the choice of formulation of the Covariance Determination state vector, as the state vector at t_i is directly mapped to the observed covariance:

$$\frac{\partial \boldsymbol{z}}{\partial \boldsymbol{x}} = \boldsymbol{I} \tag{2.27}$$

The second term of the Jacobian matrix is a compound of the correction due to the consider parameters variance to the noise only covariance, giving the consider covariance at reference epoch, and the propagation of the consider covariance from the reference epoch to the epoch t_i:

$$\begin{aligned} \boldsymbol{x} = \boldsymbol{f}(t_i, \boldsymbol{C}) &= \boldsymbol{\Phi}(t, t_0) \boldsymbol{P}_c\left(t_0, \boldsymbol{y}_0^{ref}\right) \boldsymbol{\Phi}^T(t, t_0) \\ &= \boldsymbol{\Phi}(t_i, t_0)(\boldsymbol{P} + \boldsymbol{K}^T \boldsymbol{C} \boldsymbol{K}) \boldsymbol{\Phi}^T(t_i, t_0) \end{aligned} \tag{2.28}$$

As detailed in [Lopez-Jimenez, Pastor, Escobar, Setty, & Agueda, 2019], the consider covariance matrix is propagated via the complete transition matrix, $\boldsymbol{\Phi}(t_i, t_0) \in \mathbb{R}^{n_y} \times \mathbb{R}^{n_y}$.The complete transition matrix is a square matrix of dimensions equal to the dimensions of the noise-only covariance matrix. Not only position and velocity covariance terms are propagated but also dynamical covariance terms (such as drag coefficient or solar radiation pressure coefficient terms) as they affect the orbital state covariance terms increasing their uncertainty. Finally, the cost function defined entails a minimization of the difference between the observed and modelled covariance in a least-squares fashion :

$$\begin{aligned} J = min \left| \left(\Delta \boldsymbol{z} - \boldsymbol{H}_y^* \Delta \boldsymbol{y}_0\right)^{\boldsymbol{T}} \left(\Delta \boldsymbol{z} - \boldsymbol{H}_y^* \Delta \boldsymbol{y}_0\right) \right| \rightarrow \\ \left(\boldsymbol{H}_y^{*\,T} \boldsymbol{W}^* \boldsymbol{H}_y^*\right) \Delta \boldsymbol{y}_0^{lsq} = \left(\boldsymbol{H}_y^{*\,T} \Delta \boldsymbol{z}\right) \end{aligned} \tag{2.29}$$

Due to the non-linearity of $\boldsymbol{h}$, the described process becomes iterative with the continuous substitution of the $\boldsymbol{y}_0^{ref}$ by the most recently computed $\boldsymbol{y}_0^{lsq}$. Proper care should be given to the weighting of the different observations, implemented through the $\boldsymbol{W}^*$ matrix. As they are part of the same covariance matrix and obtained using a common methodology, there is not a clear distinction between the quality of the terms. A first approximation can be assumed by giving a bigger relevance to diagonal terms of the position covariance on the first place, on the second place

the cross-coupled terms of the position covariance, on the third place the diagonal velocity components and lastly the cross-coupled velocity components. The effect on the solution of this approximation will ensure that position diagonal terms of the observed covariance are properly fitted by the consider covariance, as they represent the most important terms when treating covariance realism.

Another important remark should be made on the convergence criteria defined for the Covariance Determination algorithm. Different convergence criteria are employed in order to study the convergence rate and the quality of the solution:

- Maximum number of iterations: to avoid infinite loops, a maximum number of iterations is defined.
- Maximum number of divergent iterations: to avoid continuous divergence once a local minima has been approximated, the algorithm will monitor the continuous divergences to decide whether an improvement on the final solution is achieved or not. If a certain number of consecutive divergences is met, the algorithm will stop as no further improvement on the solution may be achieved.
- Decrement of the WRMS: to monitor the improvement on the quality of the solution, the algorithm will determine the rate of decrement of the WRMS, the weighted sum of standardized residuals, as a measure of the convergence rate. Below a certain threshold, the solution quality will stagnate or produce little improvement with consecutive iterations.
- Absolute value of WRMS: to monitor the overall quality of the solution, if a certain threshold condition is met the algorithm will stop as an accurate solution will have been computed.

Finally, a workflow of the iterative process of the Covariance Determination algorithm is presented illustrating the previously defined algorithm in a more graphical and compact fashion:

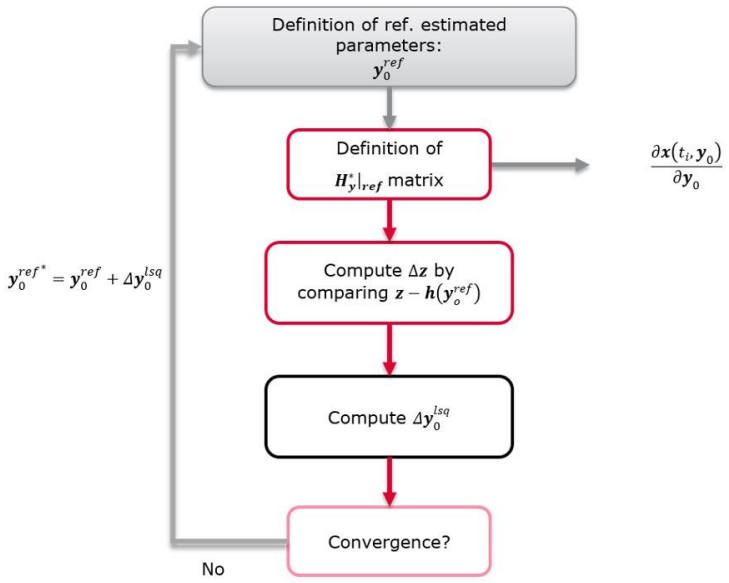

Figure 6 Iterative Covariance Determination algorithm

As mentioned previously, both observations and state vector of the Covariance Determination problem are expressed in a local reference frame (TNW). However, the propagation of the covariance matrices is done in an inertial reference (J2000). Initially, the consider covariance is obtained at t_0 in a TNW frame. A frame transformation, using Equation (2 .3), is performed from TNW to J2000 frame. Then, a propagation of the consider covariance from t_0 to t_i is performed, obtaining the consider covariance at the epoch of the measurements. Finally, a frame transformation is applied to express the consider covariance in the TNW frame using Equation (2 .2). This procedure is required for the evaluation of the residual in the BLS algorithm.

The present section has defined the Covariance Determination algorithm, together with the assumptions and processes that it entails. Next section will deal with the methodology employed for the computation of the observed covariance, the key input to the Covariance Determination algorithm.

2.4 Observed covariance generation

The generation of the observed covariance entails the processing of orbital differences, thus orbital uncertainty evolution, during the orbit prediction process. The presented method is not within the scope of this Thesis as it is integrated In GMV's SST software suite and already verified. However, to motivate the use of the aforementioned method, the present section is included. The covariance matrix is mathematically defined as:

$$\frac{1}{N}\sum_{i=0}^{N}[\boldsymbol{x}_i - E(\boldsymbol{x})][\boldsymbol{x}_i - E(\boldsymbol{x})]^{\boldsymbol{T}} \qquad (2.30)$$

The previous formulation processes orbital differences of a complete set of orbit estimations and predictions with respect to a reference state to derive a covariance matrix that is representative of the state uncertainty. However, the formal definition of the covariance matrix is only feasible during simulations, as an infinite number of independent measurements and independent ODs can be processed, leading to a representative sampling of orbital differences. However, in real operational environments this is not attainable, hence a different processing strategy is chosen.

In the observed covariance method, the observed covariance is obtained by comparing high-quality determined orbits against predicted ones. The method is based on a purely statistical consistency analysis of orbital differences between predicted and determined orbits from independent and uncorrelated ODs. A graphical scheme of the method is provided in Figure 7. Each orbital comparison is assembled in the corresponding prediction time bin, where orbits with equal ephemeris (describing the same state at the same epoch) are compared. What distinguishes them is the time elapsed between the epoch of comparison and the time when the propagation started. To illustrate this, looking at Figure 7, take for instance the first orbital comparison: the first OD has delivered an estimated state (i.e. Determined orbit (i)) plus a predicted state (i.e. Predicted orbit (i)) that spans over time; a subsequent OD (i.e. Determined orbit (ii)) delivers another estimated orbit but in a different period from the first OD and a different propagated orbit (i.e. Predicted orbit (ii)); the difference between the Predicted orbit (i) and Determined orbit (ii) over the ephemeris that both share will define the orbital differences tagged at Prediction time t_0 *to* t_1.

Therefore, by aggregating orbital differences between pairs of predicted and determined orbits from independent and uncorrelated ODs, it is possible to obtain the evolution of the covariance matrix along the prediction time. To do so, each pair is evaluated and statistics along certain prediction time window obtained. The prediction time is referred to as the relative time with respect to the epoch of the last observation.

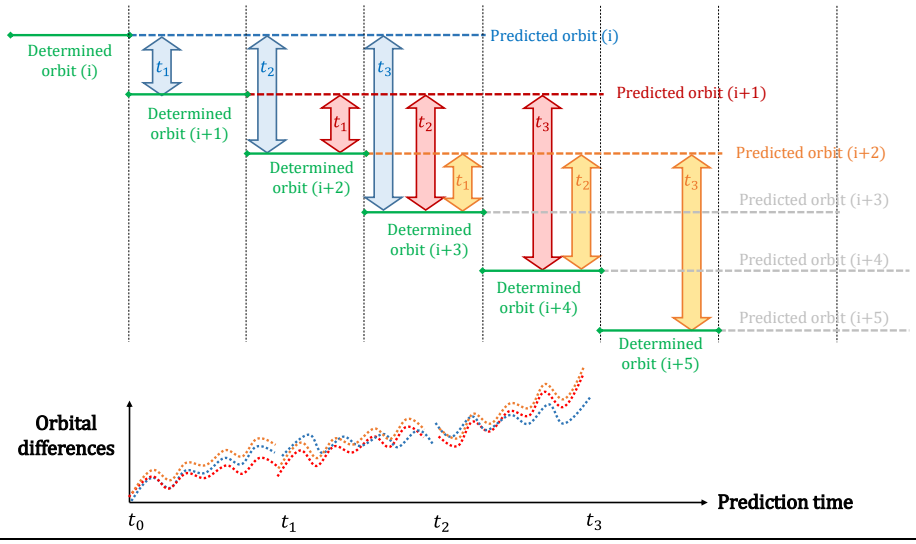

Figure 7 Sketch of the orbital differences aggregation process for the generation of observed covariance. The different colours describe the relative orbital differences with different ODs between a determined orbit and a predicted one. This differences are time-tagged taking into account the relative time elapsed between the start of the prediction period and the determined orbit.

The final aggregation of orbital differences leads to Figure 8. By considering a sufficient amount of independent orbits, a statistical representation of the evolution of uncertainty over time can be derived. Assuming that our uncertainty can be approximated as a Gaussian distribution, the statistical trend can be fitted and represented by a covariance matrix, the so-called observed covariance. This method has been successfully applied to derive covariance for operational orbits [Díez, et al., 2019], and therefore it represents a validated and independent tool to be used during the completion of this Thesis.

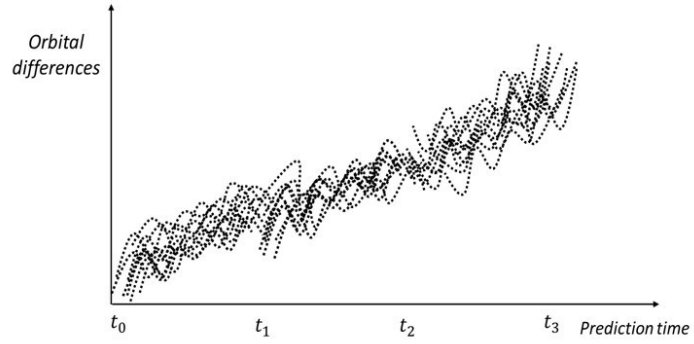

Figure 8 Aggregation of the orbital differences along the prediction time for the generation of an observed covariance.

The previous section has detailed the methodology to effectively produce an observed covariance, a statistical evolution of the orbit uncertainty during the propagation period. Next section will deal with the consider parameters to be contemplated in the Covariance Determination algorithm, based on the relevant orbital perturbations that affect the most the uncertainty realism of the a-priori covariance.

2.5 Consider parameters

The consider parameters modelled in the Covariance Determination algorithm represent the non-modelled sources of uncertainty that affect the provision of a realistic covariance during the orbit estimation and prediction process. In section 2.1.3, a definition of the non-conservative orbital perturbations models that have a greater impact in the covariance realism problem is given. Thus, the consider parameters to model will tackle the aforementioned orbital perturbations and another special case related to a measurement modelling error.

The modelled consider parameters will be defined following the assumptions and considerations detailed in section 2.2. As commented previously, two types of consider parameters are considered: those acting directly to the reconstruction of the observations through the measurement models and those acting indirectly to the observations as part of the dynamic models.

2.5.1 Atmospheric Drag force model error

As seen in section 2.1.3.1, the most important contribution in the covariance unrealism when performing orbit determination and prediction processes in the LEO regime is the modelling of atmospheric forces. These forces act upon orbiting bodies and are modelled in the Drag acceleration (as shown in Equation (2 .4)). Especially for low Earth orbits, the Drag acceleration and the error incurred in the modelling of this non-conservative force supposes the largest position uncertainty growth in the along-track direction. Recalling the formulation of the Drag acceleration, a new formulation is proposed where a consider parameter c_{AE} is included:

$$\boldsymbol{D} = -\frac{\alpha}{2B}(1 + c_{AE})|\boldsymbol{v}|\boldsymbol{v} \qquad (2 .31)$$

Where B is the ballistic coefficient (that is derived from the computation of the mass, drag coefficient and cross-sectional area). The rest of the parameters have been explained in Equation (2 .4). B will be a dynamical parameter estimated during the orbit determination process. α is the density of the atmosphere, dependent on several factors as explained in Section A, whose value will be derived from the implemented models on GMV's orbit determination software (using the MSISe-90 atmospheric model). Finally, c_{AE} will be the consider parameter implemented and

will represent the error incurred when modelling the atmospheric drag force. The consider parameter can be best regarded by the following equation:

$$c_{AE} \sim N(0, \sigma_{AE}) \tag{2 .32}$$

In order to compute the partial derivative matrix $\boldsymbol{H_c}$, Equation (2 .15) applies.

2.5.2 Solar Radiation Pressure model error

In section 2.1.3.2, the relevance of the uncertainty in the modelling of the solar radiation pressure force is detailed. The classical formulation of the solar radiation pressure force is changed so as to account for errors in the modelling. Recalling the formulation for the SRP acceleration from Equation (2 .6) and adding a consider parameter to model the inaccuracy in the model:

$$\boldsymbol{SRP} = -\frac{C_R W A\,(1 + c_{SRP})}{mc}\boldsymbol{e_s} \tag{2 .33}$$

c_{SRP} represents the consider parameter and hence the errors in the modelling of the solar radiation pressure force. The consider parameter formulation can be best perceived by inspecting the following equation:

$$c_{SRP} \sim N(0, \sigma_{SRP}) \tag{2 .34}$$

In order to compute the partial derivative matrix $\boldsymbol{H_c}$, Equation (2 .15) applies.

2.5.3 Sensor calibration parameters error

A special case contemplated in the Covariance Determination algorithm is the effect of the uncertainty when defining the measurement models employed to compute the simulated measurements. Measurement models employed for classical orbit determination processes are well-known and defined (see [ESA, Mathematical Models and Algorithms, 2009]). However, an uncertainty in the definition of several quantities, like measurement biases, translates into an uncertainty of the measurement model which, in the end, affect the computation of a realistic covariance.

Considering that a typical SST sensor obtains range, range-rate and angular measurements (either azimuth and elevation or right ascension and declination), measurement biases are defined as follow:

$$z^* = z + c_z \tag{2 .35}$$

Where z refers to any type of SST sensor measurement (i.e. range, range-rate, azimuth, elevation, etc.) as measured by the sensor, z^* refers to the corrected measurement and c_z refers to the added consider parameter. Note that in the defined station calibration consider parameters, a direct impact on the measurement models is observed. The derivatives that will form the $\boldsymbol{H_c}$ matrix can be computed directly, due to the simplicity of the consider parameter model defined:

$$\boldsymbol{H}_c = \frac{\partial \boldsymbol{z_k}}{\partial \boldsymbol{c_k}} = \boldsymbol{I}_{nb \times nb} \tag{2 .36}$$

Where nb is the number of consider parameters implemented as biases in the measurement model. The partials of the matrix are computed per measurement and consider parameter, as the subscript k denotes. The consider parameter formulation of the sensor calibration parameters can be best perceived by inspecting the following equation:

$$c_z \sim N(0, \sigma_z) \tag{2 .37}$$

During this section, all relevant sources of uncertainty have been addressed by carefully defining several consider parameters. After the definition of the different implemented consider parameters, it is time to present the validation chain that will help verify the devised methodology.

2.6 Covariance realism metrics

The present section proposes a series of consistent and robust metrics to test the realism of any covariance matrix given an experimental distribution of orbital states. As introduced in section 1.2, different conditions must be fulfilled for a covariance matrix to be considered realistic. Each condition yields to the definition of a unique metric that should be fulfilled to ensure covariance realism:

- **Unbiased average orbital state:** the average value for the orbital differences of the complete distribution should lie close to the true state. Biases ten times smaller than the typical standard deviation are considered as acceptable.

- **Study of the normality of the orbital differences:** to ensure that the orbital differences of the complete distribution of estimated and propagated states are normal and can be approximated by a multivariate Gaussian distribution (i.e. a covariance matrix) normality tests are employed.
  From [Vallado & Seago, Covariance realism, 2009] the formulation of a statistical test of hypothesis is presented, where a typical significance value for normality tests is established at 5% (indicating that there is a 5% chance to reject the null hypothesis when true, that is, to reject a normal distribution when it is actually normal). Any normality test computes a test statistic and a p-value, being the most relevant the latter as it is indicative of the probability of obtaining a test statistic at least as extreme as the computed when the hypothesis holds true. Summarizing, if the p-value is lower than the significance level established then the null hypothesis is rejected whereas if larger, the hypothesis cannot be rejected (which does not indicate that is necessarily true).
  From [Vallado & Seago, Covariance realism, 2009] an analysis on different normality tests on empirical distributions is done. Michael's test is considered more robust and powerful than the regular Kolmogorov test when testing normality on orbital propagation processes. Hence, for testing normality in orbit propagation processes, Michael's test is selected for this project. From [Michael, 1983] and [Royston, 1993], the required theoretical background is retrieved, where a graphical methodology to perform the test is described. The test defines the procedure to plot the standardized empirical Cumulative Distribution Function (CDF) versus the theoretical CDF, defining some bounds as confidence regions. These bound are defined by the following formulation:

$$y_i = sin^2\left(arcsin\left(t_i^{\frac{1}{2}}\right) \pm \frac{1}{2}\pi d_{SP}\right) \tag{2 .38}$$

$$t_i = \frac{i - \frac{1}{2}}{n} \tag{2 .39}$$

  Where y represents the ordinate of the P-P graph and t represents the abscissa. From the previous formulation, i represents the sample index (within the complete ordered distribution), i.e. considering a distribution of n samples i ranges from 1 to n. The d_{SP} value represents the test statistics which in turn is dependent on the significance level desired and which defines the boundaries of the acceptance region. Finally, the CDF function of the empirical distribution is plotted against the confidence boundary regions defined in Equation (2 .38) and the null hypothesis is rejected if any point of the empirical CDF infringes the bounds. The empirical CDF is standardized and the abscissa is defined as:

$$f_i = \Phi\left(\frac{y_i - \bar{y}}{\sigma}\right) \tag{2 .40}$$

Where f_i is the transformed ordinate of the empirical data point, Φ is the standard cumulative distribution function, $\bar{y}$ the mean of the sample to test and σ the standard deviation. The interpretation of PP plots is that each sample of the distribution is analyzed to check what percentage of data lies at or below the analyzed sample, thus comparing the spread of the empirical distribution against a theoretical one (and for this it is important that the empirical distribution is standardized).

- **Covariance containment:** to ensure the covariance is able to capture the state uncertainty (position) of the cloud of MC points, which represents a sampling of the true probability density function. To do so, a similar approach to [Folcik, Lue, & Vatsky, 2011] is followed by defining the containment metrics through the computation of the Mahalanobis distance (see [Mahalanobis, 1936] for further reference) to estimate the percentage of MC points lying inside a k-sigma ellipsoid at different epochs. The Mahalanobis distance is a measure of the statistical distance between an orbital state with respect to a certain normal distribution (characterized by a mean and a covariance). The aim of the test is to characterize the Mahalanobis distance of each and every point of a given distribution to check if the supposed dispersion (expressed as the covariance matrix) is able to represent the true uncertainty (distribution of orbital differences). The formulation of the Mahalanobis distance is as follows:

$$M = \sqrt{(\boldsymbol{x} - \overline{\boldsymbol{x}})^{\boldsymbol{T}} \boldsymbol{P}^{-\mathbf{1}} (\boldsymbol{x} - \overline{\boldsymbol{x}})} \tag{2.41}$$

Where $\boldsymbol{x}$ is the state vector of the distribution to be tested, $\overline{\boldsymbol{x}}$ the mean of the average distribution and $\boldsymbol{P}$ the covariance matric associated with the distribution.

2.7 Validation

The present section will define a thorough validation chain within a simulated realistic environment to provide solid evidence that the Covariance Determination methodology can deliver a sound covariance realism improvement. Although the ultimate objective of the Covariance Determination algorithm is to be used with real operational orbits, the validation chain will demonstrate the performance of the methodology in a simulated environment and the effect of several uncertainty sources in the degradation of the covariance realism.

The simulation environment has been set up with the capability to simulate realistic orbits, SST sensor measurements and ultimately process a representative population of solutions to generate the so-called observed covariance. The different effects of the dynamical and measurement model errors have been implemented as systematic errors over orbital arcs, as these are the non-modelled errors that the Covariance Determination methodology aims to capture.

The environmental conditions of the validation cases have been carefully chosen so as to be representative of the real operational case that will be treated afterwards. Finally the generation of the observed covariance is reviewed briefly using the theory introduced in section 2.4.

2.7.1 Validation chain workflow

To validate the Covariance Determination algorithm and its implementation, it is mandatory to test if the modelled consider parameters and the methodology described during sections 2.2, 2.3 and 2.4 can capture the different sources of uncertainty that affect the provision and propagation of the noise-only covariance.

The validation chain aims at providing a sufficiently representative population of samples so that a proper observed covariance can be built. The observed covariance matrix is to be fed to the Covariance Determination algorithm with the purpose of estimating the variance of the consider parameter and providing a realistic consider covariance by fitting it to the observed one.

To produce the population of samples, perturbations are added to the dynamic models of the different measurements and forces at stake during the OD and propagation processes. The nature of the perturbation considered is systematic during an orbital arc, this means that a fixed value for the perturbation is considered during the whole computation of a sample. Its value will be determined as sample of a zero-mean Gaussian distribution. The purpose of the validation is for the Covariance Determination algorithm to recover the standard deviation of the input consider parameter error, given a proper sampling of the PDF associated to the state estimation and prediction problem.

Careful consideration should be given to the pertubartion introduced in the models as it affects each sample of the population in a constant fashion during the whole orbital arc, hence it becomes a systematic error during the generation of measurements and estimation of the state vector. However, as each sample is affected by a unique value, leading to a different orbital estimation. By aggregation of a representative sample of orbit ephemeris, a sampling of PDF of the orbit estimation and propagation process is achieved.

The validation chain has been conceptualized as a simulation environment representative of the reality. To do so, a single radar has been considered as a representative SST sensor to take observations of a simulated RSO. In addition, to validate the implementation of the Covariance Determination algorithm, only the atmospheric drag force and range bias consider parameters have been tested, delivering a validation of a dynamical and measurement model consider parameter. The next figure introduces the workflow of the validation chain:

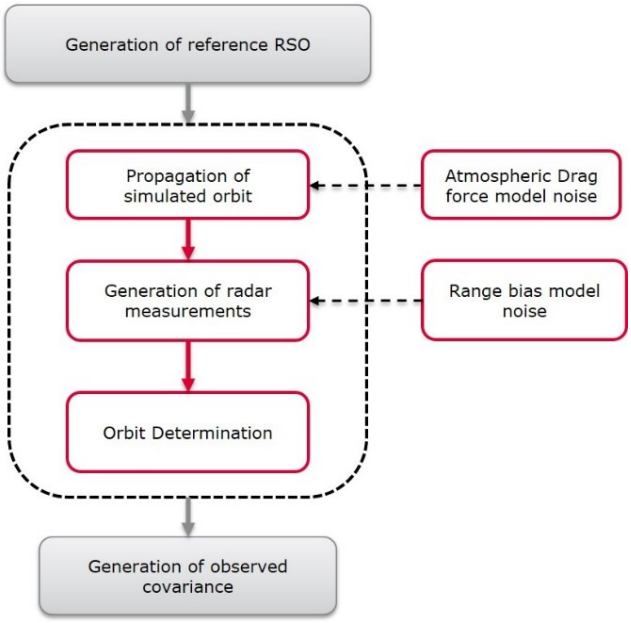

Figure 9 Validation chain workflow

Figure 9 represents the workflow defined to compute the population of samples and build the observed covariance matrix. All the validation cases use a MC based approach where each sample is unique and represents a different perturbation of the parameters being modelled (atmospheric force, solar radiation pressure or sensor calibration error). Note from Figure 9 that dynamic model perturbations and measurement model perturbations affect different processes within the validation chain, leading to different effects to the processed states (a detailed explanation is given in the following paragraphs). The steps required for the computation of a population of N samples are:

1. Generation of a reference RSO: The definition of the resident space object will be done entails the definition of the orbital and physical properties of the object summarized in an OPM format (see [CCSDS, Orbit data messages (blue book), 2009]). The OPM contains information about the state of the object (position and velocity), osculating Keplerian elements, the covariance matrix describing the uncertainty of the object as well as relevant physical parameters, like drag coefficient, cross-sectional area, solar radiation coefficient, etc. The reference RSO as well as its ephemeris will be named hereafter as reference state.

2. MC chain: The MC chain becomes the iterative part of the validation procedure that will deliver a unique MC point per trial. The steps required to produce a single solution comprise:

    a. Propagation of simulated orbit: The propagation of the reference RSO with a high-fidelity propagator leads to a series of ephemeris for a user defined time period, which will be named hereafter the simulated orbits. The atmospheric force model error is introduced in the computation of the simulated orbits leading to different orbit ephemeris which share one point in common: the initial state. If no dynamical model error is introduced, the simulated orbits will have no difference with respect to the original reference state. Because a perturbation of the dynamics is sought, the atmospheric drag model error has to be introduced in this step as later on these simulated orbits will be used to generate simulated radar measurements. Figure 11 provides a graphical representation of the population of simulated orbits produced.

b. Generation of radar measurements: The generation of radar measurements uses the previously computed simulated orbits to generate realistic simulated radar measurements to be processed by an OD algorithm afterwards. During the measurement computation, two sources of noise can be considered: typical measurement white noise of a radar station (defined as a Gaussian noise with zero mean and random seed) that perturbs each computed measurement in a unique way during an orbital arc, and sensor calibration biases, which produce a constant perturbation to the computation of measurements during the same orbital arc. Measurement white noise is introduced in the measurement computation scheme although it does not have any effect in the validation of the Covariance Determination algorithm other than proving that with real measurement conditions the methodology can work efficiently.

c. Orbit determination: Using the simulated measurements, ODs are performed, leading to a cloud of orbital states, named hereafter estimated states. A careful measurement weighting is done (by weighting the different measurements with the same dispersions as the ones introduced in the previous step) and using the same high-fidelity orbit propagator employed in the propagation of the simulated state (without considering the perturbations in the atmospheric force models). Due to the addition of 3 possible sources of error, that is measurement white noise, range bias perturbation and atmospheric drag force perturbation, the estimated orbits lead to a population of N unique samples. The cloud of solutions obtained is intended to sample the PDF characterizing the uncertainty of the OD process when unconsidered model errors are present. Figure 10 gives a graphical representation of the estimated orbits obtained, where faint blue dots represent different radar measurement and several orbits are fitted to them through an OD. Afterwards, estimated states are propagated using the same dynamical model implemented during the OD process, which results in a set of determined and predicted orbits, ready to be processed to derive the observed covariance.

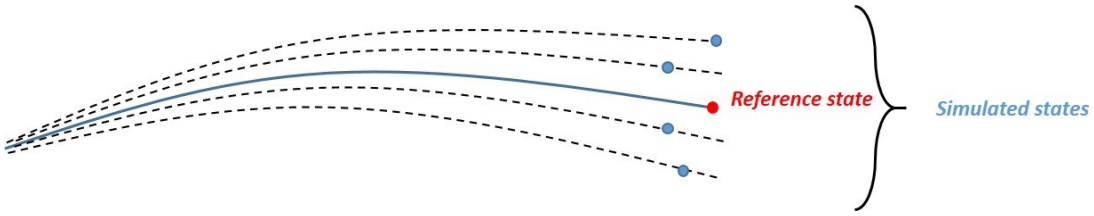

Figure 11 Graphical representation of the simulated orbits vs. the reference state, for a case with a perturbation on the atmospheric drag force. Dashed curves represent simulated states whereas the solid curve represents the reference state.

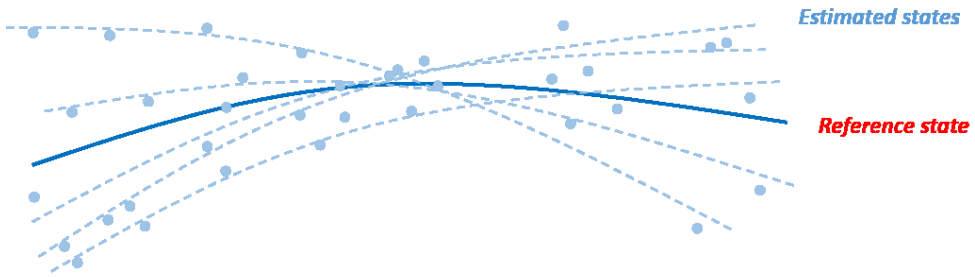

Figure 10 Estimated states obtained after the processing of the MC validation chain. Faint blue dots represents measurements while dashed curves represent the set of estimated state. In solid blue, the reference state.

A definition of the different perturbations considered in the generation of the MC points will be given next. From the previous validation chain, several perturbations, assumed as random variables following a normal distribution, affect the generation of the population of MC points. Each MC trial can be affected by:

- White noise in the measurement generation process: to simulate real working conditions and with the aim to compute realistic radar measurements, a certain random Gaussian noise is considered in the

generation of a single measurement (range, range-rate, azimuth and elevation) equivalent to the noise that a real radar sensor would experience when sensing a real orbiting body. This perturbation affects each measurement of an observation in a unique way, deviating the estimated orbit from the simulated one.

- Noise in the generation of a MC point: as the aim of the Covariance Determination algorithm is to recover the variance of a consider parameter (which affects an orbital arc in a systematic fashion, as detailed previously), a constant perturbation of a consider parameter is introduced during a whole orbital arc, leading to a unique MC point. By computing N samples affected by a set of normally distributed consider parameter perturbations, with a zero mean and certain standard deviation, a representative sampling of the uncertainty of an orbit determination process affected by unconsidered model uncertainties can be done.

The validation chain defines a clear and straightforward procedure to study the effect of the different perturbations in the orbital state estimation problem. Next section will deal with the processing of the cloud of estimated orbits to obtain the observed covariance matrix.

2.7.2 Generation of simulated observed covariance

The generation of the simulated observed covariance entails the computation of a covariance matrix statistically representative of the uncertainty of the orbit estimation and prediction problem. The previous section has dealt with the generation of a cloud of MC solutions, which will provide some insights in the effects of the different perturbations to the state estimation and propagation. However, the ultimate aim of the validation chain is to deliver an observed covariance matrix to serve as the input of the Covariance Determination algorithm.

The covariance of the estimated state vector is identical to the covariance of the orbital differences computed between N random state estimation trials if the position and velocity differences are assumed as identically distributed Gaussian random variables (i.e. unbiased and normally distributed), from [Zhang, Wu, & Cheng, 2012]. Thus, both at the estimation epoch and propagation of the state, the covariance matrix becomes of the orbital differences is assumed as a proper characterisation of the state estimation and propagation uncertainty.

For the validation of the Covariance Determination algorithm, Equation (2 .30) will be used in the derivation of a representative covariance matrix using the previously generated MC ephemeris. Ultimately, the observed covariance matrix will be obtained at different epochs providing an evolution of the covariance matrix from the estimation epoch to the prediction epochs. The observed covariance matrix will be transformed to the local TNW reference frame for posterior ingestion in the Covariance Determination algorithm. The observed covariance obtained through this process will be called hereafter simulated observed covariance.

A final remark is to be made considering the validation chain presented previously. The validation chain as presented produces a cloud of MC points and ephemeris for a specific time period, where the generation of radar measurements takes place at the same epochs (hence the generation of the estimated states) and where the propagation and generation of the predicted orbits spans over the same time period. Each MC point ephemeris is used to derive orbital differences for the same epochs, reason for which Equation (2 .30) holds. A graphical representation of the generation of the orbital differences can be found in the following figure:

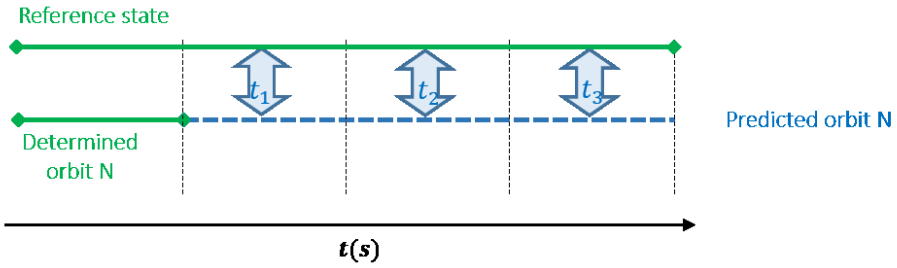

Figure 12 Graphical representation of the time scheme followed to compute the orbital differences, where all the N determined and predicted orbits span over the same period of time

As explained during section 2.4, there are two different strategies to compute an observed covariance matrix. For the validation of the consider parameters when using observed covariance derived from operational–like orbits (using the observed covariance methodology) a different simulation strategy is required . The validation chain introduced in the previous section still holds whereas the simulated epochs where the OD processes take place vary. A graphical representation of the generation of orbital differences can be found in Figure 13.

From Figure 13, there is no doubt that the period of time in which the ODs take place varies, creating a cloud of solutions representative of a real operational case, where non-correlated orbit determinations would be processed to derive an observed covariance. This simulated covariance method will be named hereafter operational simulated observed covariance.

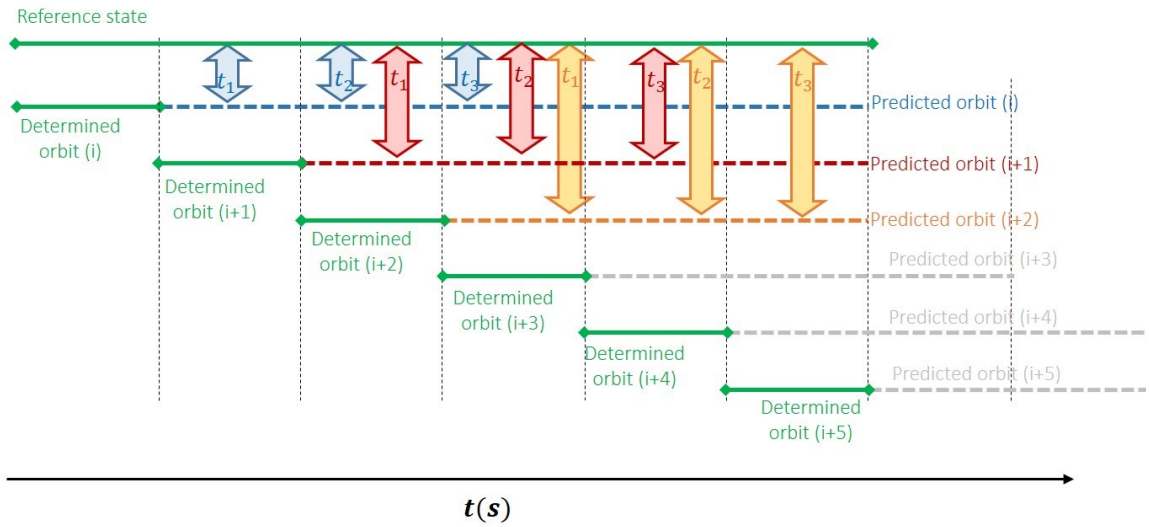

Figure 13 Graphical representation of the time scheme followed to compute the orbital differences, where all the N determined orbits are computed without overlaps, leading to different predicted orbits.

This chapter has provided the foundations upon which the novel methodology of the Covariance Determination algorithm is built, giving extensive insight into the relevant sources of uncertainty to implement and the theoretical background of the consider parameters. In addition, a thorough mathematical derivation of the Covariance Determination algorithm is provided, highlighting the most relevant assumptions considered during the definition of the methodology. The method to generate an observed covariance, either for validation or operational purposes, has been presented together with the different modelled consider parameters. Finally, extensive insight is provided into the definition of the validation chain to be processed in the validation and verification of the software. Next chapter will present the validation and verification results, product of the validation chain described in the present chapter as well as the results obtained from the application of the Covariance Determination algorithm to a real operational case, a tracking campaign of the Sentinel 3A satellite.

3

RESULTS

This chapter presents the results of the validation and real operational cases processed with the Covariance Determination algorithm. The first part of this chapter introduces the validation of the Covariance Determination algorithm applied to two different uncertainty sources, the first one being a source in the dynamic models and the second one being in the measurement models. A validation is done using both observed covariance generation approaches documented in section 2.4.

After due documentation of the verification and validation processes carried out, a real operational tracking campaign is presented using real radar measurements made publicly available by Leolabs for the Sentinel 3A satellite. The results of applying the Covariance Determination algorithm to the tracking campaign of the Sentinel 3A satellite are analysed in a similar fashion as the validation cases presented before.

3.1 Validation of the Covariance Determination algorithm

The present section intends to proof with strong evidence not only the fact that the implementation of the Covariance Determination algorithm is a success but that it contributes towards the covariance realism improvement in batch least-squares OD and propagation processes.

First, a detailed description of the boundary conditions defined for the validation and verification test cases is provided, where special emphasis is given to the definition of a realistic simulation scenario. Second, a thorough extensive analysis is performed on the output of the different test cases tried, where remarkable insight is derived from the computation of each case. Third, a validation of the Covariance Determination algorithm, the modelling and implementation of different consider parameters is given, demonstrating the powerful capabilities of the novel methodology.

Four different cases are presented were different features of the Covariance Determination algorithm are tested. In the following table, the different test cases are listed:

Table 3 Test cases used in the verification and validation of the Covariance Determination algorithm

Test case	Consider parameter	Observed covariance
Case A	Measurement noise only	Simulated observed covariance
Case B	AE (Atmospheric Drag Model Error)	Simulated observed covariance
Case C	RBE (Range Bias Model Error)	Simulated observed covariance
Case D	AE (Atmospheric Drag Model Error)	Operational simulated observed covariance (observed covariance method)

3.1.1 Simulation scenario

The simulation scenario has been conceived as a realistic representation of a tracking campaign of an object similar to the Sentinel 3A satellite, as this represents the real operational case that will be dealt with after the verification and validation of the algorithm.

To define the simulation scenario, some boundary conditions have to be fixed in order to ensure the repeatability of the simulated results: reference orbital state and physical characteristics of the reference RSO, dynamic model employed in the computation of the solutions and measurement model employed.

3.1.1.1 Reference RSO

The orbit and physical properties of the reference RSO are listed in Table 4. The orbit has been taken from a public TLE of Sentinel -3A satellite (41335) from [JSpOC, 2019]:

Table 4 Simulated RSO orbit and physical properties

Reference RSO	
Semi-major axis	7186.877 km
Eccentricity	0.001113
Inclination	98.72 deg
RAAN	77.03 deg
Mass	100 kg
Area	10 m^2

The physical properties have been assumed by considering a typical space debris object located in a LEO region, using the work developed by [Sáez-Bo, Pastor-Rodríguez, & Ayuga-García, 2018].

3.1.1.2 Dynamic model

The dynamic model employed in the simulation of the different test cases is listed in the following table:

Table 5 Dynamic model employed for the validation and verification

Full dynamical model	
Gravity field (Static)	EIGEN.GRGS.RL03.v2 16x16
Third body perturbations	Sun & Moon
Polar motion and UT1	IERS C04 08
Pole Model	IERS 2010 conventions
Precession/ Nutation	IERS 2010 conventions
Atmospheric Model	NLRMSISe-90;
Solar Radiation Pressure	Constant area (S2
Geodetic surface	ERS-1
Reference frame	J2000 ECI

A simpler dynamic model than the one presented in Table 2 is used in the validation of the code. Note that by implementing the same model in the definition of the reference state ephemeris, the simulated orbits and the estimated orbits, its orbital differences will only depend on the different perturbations introduced.

3.1.1.3 Measurement model

The measurement model employed for the generation of the radar measurements can be found in [ESA, Mathematical Models and Algorithms, 2009]. The radar used in the validation methodology has the following geodetic coordinates:

Table 6 Geodetic coordinates of simulated radar station

Geodetic coordinates of SST radar	
Longitude (deg)	-5.5911
Latitude (deg)	37.16643
Height (km)	0.1423

The simulated radar station is located in the northern hemisphere and is defined to have a broad FOV and sufficient power to ensure observability of the defined reference RSO:

Table 7 SST radar simulated properties

SST radar physical properties	
Radar FOV	Pyramidal Asymmetric
Radar Pointing direction (azimuth)	180 deg
Radar Pointing direction (elevation)	75 deg
Radar Aperture Semi-Angle (+X)	43.20 deg
Radar Aperture Semi-Angle (-X)	43.20 deg
Radar Aperture Semi-Angle (+Y)	30 deg
Radar Aperture Semi-Angle (-Y)	30 deg
Reference RCS	0.01 m^2

Finally, typical SST radar noise is assumed during the generation of measurement. The typical zero-mean Gaussian noises assumed are listed in the following table:

Table 8 Typical SST radar noises assumed for the generation of measurement in the validation cases.

Measurement	Sigma
Two-way range	10 m
Azimuth and elevation	300 mdeg
Two-way range-rate	1000 mm/s

The simulation environment has been carefully exposed by detailing all the design choices assumed during the definition of the realistic scenario. Next section will go through the relevant outputs produced during the validation and verification cases described in Table 3.

3.1.2 Validation and Verification test cases

The verification and validation cases defined in the present section study the effect of the different consider parameters in the state estimation and prediction problem, both in the definition of the orbital state and the definition of its associated uncertainty, yielding an observed covariance to be ingested by the Covariance Determination algorithm. The result of the different test cases is the validation and verification of the implementation of the methodology as well as the consider parameters modelled.

Regarding the generation of the observed covariance, different methodologies apply for the different test cases. Thus, for the different test cases the following dates are used in the simulation of measurements and in the propagation of the predicted orbits:

Table 9 Summary of the features for each of the different cases devised

Test case	Observed covariance	Reference orbit	Estimation epoch for OD	Predicted orbit
Case A	Simulated observed covariance	01-01-2019 to 08-01-2019	01-08-2019	08-01-2019 to 16-01-2019
Case B	Simulated observed covariance	01-01-2019 to 08-01-2019	01-08-2019	08-01-2019 to 16-01-2019
Case C	Simulated observed covariance	01-01-2019 to 08-01-2019	01-08-2019	08-01-2019 to 16-01-2019
Case D	Operational simulated observed covariance	01-01-2018 to 01-07-2018	*	*

Case D stands out as the odd test case since to simulate different operational realistic orbits, the process carried out to perform the generation of the MC solutions was different (described in section 2.7.2) yielding to a more complex orbital processing. Analogous to a real tracking campaign, simulated measurements were generated considering batches of 5 days yielding to an OD (i.e. estimated orbit) within the considered period. The estimated state is then propagated 8 days ahead using a high-fidelity propagator. The generation of determined and predicted solution takes the following scheme: a first batch would span from the 01-01-2018 to 06-01-2018 and the propagation period would take place from 06-01-2018 to 14-01-2018; the next batch of measurements would take place from 02-01-2018 to 07-01-2018, with a propagation from 07-01-2018 to 15-01-2018.

For case A, B and C a sample of 10,000 MC solutions have been processed, using the MC chain introduced in section 2.7. The choosen number of samples has been found to describe with sufficient accuracy the state uncertainty of the OD process (from [Flegel & Bennett, 2018]). The different analysis included ensure the quality of the solutions obtained through the OD process as well as the degree to which the uncertainty of the orbit can be characterized by the different covariance matrices. Each test case is evaluated using the covariance realism metrics presented in section 2.6, giving a consistent and common approach for each test. The author deemed irrelevant to include normality test results for the first 3 test cases, as the sufficient population sample and the generation of normally distributed perturbations ensure the normality of the final distributions. However, the last test case does not hold on the same assumptions, reason for which testing for normality becomes an important part of the validation process.

3.1.2.1 Case A

The first test case devised aims at addressing the covariance consistency of the validation methodology. It is key to the verification and validation of the Covariance Determination algorithm to ensure the quality of the observed covariance and to validate the hypothesis posed during Section 2.4 on the similarity between state uncertainty and observed covariance. The present case formulation can be summarized in the following table:

Table 10 Features of Case A

Test case A	
Consider parameter	Measurement noise only
Observed covariance	Simulated observed covariance
Number of simulated points	10000
Reference orbit	01-01-2019 to 08-01-2019
Estimation epoch for OD	01-08-2019
Predicted orbit	08-01-2019 to 16-01-2019

The present case does not consider the addition of any perturbation to the orbit determination process through the consider parameters yet typical measurement noise in the measurement computation step is considered as described in section 2.7.1. For the complete sample of MC points, an observed covariance is derived at different epochs describing the uncertainty on the state estimation problem at different epochs.

Before proceeding, a validation on the consistency of the different ODs is carried out. As mentioned, the generation of measurements is only affected by the addition of a random Gaussian noise, however it is expected to be well captured since the input noise is defined beforehand. The following histogram depicts the weighted RMS of the residuals of the resulting OD:

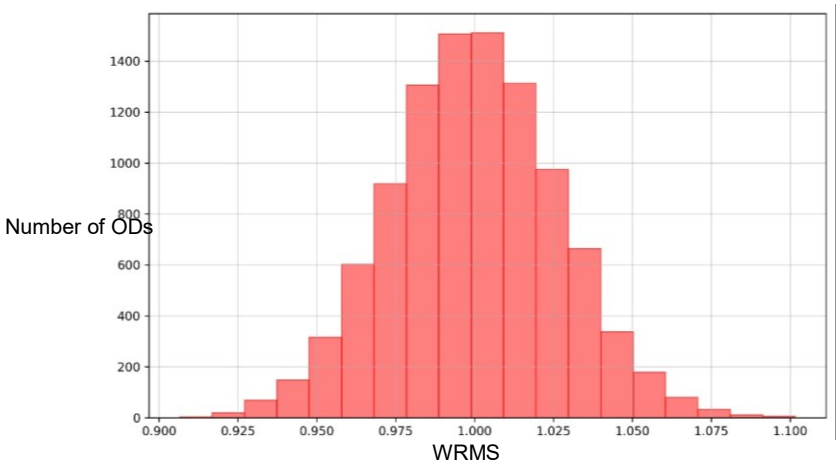

Figure 14 WRMS of the OD processes for test Case A

From the previous figure, the processed ODs have been properly weighted and the measurement model generation yields a Gaussian distribution of the residuals (due to the addition of white noise during measurement generation). The quality of the ODs has been verified by checking the rejection rates of the processed measurements (around 0%) and the availability of enough tracks for the correct estimation of the parameters (minimum two per day). The simulated observed covariance, computed using the resulting cloud of MC points, is compared component by component to the 10000 noise-only covariance matrices. The following figure represents the histograms of the relative differences between the observed covariance and the N estimated covariance matrices:

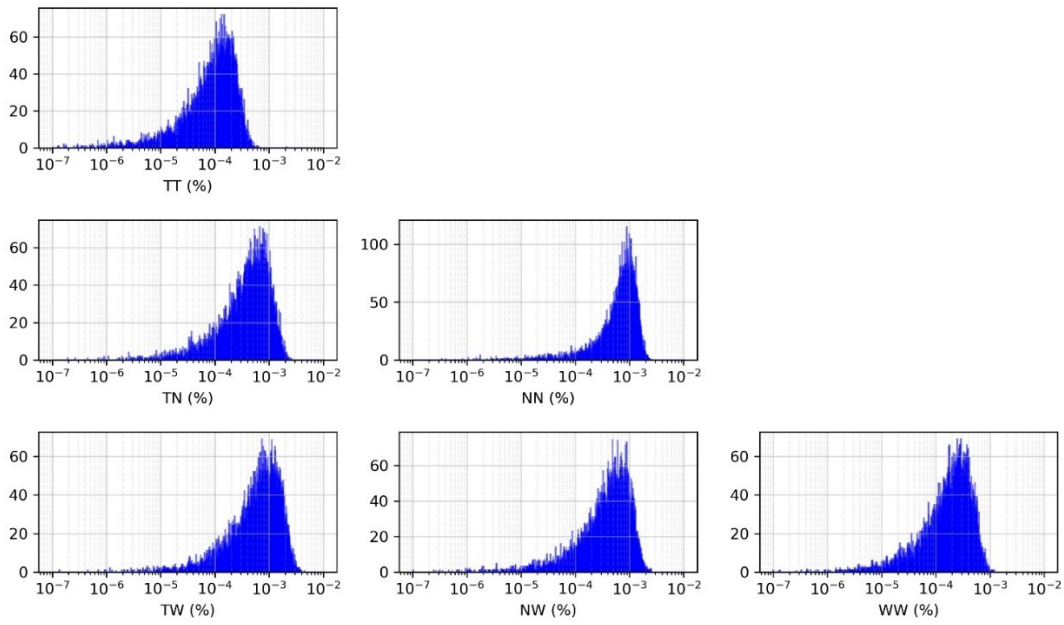

Figure 15 . Histogram of the relative differences between noise-only covariance matrices. TNW position elements are compared against an average value for the complete set of noise-only covariance matrices for test Case A

Note that the relative differences of the observed covariance versus the N estimated covariance matrices are below 0.01% for all the position elements. A final validation is provided to evaluate the containment of the noise-only covariance matrices through time, as the state is propagated from the estimation epoch. The analysis developed in [Folcik, Lue, & Vatsky, 2011] is reproduced computing the Mahalanobis distance of the MC points with respect to its mean state and its average noise-only covariance matrix. The results are listed in the following table:

Table 11 Covariance containment test for Case A for the noise-only covariance (left) and the consider covariance (right). Colour scale is applied to each column to compare the theoretical value against the measured, where a similar colour denotes proximity of both values. t_0 stands for estimation epoch and subsequent prediction times are expressed relative to it.

Time	Noise-only covariance				Consider covariance			
	1-σ	2-σ	3-σ	4-σ	1-σ	2-σ	3-σ	4-σ
t_0	19.72%	73.68%	97.26%	99.87%	19.64%	73.97%	97.05%	99.88%
t_0 + 1 day	20.20%	74.04%	97.23%	99.89%	19.84%	73.64%	97.28%	99.91%
t_0 + 2 days	19.62%	74.06%	97.07%	99.86%	19.88%	74.00%	97.11%	99.91%
t_0 + 3 day	19.91%	73.79%	97.08%	99.87%	19.71%	73.87%	97.16%	99.91%
t_0 + 4 days	19.42%	73.87%	97.13%	99.87%	19.37%	74.44%	97.20%	99.89%
t_0 + 5 days	19.79%	73.94%	97.24%	99.86%	19.49%	73.86%	97.18%	99.89%
t_0 + 6 days	19.35%	74.05%	97.05%	99.87%	19.51%	74.11%	97.28%	99.89%
Theoretical	19.90%	73.90%	97.10%	99.87%	19.90%	73.90%	97.10%	99.87%

Special detail will be given in the interpretation of the previous results. From [Folcik, Lue, & Vatsky, 2011], position covariance defines the ellipsoidal volume that represents the position uncertainty region, centred at the estimated state, provided that uncertainties are Gaussian and orbital differences small. A computation of the Mahalanobis distance between a MC point and its average state (i.e. the expectancy of the distribution) can be understood as determining whether the MC point will lie inside or outside a $k\sigma$ ellipsoid. In the previous table, for a 3-dof (degrees-of-freedom) multivariate normal distribution the theoretical statistics are shown in the last row.

For an increasing $k\sigma$ region of confidence, the percentage of points of the whole distribution lying inside the different ellipsoidal volumes is defined. The Mahalanobis distance of each of the MC points has been computed using Equation (2 .41), where orbital differences are expressed in a local TNW frame, taking the average state as the reference state to express the local frame, and the average noise—only covariance as the covariance matrix of the distribution. A colour scale has been defined to ease the understanding of the metrics provided, where the closer the colour of the cell to the theoretical value the closer is the containment statistic to the theoretical one.

Inspecting Table 11 strong similarities are found in the results presented for both containment tests. This eventually yields to the conclusion that both covariance matrices are representative of the uncertainty of the orbital state estimation.

3.1.2.2 Case B

The second test case devised addresses the impact of the atmospheric drag force model consider parameter, once the generation of the observed covariance is validated through Case A.

Case B is key to understand the role of dynamic model errors when performing ODs and subsequent orbit propagations, more concretely the effect of errors in the modelling of the atmospheric drag force. As seen in section 2.1.3.1, this non-conservative orbital perturbation represents the major contribution to covariance unrealism in the LEO orbital regime. An extensive analysis is made on the impact of un-modelled uncertainties in the definition of a realistic covariance as well as the degradation of the consistency and containment of the noise-only covariance with time.

In the following table, the relevant features of Test Case B are listed:

Table 12 Features of Case B

Test case B	
Consider parameter	AE (Atmospheric Drag Model Error)
Observed covariance	Simulated observed covariance
Number of simulated points	10000
Reference orbit	01-01-2019 to 08-01-2019
Estimation epoch for OD	01-08-2019
Predicted orbit	08-01-2019 to 16-01-2019

The present case introduces a certain perturbation in the atmospheric drag force model by means of a non-null consider parameter. Recalling the equation for the drag force model (Equation (2 .31)) a gaussian atmospheric drag force model perturbation is introduced, following:

$$c_{AE} \sim N(0, \sigma_{AE} = 5\%) \tag{3 .1}$$

Recalling section 2.7, the consider parameter value is constant during an orbital arc but varies from MC trial to MC trial, leading to a cloud of solutions sampling the PDF of the state estimation. In terms of covariance consistency, the weighted RMS and the differences among the estimated (MC) covariance matrices have been analysed, obtaining similar results as those presented for Case A.

Figure 16 represents a histogram of the WRMS of the different ODs. The quality of the ODs has been verified by checking the rejection rates of the processed measurements (around 0%), the availability of enough tracks for the correct estimation of the parameters (minimum two per day).

Figure 17 displays the histograms of the relative differences between the average noise-only covariance and the N estimated covariance matrices. One may expect to obtain worse solutions for the processed ODs, as a perturbations to the atmospheric drag force model are introduced. However both WRMS and relative differences of the noise-only covariance matrices are similar to Case A. Thus, consistency among the computed ODs seems to be demonstrated although a real covariance consistency and containment is not achieved (as results will show later).

Figure 18 shows the correlation of the error in the estimated $\mathrm{C_D}$ with the atmospheric model perturbation introduced. The population of estimated $\mathrm{C_D}$ describes almost a 1:1 correlation with the perturbation of the model introduced, where the drag coefficient error is computed having as a reference the $\mathrm{C_D} = 0.4$ defined in section 3.1.1.1. A certain noise is appreciated due to the measurement model noise present in the generation of each MC sample.

The propagation of both the estimated state and the covariance matrix yield to divergences between the reference orbit and the N MC samples. In Figure 19, Figure 20 and Figure 21, the effect of perturbations in the atmospheric drag force model is analysed by plotting the orbital differences of the MC points and its propagated states with respect to the reference orbit (expressed in the local TNW frame).

Note that in Figure 20 and Figure 21 the label has been eliminated to allow readability of the plot. Inspecting the previous figures, there is no doubt that the contribution of the atmospheric drag force perturbation yields a drift of the object's position in the along-track direction. No observable drift is found in the other two directions, as orbital differences are almost constant through the propagation period (small differences are observed with respect to the reference state as well as a dispersion of the points for equal model perturbation due to the measurement noise introduced).

From inspection of Figure 19, Figure 20 and Figure 21, there is a clear correlation between perturbations in the atmospheric model and orbital differences in the along-track direction. Not only that but, with propagation, the effect of a perturbation in the atmospheric model increases. Inspecting Figure 22, the RMS of the along-track direction increases quadratically with propagation time as denoted by the perfect fit achieved with a parabola function (where the r-squared parameter denotes the error between the fit and the data, being 1 a perfect fit).

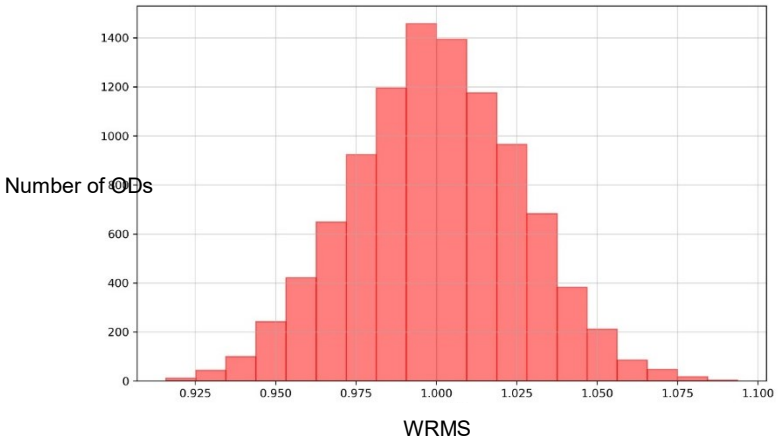

Figure 16 WRMS of the ODs for test Case B

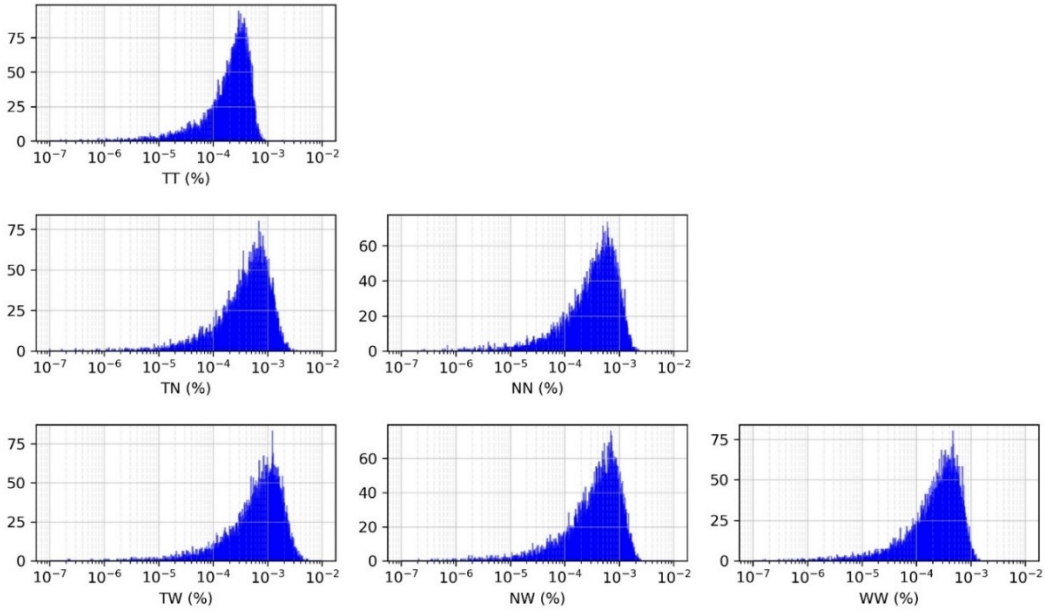

Figure 17 Histogram of the relative differences between noise-only covariance matrices. TNW position elements are compared against an average value for the complete set of noise-only covariance matrices for test Case B

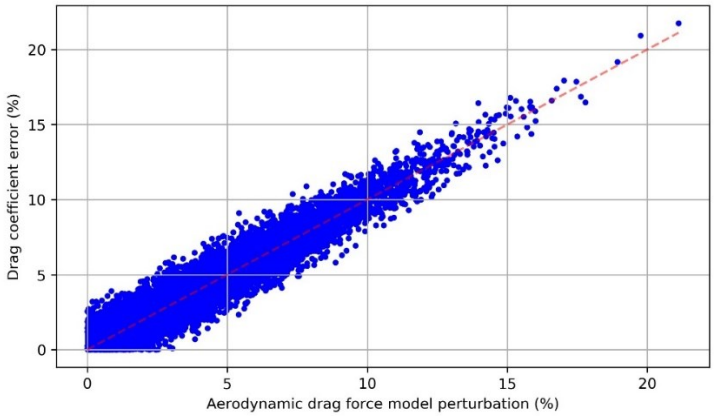

Figure 18 Drag coefficient error vs. atmospheric drag force model perturbation. In red a trend-line is plotted denoting a 1:1 correlation between the plotted variables.

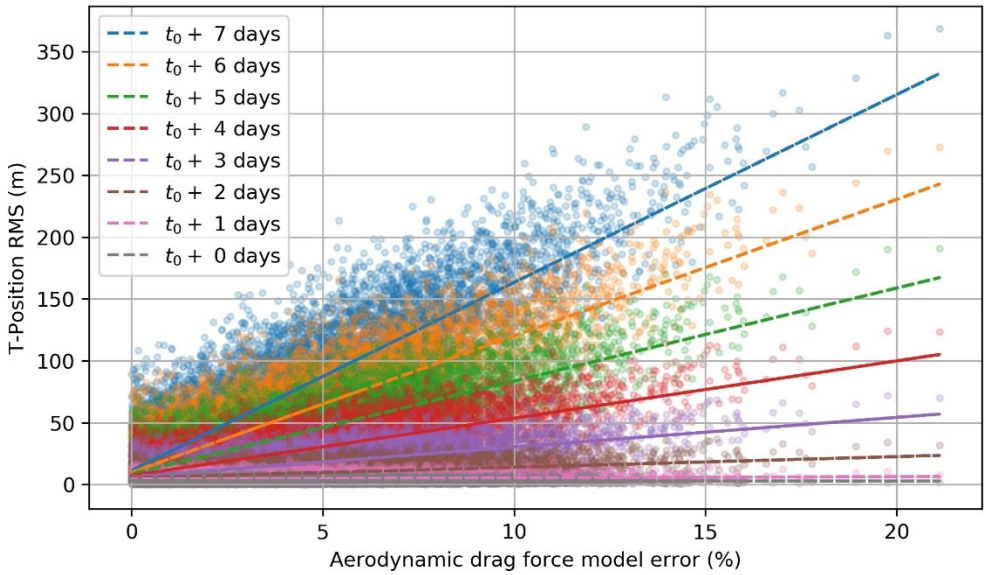

Figure 19 Atmospheric drag force model error vs. T-position RMS error for different propagation epochs

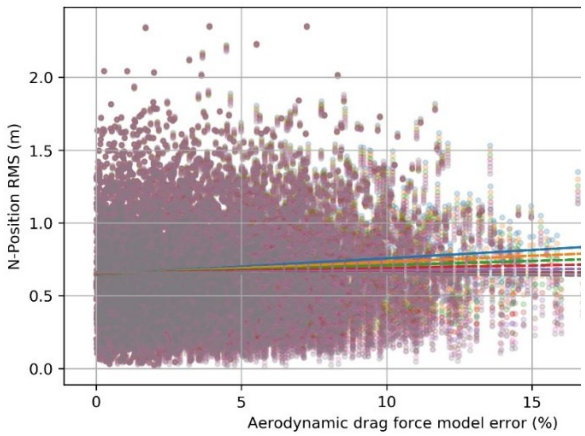

Figure 20 Atmospheric drag force model error vs. N-position RMS error for different propagation epochs. . Legend is removed for readability (same legend as Figure 19 applies)

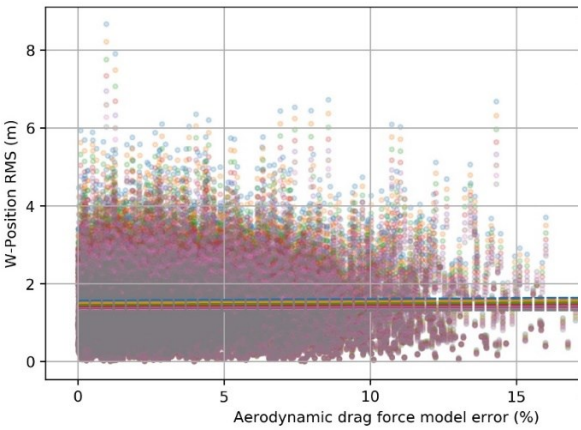

Figure 21 Atmospheric drag force model error vs. W-position RMS error for different propagation epochs. . Legend is removed for readability (same legend as Figure 19 applies)

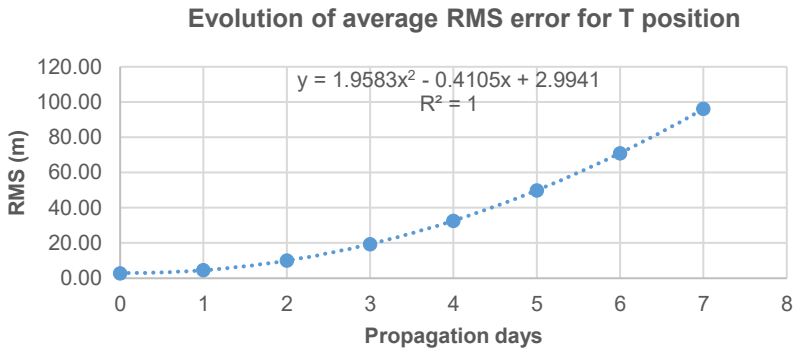

Figure 22 Evolution of along-track (T) average position RMS error with propagation time. A quadratic trend-line is adjusted to the data points providing a perfect fit.

The following table displays the results for the containment analysis on the noise-only and consider covariance at different propagation times:

Table 13 Covariance containment test for Case B for the noise-only covariance (left) and the consider covariance (right). Colour scale is applied to each column to compare the theoretical value against the measured, where a similar colour denotes proximity of both values. t_0 stands for estimation epoch and subsequent prediction times are expressed relative to it.

Time	Noise-only covariance				Consider covariance			
	1-σ	2-σ	3-σ	4-σ	1-σ	2-σ	3-σ	4-σ
t_0	19.61%	74.03%	97.06%	99.89%	19.64%	73.97%	97.05%	99.88%
t_0 + 1 day	18.56%	70.66%	96.48%	99.83%	19.84%	73.64%	97.28%	99.91%
t_0 + 2 days	12.54%	55.92%	86.31%	97.17%	19.88%	74.00%	97.11%	99.91%
t_0 + 3 day	9.28%	42.58%	72.89%	88.93%	19.71%	73.87%	97.16%	99.91%
t_0 + 4 days	7.20%	34.77%	62.24%	79.96%	19.37%	74.44%	97.20%	99.89%
t_0 + 5 days	5.47%	26.70%	49.64%	66.14%	19.49%	73.86%	97.18%	99.89%
t_0 + 6 days	4.66%	21.98%	42.08%	57.49%	19.51%	74.11%	97.28%	99.89%
Theoretical	19.90%	73.90%	97.10%	99.87%	19.90%	73.90%	97.10%	99.87%

In the previous analysis, the average noise-only covariance matrix is used to run the covariance containment tests and to compute the Mahalanobis distance of the distribution of points. Inspecting the previous table (left), a degradation of covariance containment for the noise-only covariance is observed, as the metrics obtained at different propagation epochs worsen with the propagation time.

Using the distribution of orbital states, an observed covariance matrix is processed. Because noise-only covariance matrices display little differences between them, an averaged noise-only covariance matrix is computed and used in the fitting process of the Covariance Determination algorithm. The results of the fitting are listed in the following table:

Table 14 Results of Case B applying the Covariance Determination algorithm

Test case B	
Atmospheric model error	$24.27\ \%^2$
Variance of estimated parameter	$5.427E-03\ (\%^4)$
LSQ solver	Gauss-Newton
Number of iterations	3
CPU time	0.0207 min

The solution provided by the Covariance Determination algorithm has estimated a variance of the atmospheric drag force model error of $24.27445\ \%^2$, i.e. a standard deviation of 4.93%, almost the 5% of the input noise model. The sigma of the estimated parameter as well as the residuals are found to be several orders of magnitude smaller than the computed value. Furthermore, a containment test is provided in Table 13 (right). It is clear that the consider covariance computed with the estimated consider parameter variance complies with the theoretical metrics of the covariance containment test. For this test, the consider covariance was employed and a Mahalanobis distance was computed for each of the MC ephemeris yielding the previous results.

To provide a conceptual approach to the covariance realism improvement provided by the Covariance Determination algorithm, Figure 23 displays the evolution of the T, N and W position sigma of the noise-only, observed and consider covariance matrices along time. The first insight is that the noise-only covariance diverges from the observed covariance, being the most notorious the degradation of the covariance realism in the along-track direction, while the other principal direction, N and W, seem to correctly represent the uncertainty of the orbital state in their respective directions.

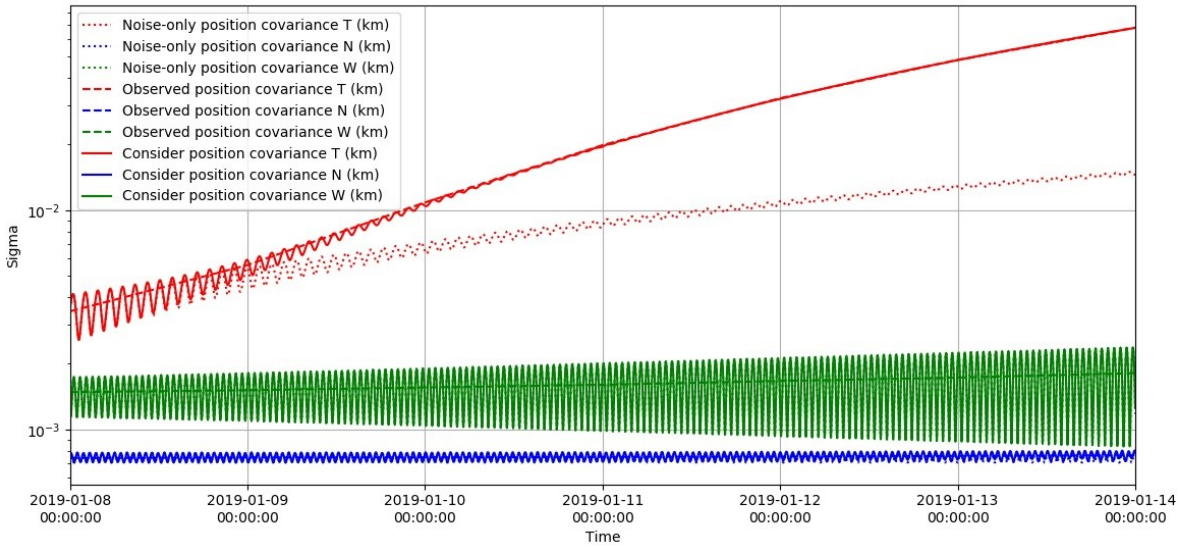

Figure 23 Evolution of the T, N and W position sigma of the noise-only, observed and consider covariance for test Case B

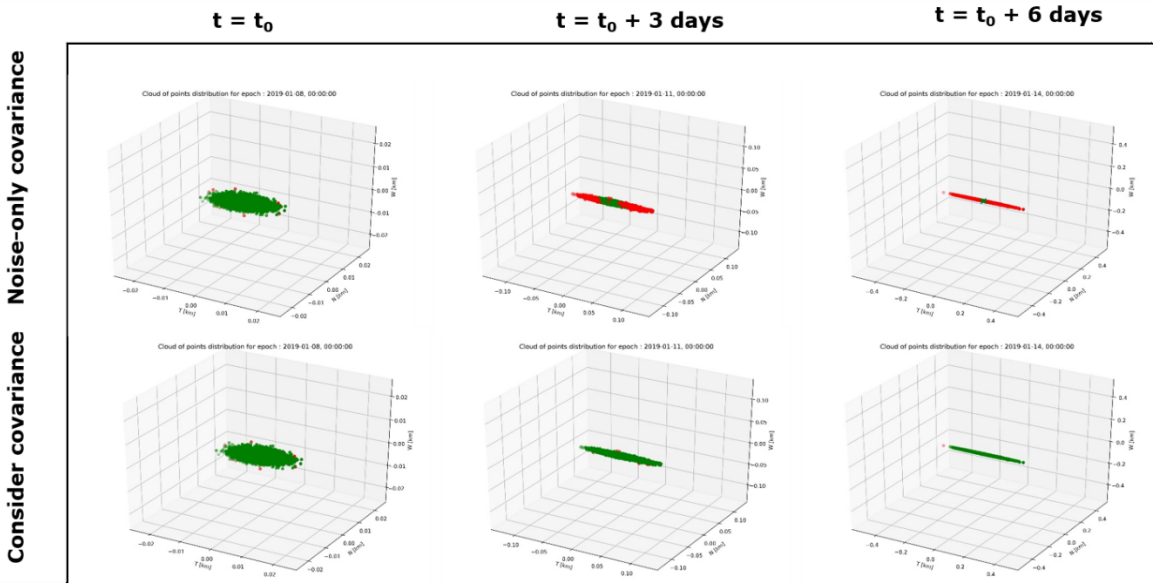

Figure 24 Position covariance containment considering a 4-σ ellipsoid for Case B. In green, the MC points whose computed Mahalanobis distance does not exceed the 4σ ellipsoid and in red the points whose distance exceeds the ellipsoid.

In Figure 24, a representation of the covariance containment analysis is provided for the noise-only and consider covariance. Note that each covariance matrix (consider and noise-only) leads to a different Mahalanobis distance for each MC point, so a graphic representation of the covariance realism degradation is appreciated in the previous figure. In addition, the main direction of uncertainty (the principal axis of the ellipsoid) coincides with the along-track direction, due to the effect of the uncertainty in the atmospheric drag model during the propagation.

Finally, the correction of the atmospheric drag consider parameter to the noise-only covariance matrix is studied. Recall that, from Equation (2 .12), the consider parameter yields a correction to the noise-only covariance matrix by means of a space transformation from the consider space to the covariance space (i.e. $\boldsymbol{K^T C K}$). The contribution matrix computed assuming a unitary atmospheric model consider parameter is the following:

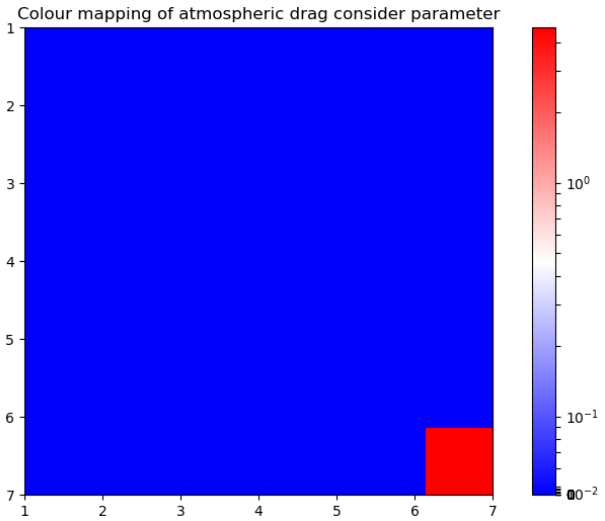

Figure 25 Colour map of the contribution of a unitary atmospheric drag consider parameter to the noise-only covariance matrix (in J2000 reference frame).

In the previous figure, the different components of the correction matrix are plotted, from 1 to 6 the different terms of the state vector (i.e. position and velocity) and in the (7,7) position the term for the variance of the drag coefficient. The atmospheric drag consider parameter contributes almost exclusively adding uncertainty in the covariance term of the drag coefficient.

3.1.2.3 Case C

The third test case devised addresses the impact of the range bias consider parameter, i.e. the effects of errors in the modelling of measurements to the covariance realism problem. The features of test Case C are listed in the following table:

Table 15 Features of Case C

Test case C	
Consider parameter	RB (Range Bias Model Error)
Observed covariance	Simulated observed covariance
Number of simulated points	10000
Reference orbit	01-01-2019 to 08-01-2019
Estimation epoch for OD	01-08-2019
Predicted orbit	08-01-2019 to 16-01-2019

The present case introduces a certain perturbation in the range bias modelling by means of a non-null consider parameter. Recalling the equation for the range measurement model (Equation (2 .35)) a gaussian range bias model perturbation is introduced, following:

$$c_{RB} \sim N(0, \sigma_{RB} = 20\ m) \tag{3 .2}$$

The same extensive analysis provided for test Case B is reproduced with the computed set of ODs and propagated states. A consistency check among the different noise-only covariance matrices is provided in Figure 26. The quality of the ODs has been verified by checking the rejection rates of the processed measurements (around 0%), the availability of enough tracks for the correct estimation of the parameters (minimum two per day).

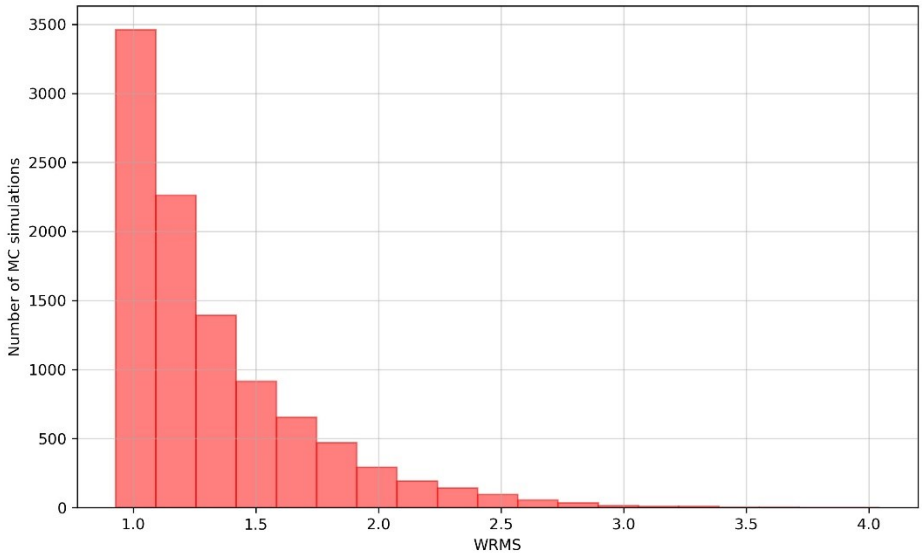

Figure 26 WRMS of the ODs for test Case C

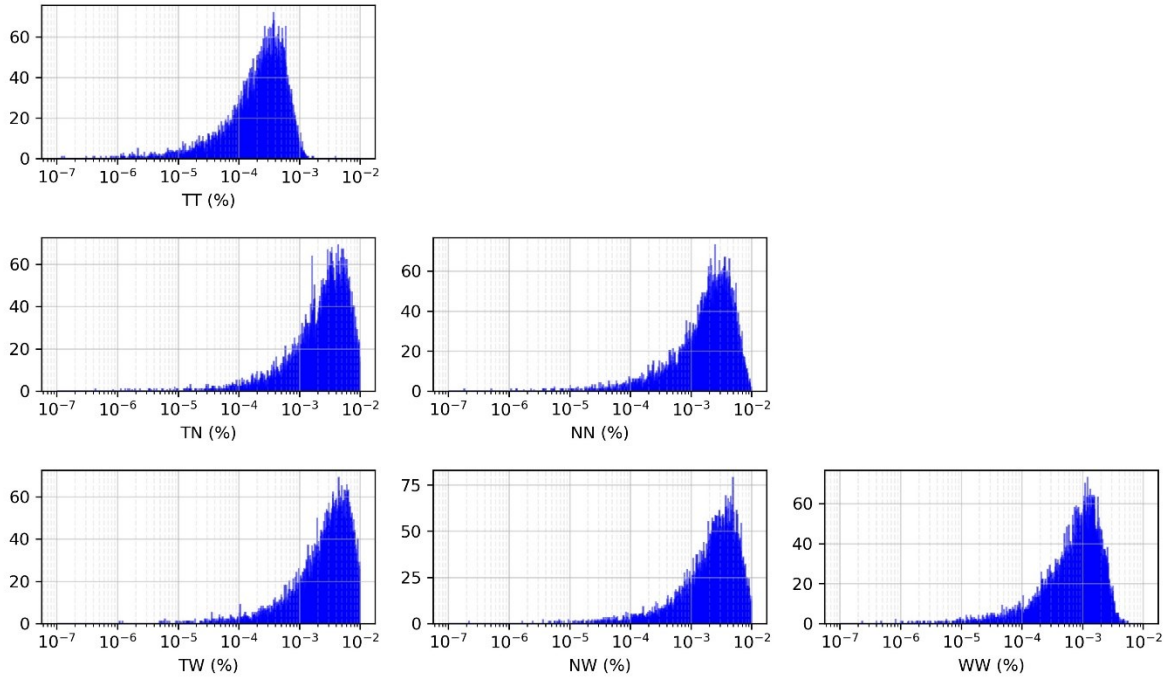

Figure 27 Histogram of the relative differences between noise-only covariance matrices. TNW position elements are compared against an average value for the complete set of noise-only covariance matrices for test Case C.

Figure 27 displays the histograms of the relative differences between the average noise-only covariance and the N estimated covariance matrices. A difference is appreciated with respect to the results obtained for test Case B. Through careful comparison of the solution obtained for both cases, in terms of noise-only covariance consistency, the estimated covariance matrices have greater differences between them (although relatively small compared to the actual values of the covariance matrix). Looking at Figure 26, the WRMS of the population of ODs does not follow a Gaussian distribution centred at a mean value 1, it is not symmetric and the ODs appear to be not properly weighted due to the addition of measurement biases, which increase the expected residuals of the OD.

Figure 28, Figure 29 and Figure 30 represent the evolution of the orbital differences as a consequence of the introduced perturbation for different propagation epochs. There is no doubt that a perturbation in the range bias yields increasing orbital differences with propagation time. This is observed mainly in the along-track direction, where the orbital differences grow with propagation time and range bias error. Contrary to that, orbital differences

in the N and W direction remain constant through propagation although they do depend on the introduced range bias perturbation.

To further study the effect of perturbations in the range bias to state estimation and prediction and its correlation with propagation time, the variation of the average RMS in the along-track directions at different propagation epochs is presented in Figure 31. Note that a quadratic polynomial is selected, despite the component of the range bias perturbation is almost negligible (a linear fitting would provide an almost perfect fit). The evolution of the orbital uncertainty due to errors in the modelling of the range bias produces a quasi-linear error growth compared to the clearly quadratic progression observed in Figure 22.

A covariance containment analysis is carried out to check the performance of the average noise-only covariance:

Table 16 Covariance containment test for Case C for the noise-only covariance (left) and the consider covariance (right). Colour scale is applied to each column to compare the theoretical value against the measured, where a similar colour denotes proximity of both values. t_0 stands for estimation epoch and subsequent prediction times are expressed relative to it.

Time	Noise-only covariance				Consider covariance			
	1-σ	2-σ	3-σ	4-σ	1-σ	2-σ	3-σ	4-σ
t_0	2.94%	14.12%	26.81%	37.24%	20.36%	73.84%	96.98%	99.92%
t_0 + 1 day	2.49%	12.33%	23.30%	33.19%	19.84%	73.61%	97.23%	99.90%
t_0 + 2 days	2.83%	15.41%	29.04%	40.89%	20.53%	73.88%	96.85%	99.91%
t_0 + 3 day	1.96%	10.17%	20.24%	29.37%	19.19%	74.02%	97.10%	99.88%
t_0 + 4 days	2.07%	11.14%	21.51%	30.29%	19.85%	74.14%	96.95%	99.89%
t_0 + 5 days	1.76%	8.78%	18.16%	26.53%	19.33%	74.20%	97.09%	99.90%
t_0 + 6 days	1.82%	10.34%	19.40%	27.75%	19.85%	74.07%	96.97%	99.92%
Theoretical	19.90%	73.90%	97.10%	99.87%	19.90%	73.90%	97.10%	99.87%

Inspecting the previous table, there is no doubt that the noise-only covariance (left) fails to properly characterize the real uncertainty of the state estimation and prediction problem. The observed covariance is ingested by the Covariance Determination algorithm together with the rest of the required inputs (derived from a previously computed OD). The results of the fitting are listed in the following table:

Table 17 Results of Case C applying the Covariance Determination algorithm

	Test case C
Range bias model error	$424.89\ m^2$
Variance of estimated parameter	$1.439\ E-02\ m^4$
LSQ solver	Gauss-Newton
Number of iterations	3
CPU time	0.0225 min

The solution provided by the Covariance Determination algorithm has estimated a variance of the range bias model error of $424.89\ m^2$, i.e. a standard deviation of 20.61 m, almost the 20 m of the input noise model. The sigma of the estimated parameter as well as the residuals are found to be several orders of magnitude smaller than the computed value. Furthermore, a containment test is provided in the following table:

Inspecting Table 16, it is clear that the consider covariance (right) computed with the estimated consider parameter variance complies with the theoretical metrics of the covariance containment test. For this test, the consider covariance was employed and a Mahalanobis distance was computed for each of the MC points yielding the previous results.

To provide a conceptual approach to the covariance realism improvement provided by the Covariance Determination algorithm, Figure 32 displays the evolution of the T, N and W position sigma of the noise-only, observed and consider covariance matrices along time.

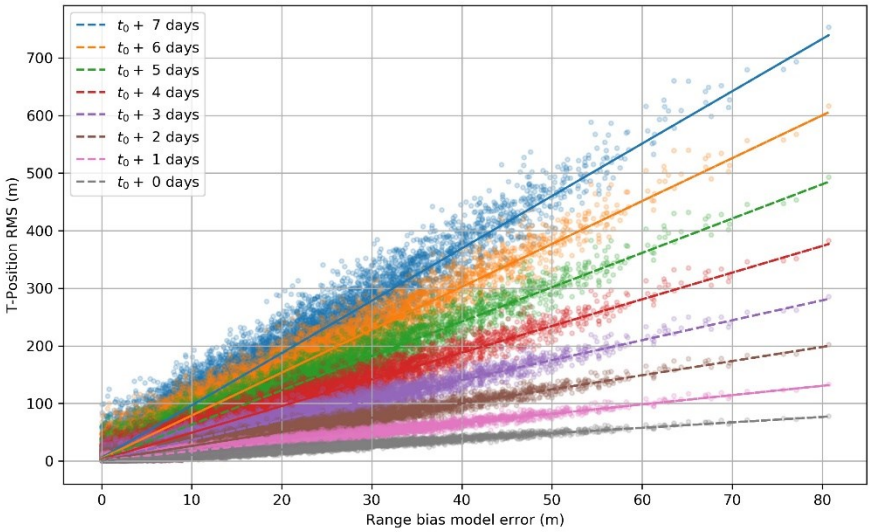

Figure 28 Range bias model error vs. T-position RMS error for different propagation epochs for Case C

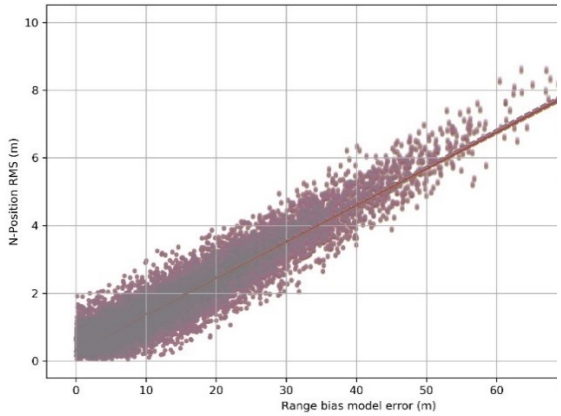

Figure 29 Range bias model error vs. N-position RMS error for different propagation epochs. Legend is removed for readability (same legend as Figure 28 applies)

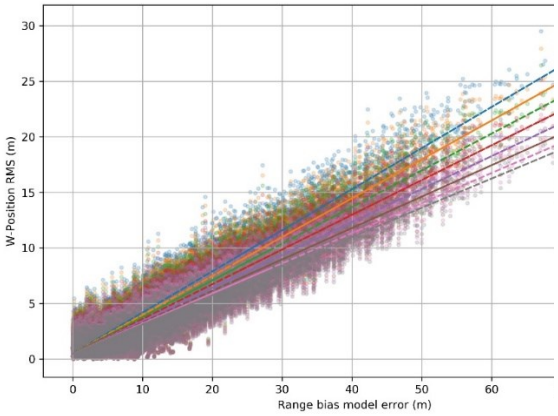

Figure 30 Range bias model error vs. W-position RMS error for different propagation epochs. Legend is removed for readability (same legend as Figure 28 applies)

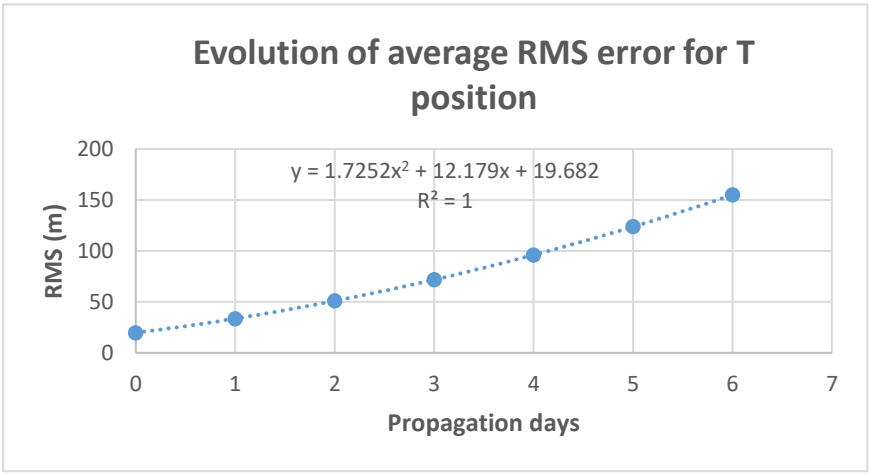

Figure 31 Evolution of along-track (T) average position RMS error with propagation time. A quadratic trend-line is adjusted to the data points providing a perfect fit.

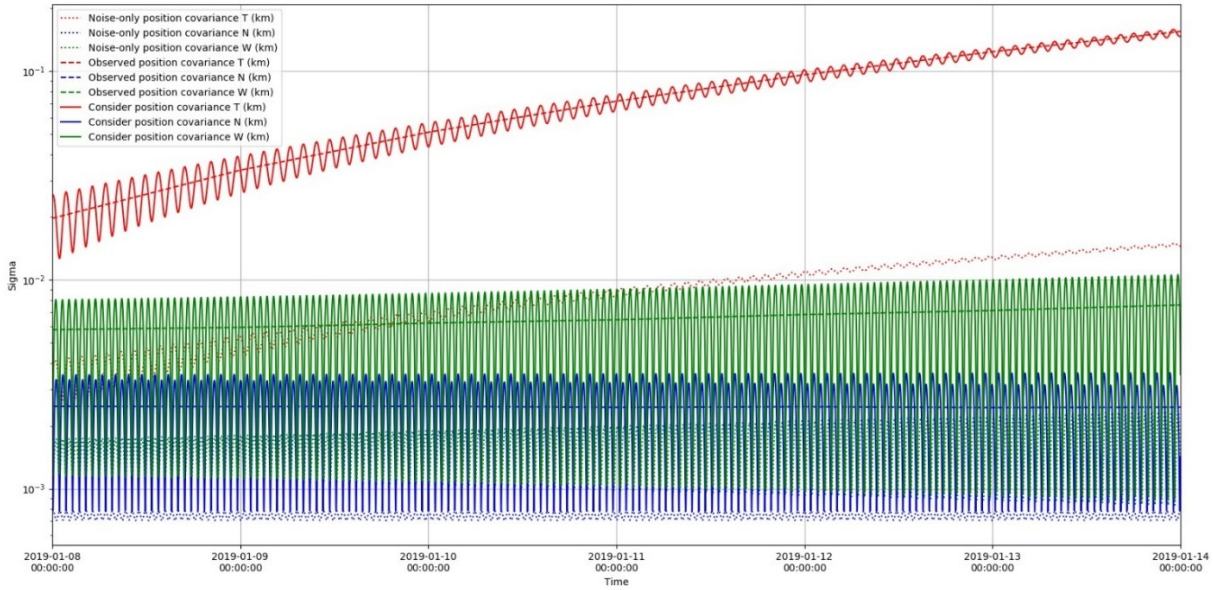

Figure 32 Evolution of the T, N and W position sigma of the noise-only (dotted), observed (dashed) and consider covariance (solid) for test Case C. Due to bad readability of the plot, the legend is summarized: In red, the evolution of the along-track uncertainty, in green the evolution of the normal uncertainty and in blue the evolution of the radial uncertainty.

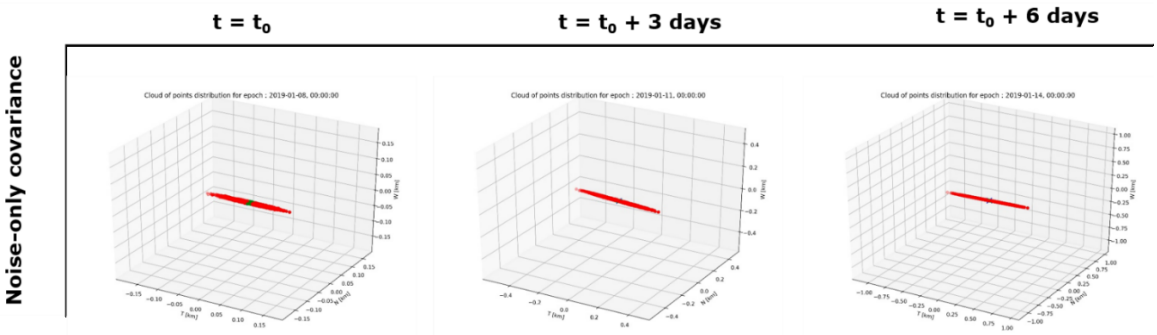

Figure 33 Position covariance containment considering a 4-σ ellipsoid for Case C. In green, the MC points whose computed Mahalanobis distance does not exceed the 4σ ellipsoid and in red the points whose distance exceeds that of the 4σ ellipsoid.

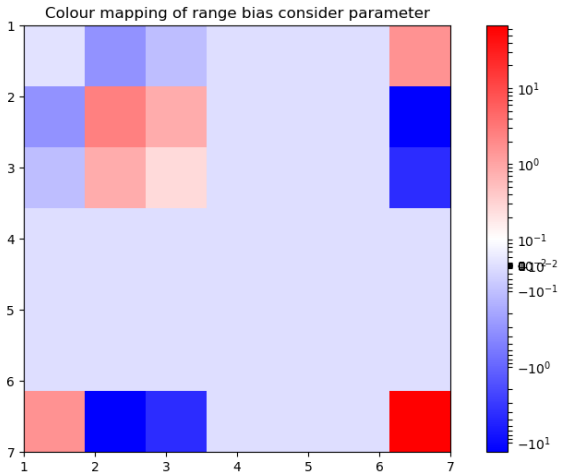

Figure 34 Colour mapping of the correction introduced by a unitary range-bias consider parameter to the noise-only covariance matrix (in J2000 reference frame).

Figure 32 shows the evolution of the T, N and W position sigma of the noise-only, observed and consider covariance matrices along time. Note that the noise-only covariance diverges from the observed covariance, being the most notorious the degeneration of the covariance realism in the along-track direction, while the other principal direction, N and W, also display non-negligible divergences.

A representative plot of the uncertainty realism degradation of the noise-only covariance is displayed in Figure 33. In the figure, a representation of the covariance containment analysis is provided for the noise-only. From the results listed in Table 16 and Figure 33, there is no doubt that the noise-only covariance is unable to represent the true uncertainty of the state estimation. To avoid redundancy, the consider covariance is not included in the previous figure, as a similar evolution is observed in Figure 24 (and because the aim of the figure is to graphically represent the unrealism of the noise-only covariance).

Analogous to the previous test case, the contribution of the range bias consider parameter to the correction of the noise-only covariance matrix is analysed. Assuming a unitary range bias consider parameter, the contribution matrix results in Figure 34. The different components of the correction matrix are plotted, from 1 to 6 the state vector components and in the 7th row and column the components related to the drag coefficient (considering a state vector of position and velocity plus an estimated drag coefficient). The range bias consider parameter contributes to the uncertainty realism of the position components of the covariance matrix and the uncertainty of the drag coefficient and correlations between the drag coefficient and the position components. This is also noticeable from Figure 32 since the noise-only covariance matrix and the observed covariance matrix display divergences at estimation epoch (while in test Case B this was not observed).

3.1.2.4 Case D

The fourth and last test case devised addresses the impact of the atmospheric drag force model consider parameter when processing realistic orbits to compute an observed covariance using the observed covariance methodology. Test case D is key to demonstrate that the developed methodology not only works within an unrealistic environment but a rather realistic simulated one.

As mentioned in the introduction of this section, test case D will employ realistic orbits, by simulating batches of measurements spanning through different periods of time. Hence, the population sample for the whole development of the observed covariance is scarcer, yielding to an insufficient sampling of the state uncertainty. In the following table, the relevant features of Test Case D are listed:

Table 18 Features of Case D

	Test case D
Consider parameter	AE (Atmospheric Drag Model Error)
Observed covariance	Realistic simulated observed covariance
Number of simulated points	181
Reference orbit	01-01-2018 to 01-07-2018
Measurement generation	5 days batch
Estimation epoch for OD	End of measurement period
Predicted orbit	Estimation epoch + 7 days

The estimation epoch and the epoch of the last measurement of the batch do not coincide. The present case introduces a certain perturbation in the atmospheric drag force model by means of a non-null consider parameter. Recalling the equation for the drag force model (Equation (2 .4)) a gaussian atmospheric drag force model perturbation is introduced, following:

$$c_{AE} \sim N(0, \sigma_{AE} = 5\%) \tag{3 .3}$$

In terms of covariance consistency, the weighted RMS and the differences among the estimated (MC) covariance matrices have been analysed. The following figure represents a histogram of the WRMS of the different ODs:

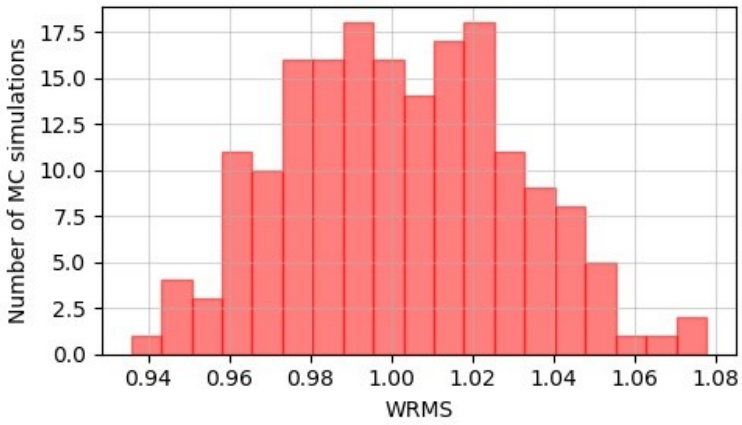

Figure 35 WRMS of the ODs for test Case D

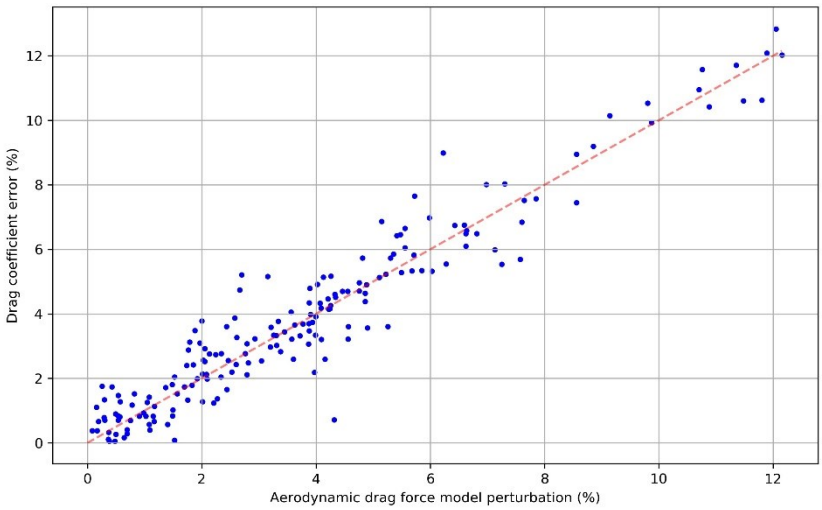

Figure 36 Drag coefficient error vs. atmospheric drag force model perturbation for test Case D

The resulting histogram of the WRMS of the different ODs resembles that of test Case B, although the distribution is computed with a much smaller population. The author deemed unnecessary to include a figure displaying the results of the analysis for the differences among computed covariance matrices, since the differences with respect to test Case B results are minimum and to avoid redundancy. Analogous to test case B, the perturbation of the atmospheric model is absorbed in the estimation of the drag coefficient (see Figure 36). At estimation epoch, it does not yield to orbital differences with respect the reference state, however, when propagated, a similar behaviour is appreciated when computing the orbital differences of the MC points with respect the reference state (see Figure 37, Figure 38 and Figure 39).

A test for normality is included as the population considered for this case is more subject to infringe with the normality requirements established for a realistic covariance. Due to a lower number of samples, the population is more sensitive to outliers in the distribution, thus a statistical test should be carried out to ensure Gaussianty of the distribution. The first covariance realism metric proposed in Section 2.6 is the test for an unbiased mean orbital state considering the aggregation of the complete orbital distribution. The averaged error of the distribution is listed in Table 19 together with its relative magnitude with respect the standard deviation of the distribution. Inspecting Table 19, the bias of the distribution is not found significant as in most of the cases, even during propagation, the relative value of the bias when compared with the standard deviation of the distribution is found to be 10 times smaller.

As exposed in section 2.6, the tests employed for testing the normality hypothesis are the graphical P-P plot using Michael's confidence boundary regions, with a significance level of 5%. The results of the normality tests can be found in Figure 37, Figure 38 and Figure 39. From inspection of the tests, the distributions are found to be normal. As none of the distributions is found to infringe the boundaries of the defined confidence regions, the univariate distribution are assumed normal since the null hypothesis of normality cannot be rejected. Note that in Figure 39 few points infringe the confidence regions, this is only indicative that at estimation epoch the normality of the W direction is rejected but as propagation occurs a normal distribution can be safely assumed.

Table 19 Averaged and relative error of the distribution in the T, N and W directions, where t_0 stands for estimation epoch and subsequent prediction times are expressed relative to it

$\boldsymbol{Epoch}$	$\Delta T\ (m)$	$\Delta N\ (m)$	$\Delta W\ (m)$	$\Delta T/\sigma_T(\%)$	$\Delta N/\sigma_N(\%)$	$\Delta W/\sigma_W(\%)$
$\boldsymbol{t_0}$	0.326	0.132	0.188	7.06	8.48	11.24
$\boldsymbol{t_0+1}$	0.505	-0.054	-0.184	6.94	-7.27	-11.15
$\boldsymbol{t_0+2}$	0.047	-0.120	-0.209	0.37	-7.22	-11.78
$\boldsymbol{t_0+3}$	-0.192	0.076	0.183	-0.90	10.08	10.31
$\boldsymbol{t_0+4}$	-0.023	0.099	0.233	-0.07	13.94	12.19
$\boldsymbol{t_0+5}$	-0.341	-0.101	-0.190	-0.67	-13.10	-9.82
$\boldsymbol{t_0+6}$	-1.152	-0.083	-0.258	-1.63	-12.04	-12.40

Table 20 Covariance containment test for Case D for the noise-only covariance (left) and the consider covariance (right). Colour scale is applied to each column to compare the theoretical value against the measured, where a similar colour denotes proximity of both values. t_0 stands for estimation epoch and subsequent prediction times are expressed relative to it.

Time	Noise-only covariance				Consider covariance			
	1-σ	2-σ	3-σ	4-σ	1-σ	2-σ	3-σ	4-σ
t₀	2.94%	14.12%	26.81%	37.24%	9.88%	44.77%	75.00%	88.95%
t₀ + 1 day	2.49%	12.33%	23.30%	33.19%	20.93%	64.53%	87.79%	97.67%
t₀ + 2 days	2.83%	15.41%	29.04%	40.89%	19.77%	71.51%	96.51%	99.42%
t₀ + 3 day	1.96%	10.17%	20.24%	29.37%	24.42%	72.67%	94.77%	99.42%
t₀ + 4 days	2.07%	11.14%	21.51%	30.29%	19.77%	68.02%	96.51%	100.00%
t₀ + 5 days	1.76%	8.78%	18.16%	26.53%	23.84%	72.67%	94.77%	99.42%
t₀ + 6 days	1.82%	10.34%	19.40%	27.75%	20.35%	70.93%	96.51%	100.00%
Theoretical	19.90%	73.90%	97.10%	99.87%	19.90%	73.90%	97.10%	99.87%

Finally, the containment metrics are presented in Table 20 leading to the same conclusion deduced from Case B: the noise-only covariance (left) fails to properly characterize the uncertainty of the state vector. The observed covariance is generated using the observed covariance method for operational orbits described in section 2.4 and 2.7.2. Once processed, the observed covariance is ingested by the Covariance Determination algorithm together with the rest of the required inputs (derived from a previously computed OD). The results of the fitting are listed in the following table:

Table 21 Results of Case D applying the Covariance Determination algorithm

Test case D	
Atmospheric model error	$26.49\ \%^2$
Variance of estimated parameter	$2.566\ E-03$
LSQ solver	Gauss-Newton
Number of iterations	3
CPU time	0.0251 min

The solution provided by the Covariance Determination algorithm has estimated a variance of the atmospheric drag force model error of $26.49\ \%^2$, i.e. a standard deviation of 5.147%, almost the 5% of the input noise model. The sigma of the estimated parameter as well as the residuals are found to be several orders of magnitude smaller than the computed value. Inspecting Table 20, it is clear that the consider covariance computed with the estimated consider parameter variance complies with the theoretical metrics of the covariance containment test. For this test, the consider covariance was employed and a Mahalanobis distance was computed for each of the MC points yielding the previous results.

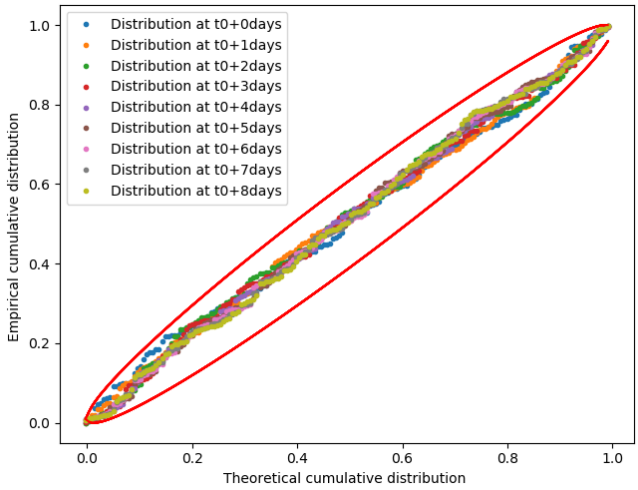

Figure 37 Normality test on the orbital differences of T direction at different propagation periods

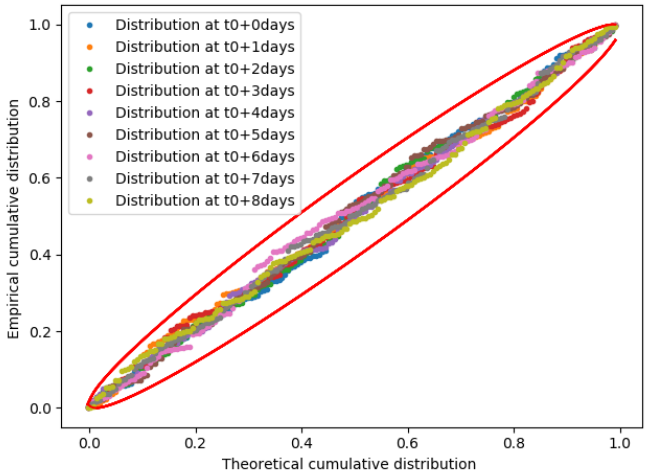

Figure 38 Normality test on the orbital differences of N direction at different propagation periods

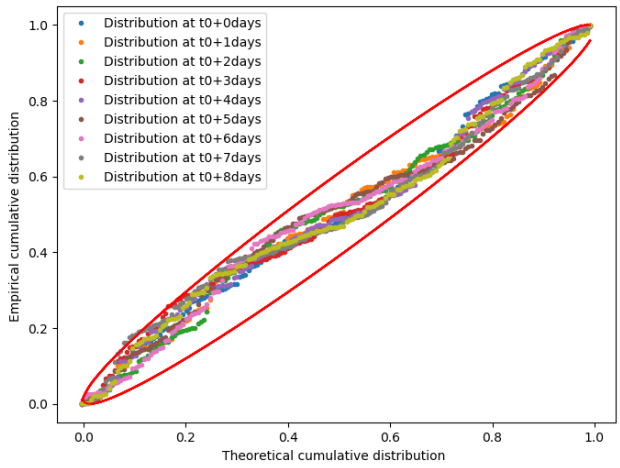

Figure 39 Normality test on the orbital differences of W direction at different propagation periods

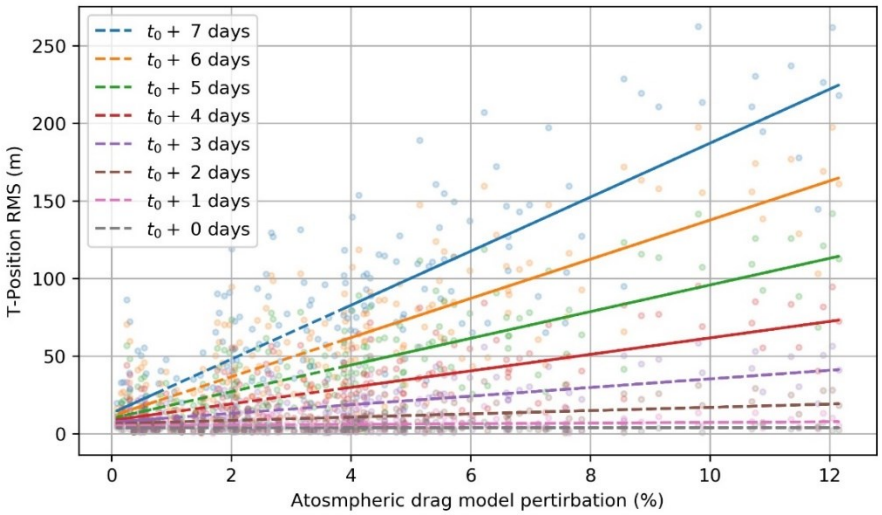

Figure 40 Atmospheric drag force model error vs. T-position RMS error

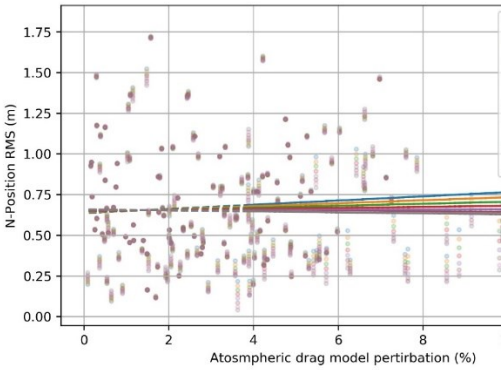

Figure 41 Atmospheric drag force model error vs. N-position RMS error. Legend is removed for readability (same legend as Figure 40applies)

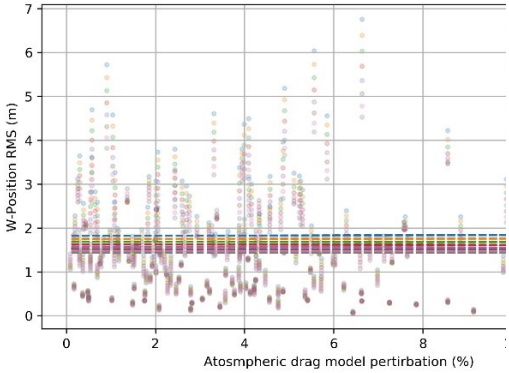

Figure 42 Atmospheric drag force model error vs. W-position RMS error. Legend is removed for readability (same legend as Figure 40 applies)

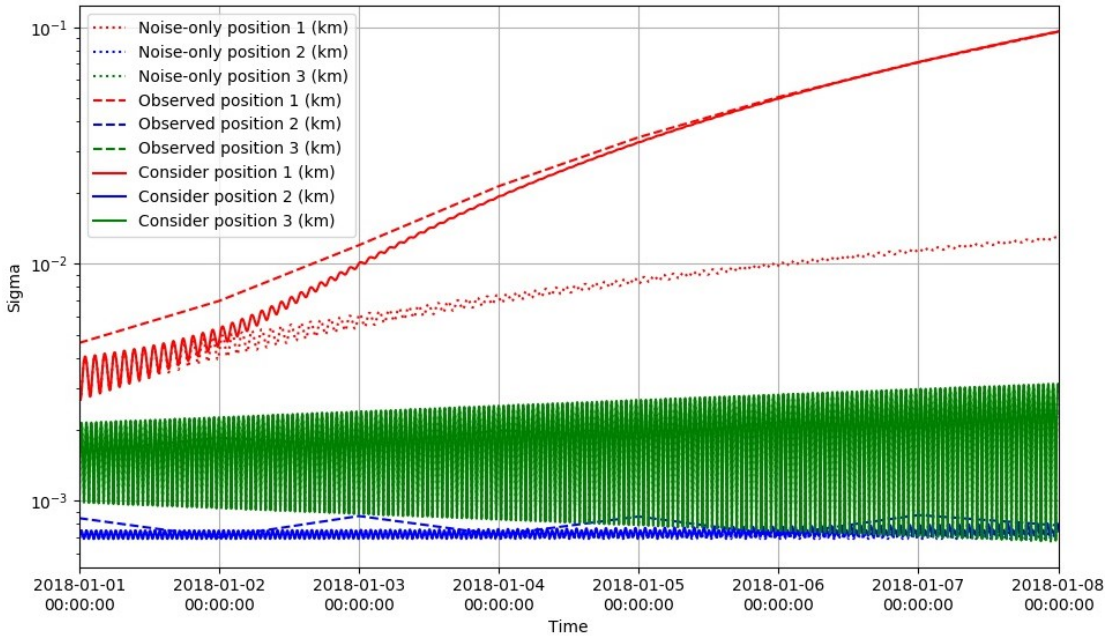

Figure 43 Evolution of the T, N and W position sigma of the noise-only, observed and consider covariance for test Case D.

To provide a more conceptual view on the goodness of the fit made by the Covariance Determination algorithm and the poor state uncertainty representation that the noise-only covariance defines, Figure 43 shows the evolution of the T, N and W position sigma of the noise-only, observed and consider covariance matrices along time. Similar to test Case B, the noise-only covariance diverges, as it is propagated, from the observed covariance. The consider covariance, implementing the corrections introduced with the consider parameters, is capable to provide a best-fit of the observed covariance. Note that compared to case B, some differences are appreciated at estimation epoch between the consider and noise-only covariance. Because the estimation epoch and the epoch of the last measurement of the processed batch do not coincide, from batch to batch a certain variability of the orbital differences is appreciated, reason for which at estimation epoch the observed and consider covariance do not coincide.

During the present section, a thorough series of incremental validation tests have been proposed and analysed to demonstrate the relevance, performance and possible applications of the Covariance Determination methodology. From the simplest case, validating the generation of an observed covariance, to the most critical, employing operational orbits, the methodology to improve covariance realism has proved to deliver remarkable results. In the following section, the results of applying the aforementioned methodology to a real case, the Sentinel 3A tracking campaign, will be detailed.

3.2 Covariance Determination applied to Sentinel 3A tracking campaign

During the previous section, a thorough validation campaign is exposed, proving insightful analysis in a wide variety of cases and model perturbations. Once validated, the software application is ready for its use in a real operational environment, fulfilling its ultimate purpose of correcting covariance unrealism in orbit determination and propagation processes.

In this section, a brief introduction on the Sentinel 3-A mission main facts and figures is provided, the main data sources to be processed during the analysis and a station residuals and biases characterization. Next, the analysis on the processed ODs, the typical residuals and orbital differences with respect to a precise orbit solution are provided. The estimation of several consider parameters is detailed and normality and containment metrics are used to evaluate the performance of the methodology.

3.2.1 Scenario definition

The scenario definition represents the introduction to the real operational tracking campaign of the Sentinel 3A satellite. In the following section key information is provided to better comprehend the results obtained during the sequential ODs, the posterior observed covariance generation and the Covariance Determination.

3.2.1.1 Main figures of the Sentinel 3A mission

In [Lopez-Jimenez, Literature Study for MSc Thesis - TU Delft, 2019], a detailed exposition of the Sentinel 3A mission can be found. In this section, a brief exposition of the relevant figures of the Sentinel 3A satellite are listed in the following table:

Table 22 Figures of Sentinel 3A mission

	Sentinel 3A
Semi-major axis	7186.877 km
Eccentricity	0.001113
Inclination	98.72 deg
RAAN	77.03 deg
Altitude	814.5 km
Wet mass	1150 kg
Dimensions	2.2x2.2x3.7 m
Cross-sectional area	4.5 to 8.5 m^2

3.2.1.2 Data sources of the study case

In [Lopez-Jimenez, Literature Study for MSc Thesis - TU Delft, 2019], a detailed exposition of the data sources that will be employed in the processing of the Sentinel 3A orbits is provided. The following table summarizes the information displayed in the Literature Study:

Table 23 Data sources for the Sentinel 3A tracking campaign

	Sentinel 3A
POD orbits	TU Delft POD orbits for Sentinel 3A
Manoeuvres	Publicly available at [ESA-Sentinel, 2019]
Radar measurements	Leolabs PFISR & MSR radar stations

A brief summary of each radar station can be found in the following table:

Table 24 Radar station features

	PFISR	**MSR**
Latitude (deg.)	65.12992	31.9643
Longitude (deg.)	-147.471	-103.233
Height (m)	213	855
FOV shape	Conical	Barrier

More information on the radar stations can be found in [O. Rodriguez Fernandez, F. Bonaventure, & M. Nicolls, 2018] and [Griffith, Nicolls, Lu, & Park, 2017]. Note that from Leolabs webpage, range, range-rate and angular measurements are available and distributed with ionospheric and bias corrections. In addition, measurements are retrieved for a specific target, in this case the Sentinel 3A satellite. Accounting for the orbital parameters of the satellite, listed in Table 23, and the radar station geodetic coordinates, pointing and Field of View (FOV) two satellite tracks can be captured at least per day per station, ensuring a proper amount of tracks to determine the orbit of the object. POD orbit metrics, typical quality and residuals information is reported in [Marc Fernandez, 2018]. Finally, a complete year of measurements will be considered for the analysis to be developed in this section, ranging from May 2018 to June 2019, hence Leolabs measurements will be retrieved for the considered period as well as POD orbit solutions.

3.2.1.3 Station calibration and typical measurement uncertainty

Prior to processing the retrieved measurements from Leolabs, a previous study aimed to characterise the typical residuals of both radar station was carried out, in order to properly weight the retrieved measurement and obtain accurate ODs. In the Leolabs webpage, statistics for the typical station biases and residuals can be obtained. Considering a 30 day period of data, the Figure 44, Figure 45, Figure 46 and Figure 47 show the evolution of measurement bias corrections as wells as residuals per day, obtained by processing their own OD.

From Figure 44 and Figure 45, the MSR radar displays variable values for the range measurement residuals, always contained within 10 to 20 m, and for the range bias within 0 and 13 m. Although having a considerable variability, its values are always found within certain thresholds. For the case of the range-rate measurements, bias and residuals have a more stable behaviour. From Figure 46 and Figure 47, the PFISR radar displays almost constant values for the residuals and for the bias of both range and range-rate observations.

From Table 25, the characterisation of typical noise and biases of observations taken with LeoLabs radars is done. However, LeoLabs does not provide values for angle measurement biases and residuals and a station calibration process was required to verify the supposed values displayed in Table 25 and define typical values for angle measurements. Internal documents of the SST department of GMV (disclosure not permitted) considered irrelevant the use of angular measurements in the computation of ODs using LeoLabs measurements, as typical RMS are in the order of 0.2 to 10 degrees while having a great variability of angle biases. Thus, considering typical values of angles RMS, the supposed weight that these measurements would have on an OD is negligible, hence the document recommends avoiding the processing of elevation and azimuth angle measurements.

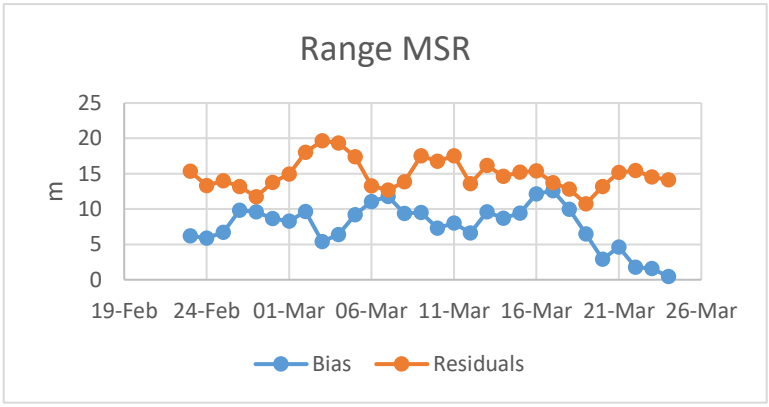

Figure 44 Range bias and residuals for the MSR radar from 23/02/2019 to 24/03/2019

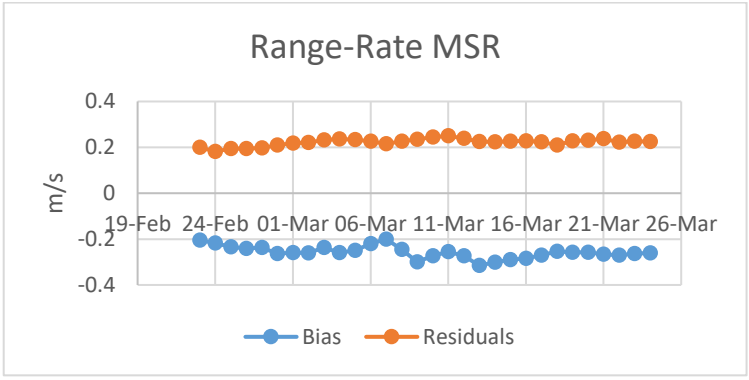

Figure 45 Range-rate bias and residuals for the MSR radar from 23/02/2019 to 24/03/2019

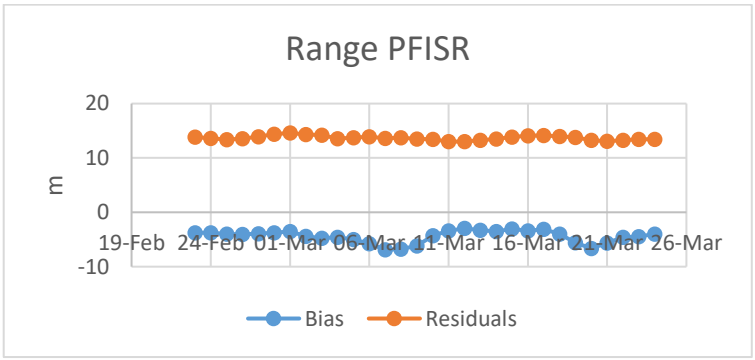

Figure 46 Range bias and residuals for the PFISR radar from 23/02/2019 to 24/03/2019

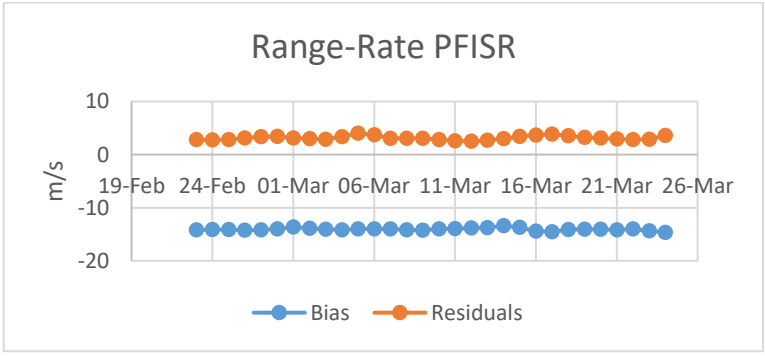

Figure 47 Range-rate bias and residuals for the PFISR radar from 23/02/2019 to 24/03/2019

Table 25 Statistics for bias and residual of MSR and PFSIR radar from 23/02/2019 to 24/03/2019 from LeoLabs

	MSR		PFSIR	
	Bias	**Residuals RMS**	**Bias**	**Residuals RMS**
Range(m)	7.653	14.902	-4.427	13.674
Range-rate (m/s)	-0.257	0.222	-14.070	3.130

Avoiding the processing of angular measurement will have an impact in the orbit determination and propagation error. From [Wiegel & Patyuchenko, 2011], radar and range-rate (i.e. Doppler) measurements are sensitive to variations in the radial and along-track component, however they lack sensitivity in the out-of-plane component and depend on the geometry of the case. For instance, an unfavourable geometry would occur when the station lies close to the orbital plane of the object as range and range-rate measurements would not capture enough information of the out-of-plane component. Thus, it is expected that the processed ODs display significant errors in the normal component when compared with POD solutions.

A preliminary process intended to determine which radar station or combination of radar stations was best suited to provide the best orbit determination solution, comparing the estimated state with the POD solution. For this analysis, a random OD batch of 7 days of measurements was considered using three different station configurations, only accounting for range and range-rate measurements. The analysis compare the estimated orbital ephemeris against the precise orbit solution to obtain a mean value of the differences, an RMS and maximum error value. From the different cases, the most promising is the case where only the MSR station is considered, although numerous references encourage using all the measurements available as the OD quality is supposed to improve (as in [Oliver Montenbruck, 2000]). The MSR station alone seems to deliver the best orbit solution as its yields the smallest mean and RMS differences. Finally, in the following table the results for the different configurations are listed:

Table 26 Comparison of the whole estimation interval between an OD with different configurations and the reference POD orbit

Comparison of OD solution vs. POD orbit				
		Radial	**Transverse**	**Cross**
MSR	**Mean(m)**	0.0241	-18.1448	0.1328
	Rms (m)	8.4271	26.0703	46.1651
	Max (m)	21.1092	61.3259	76.2945
MSR+PFSIR	**Mean (m)**	0.0464	-33.0023	0.1105
	Rms (m)	9.3114	45.0368	35.5446
	Max (m)	26.1362	95.7725	58.6109
PFSIR	**Mean (m)**	0.0402	-39.6703	0.0934
	Rms (m)	10.7694	53.3207	26.1794
	Max (m)	28.7661	104.5348	41.747

Finally, the station calibration intended to define range and range-rate measurement biases and typical RMS for the selected station. Residuals should exhibit a Gaussian distribution with 0 mean and a typical standard deviation equal to the RMS displayed in Table 25. The results of the station calibration analysis for the MSR station, considering a whole year of measurements (from 01-05-2018 to 01-06-2019) and taking into account satellite manoeuvres, are listed in the following table:

Table 27 Station calibration of the MSR radar station

	Bias (m; m/s)	**RMS (m; m/s)**
Range	-7.46961	24.677
Range-rate	-0.08408	0.288347

The study carried out to calibrate the MSR station yields important results to be considered during the OD process and to obtain best-quality orbit solutions. The biases listed in Table 27 will be considered during OD processes and the measurement weights will be defined as the RMS values computed during the calibration, giving us some insights regarding the maximum attainable accuracy of the ODs.

3.2.2 Covariance determination: practical application

The practical case of the research project represents the culmination of the work conducted during the Master Thesis and the application of the Covariance Determination methodology to a real tracking campaign of an operational satellite. The following table summarizes the most relevant features of the Sentinel 3A case:

Table 28 Features of Sentinel 3A case

Case of Sentinel 3A satellite	
Consider parameter	AE (Atmospheric Drag Model Error)
Observed covariance	Operational observed covariance
Number of simulated points	356
Reference orbit	01-05-2018 to 01-06-2019
OD period	7 days batch
Shift between ODs	1 day
Estimation epoch for OD	End of measurement period
Predicted orbit	Estimation epoch + 8 days

The dynamic model employed to perform the different ODs is summarized in the following table, where a more complete dynamic model is employed to successfully perform the orbit determination of the Sentinel 3A satellite:

Table 29 Dynamic model employed for the Sentinel 3A tracking campaign

Full dynamical model	
Gravity field (Static)	GRACE 04c 32x32
Third body perturbations	Sun & Moon
Polar motion and UT1	IERS C04 08
Pole Model	IERS 2010 conventions
Precession/ Nutation	IERS 2010 conventions
Atmospheric Model	MSISe-90; Fit performed for ballistic coefficient
Solar Radiation Pressure	Constant area (S2); Fit performed for coefficient of reflectivity
Consider relativistic gravity	Yes
Integration step	60s
Geodetic surface	ERS-1
Reference frame	J2000 ECI

It is worth mentioning that the processing method for the different batches of ODs spans over 7 days of possible measurements, each batch shifting 1 day ahead in time during a period of 1 year. This leads to a considerable amount of ODs, a total of 356 orbit estimation and subsequent propagations. After running the first analysis on the complete set of estimations and computing the orbital differences of the predicted states versus the reference POD orbits Figure 49 is obtained.

Despite rejecting ODs (Figure 49) where either during the estimation or prediction period a maneuver took place, there are some solutions describing important drifts that can be considered as spurious (probably due to problems with sensors, miscorrelations, geometry or number of available tracks, among others). The orbital differences of these estimations may pollute the processing of the operational observed covariance yielding a non-realistic and too pessimistic observed covariance. Two solutions have been implemented to surpass these difficulties, the first being the consideration of a smaller period of estimated orbits and the second beign the definition of an outlier rejection methodology.

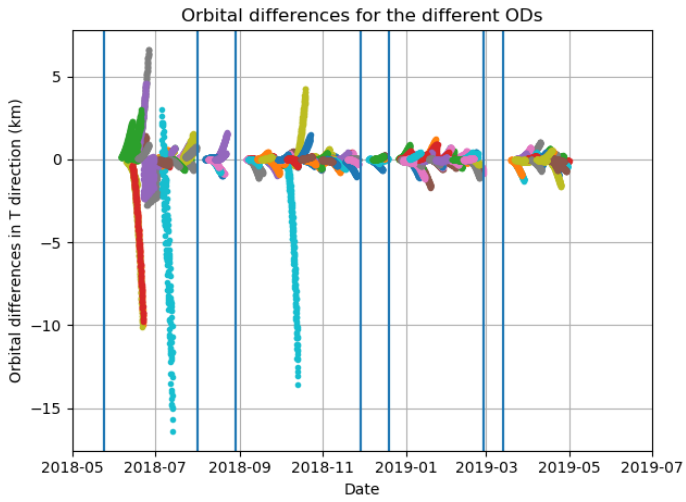

Figure 49 Orbital differences in the T direction between predicted ODs and the reference orbit for the whole year. Note that blue lines mark the epochs at which a maneuver took place, hence the OD solution is discarded due to low quality and non-negligible errors in the processing.

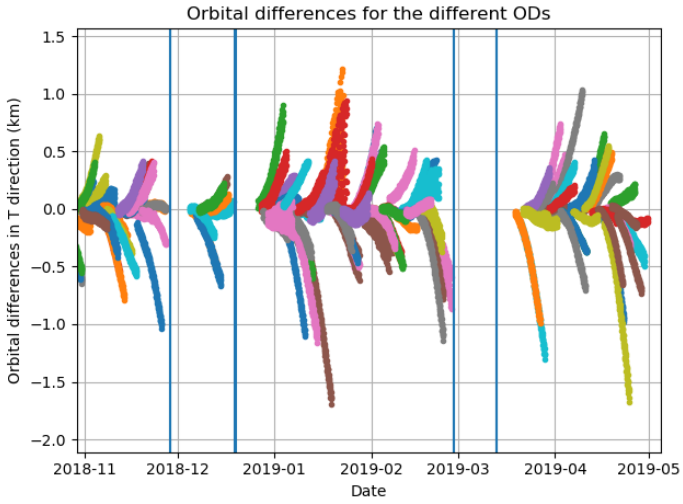

Figure 48 Orbital differences in the T direction between predicted ODs and the reference orbit for a selected period. Note that blue lines mark the epochs at which a maneuver took place, hence the OD solution is discarded due to low quality and non-negligible errors in the processing.

The selected period (Figure 48) has been chosen inspecting Figure 49, in which more stable orbits are estimated from november 2018. In addition, a rejection criteria has been established to dismiss those orbits that represent outliers to the normal distribution of orbital differences. The rejection criteria will employ a proportionality factor to reject all the orbital differences whose absolute value exceeds that of the augmented median of the whole distribution:

$$\Delta \boldsymbol{y_i} < k \cdot Median(\Delta \boldsymbol{y}) \quad (3.4)$$

The aim is that the obtained distribution can be assumed as Gaussian and a realistic covariance can be derived from it, complying with the first requirement posed during section 1.2. Different proportionality factors will be tested to decide which is the most suitable factor to reject for outliers, based on the numerical and graphical results of Michael's statistical test. Analogous to the validation section, the same metrics are employed when testing for covariance realism (defined in section 2.6). In the following table, the results for the Michael's test are listed:

Table 30 Results for Michael's test of normality at different epochs, for different rejection factors (along-track direction).

	p-value						
Factor	t_0	t_0+1	t_0+2	t_0+3	t_0+4	t_0+5	t_0+6
$k=2$	0.116542	0.662587	0.219245	0.078354	0.19673	0.478724	0.141111
$k=2.5$	0.015344	0.45968	0.436546	0.16243	0.371372	0.414509	0.273086
$k=3$	0.05533	0.073414	0.467747	0.154961	0.380622	0.451783	0.652842
$k=3.5$	7.90279E-05	0.073414	0.430101	0.047774	0.623179	0.577852	0.680931

The author deemed unnecessary to include all the P-P graphics for the Michael's statistical test for different scaling factors, however from the previous table it is clear that the rejection criteria which complies with the normality condition (assuming a significance level of 5 %) at all epochs is the $k=3$ and lower value. $k=3$ is finally selected as it yields to the less restrictive rejection criteria (leading to a 5% rejection of samples) whereas lower values displayed higher rejection rates (about 10% and higher). A P-P plot of Michael's test is included for the definitive rejection factor in Figure 50, Figure 51 and Figure 52.

After all ODs were processed, the covariance realism metrics are used to analyze the complete distribution of orbital differences. The following table lists the results of the average orbital error:

Table 31 Averaged and relative error of the distribution in the T, N and W directions, where t_0 stands for estimation epoch and subsequent prediction times are expressed relative to it

Prediction epoch	$\Delta T\ (m)$	$\Delta N\ (m)$	$\Delta W\ (m)$	$\Delta T/\sigma_T(\%)$	$\Delta N/\sigma_N(\%)$	$\Delta W/\sigma_W(\%)$
t_0	-11.71	-0.20	2.12	-45.27	-16.98	21.43
t_0+1	-10.84	0.69	3.14	-22.67	49.34	34.03
t_0+2	-9.69	-0.25	-6.37	-12.55	-14.75	-70.64
t_0+3	-14.17	-0.55	-2.77	-12.32	-25.15	-25.49
t_0+4	-21.58	0.22	7.88	-13.07	9.69	77.87
t_0+5	-20.69	0.56	2.46	-9.07	18.61	19.21
t_0+6	-30.97	-0.36	-9.14	-10.16	-10.35	-82.84
t_0+7	-41.66	-0.45	-1.43	-10.96	-12.44	-9.71
t_0+8	-50.43	0.20	10.71	-11.00	4.41	88.49

Inspecting Figure 50, there is no doubt that the distribution of orbital differences in the along-track direction does not invalidate the null hypothesis of normality. From test Case B and D and from the section 2.1.3.1, the major impact to covariance realism of LEO objects is the uncertainty in the modelling of the atmospheric drag force, affecting almost exclusively the uncertainty realism in the along-track direction. However, further inspection of normality for the remaining directions does not lead to the same conclusion. Orbital differences in the N and W directions invalidate the null hypothesis of normality, as it can be concluded from looking at Figure 51 and Figure 52.

From the normality tests displayed in Figure 50, Figure 51, Figure 52 and Table 31, the distribution of orbital differences at estimation epoch and during propagation cannot be assumed Gaussian and unbiased. The only direction in which orbital differences can be approximated as a Gaussian distribution are in the along-track direction. To further reinforce the rejection of normality for the N and W direction, Figure 53 provides a histogram of the orbital differences. Clearly, the orbital differences computed are far from being normally distributed. Especially, the orbital differences of the W direction display a bi-normal tendency where the distribution seems to be centred at two different mean values. The rest of the distributions are centred around 0 yet normality can only be assumed in the along-track direction (as demonstrated by the different tests).

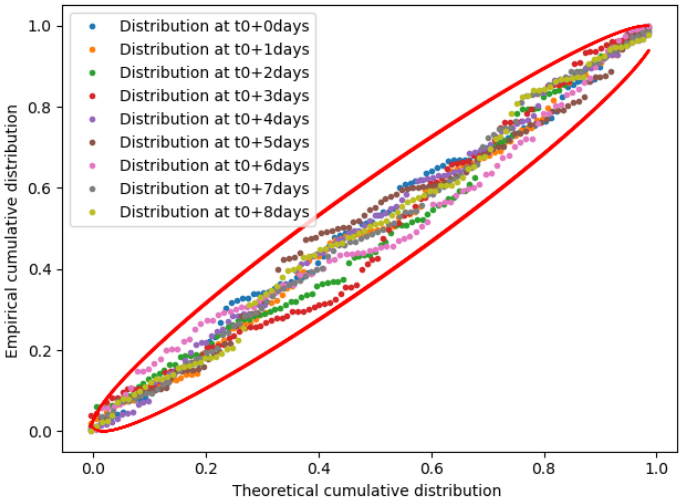

Figure 50 Michael's test of normality for the distribution of orbital differences in the T direction at different prediction times

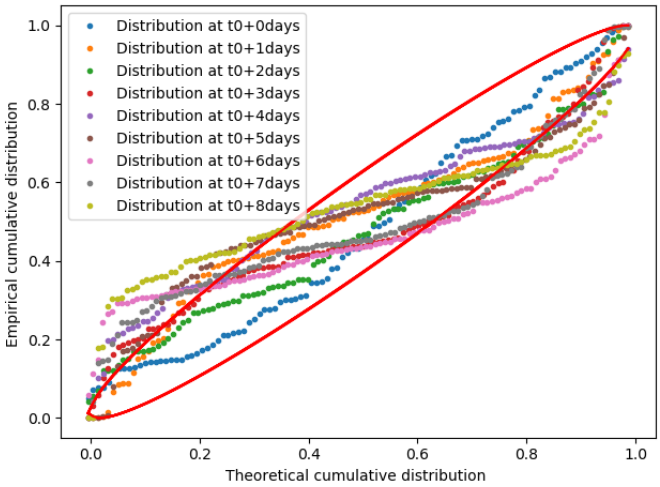

Figure 51 Michael's test of normality for the distribution of orbital differences in the N direction at different prediction times

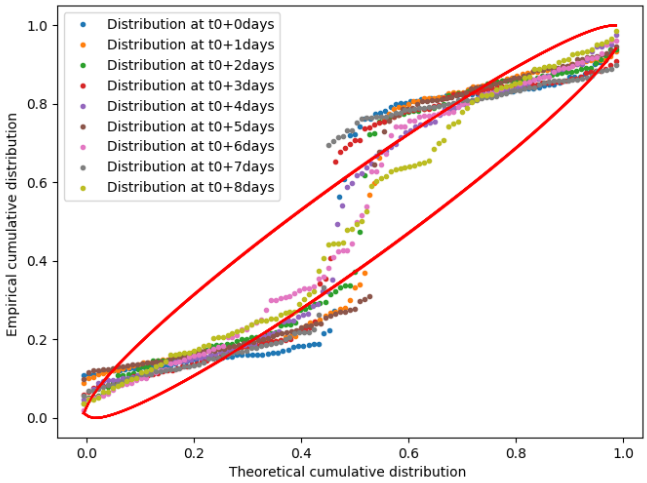

Figure 52 Michael's test of normality for the distribution of orbital differences in the W direction at different prediction times

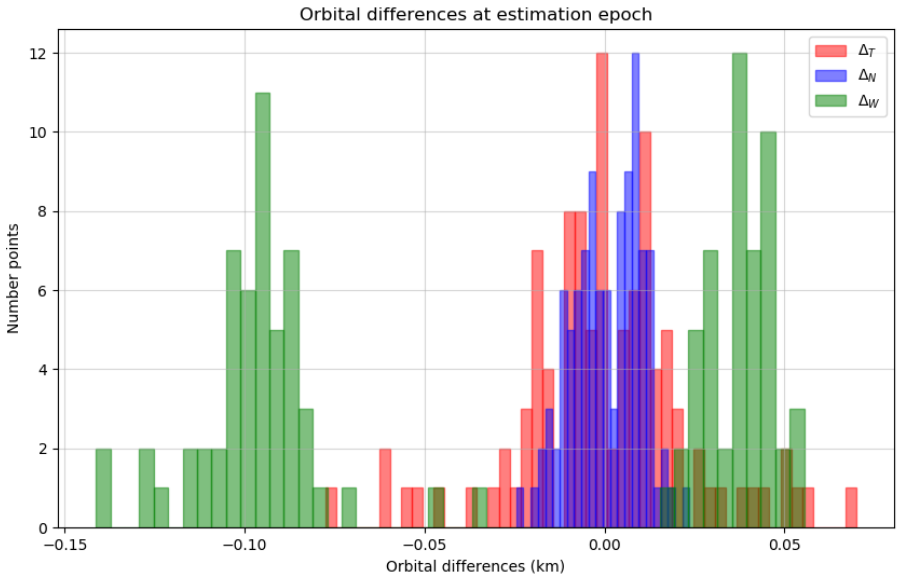

Figure 53 Orbital differences at estimation epoch for the different directions in the TNW local frame.

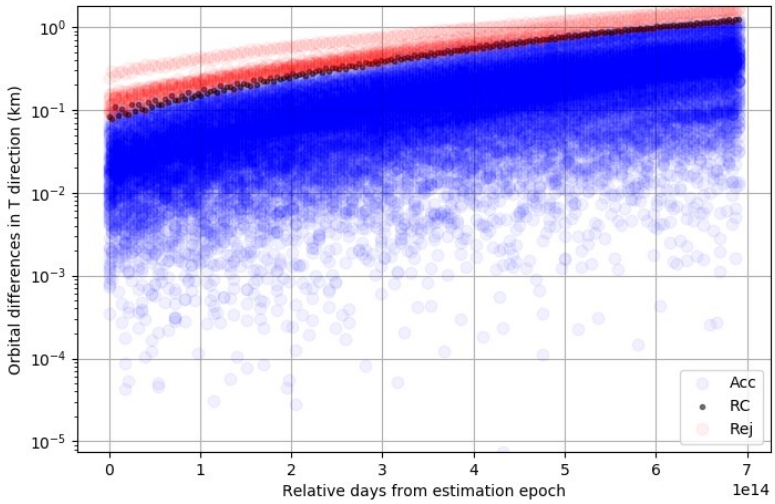

Figure 54 Aggregated orbital differences displaying the rejection criterion. A colour criteria has been defined so as to represent orbital differences: in red the rejected points, in blue the accepted points and in black the rejection criteria of each epoch (i.e. absolute median).

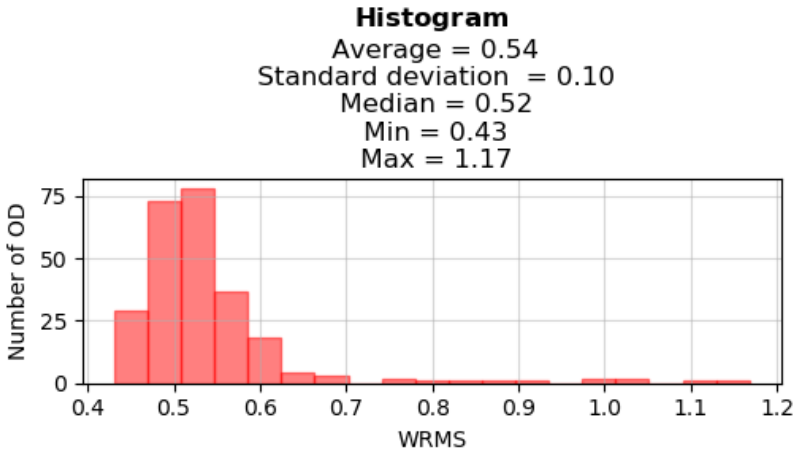

Figure 55 WRMS of the ODs for the tracking campaign of the Sentinel 3A

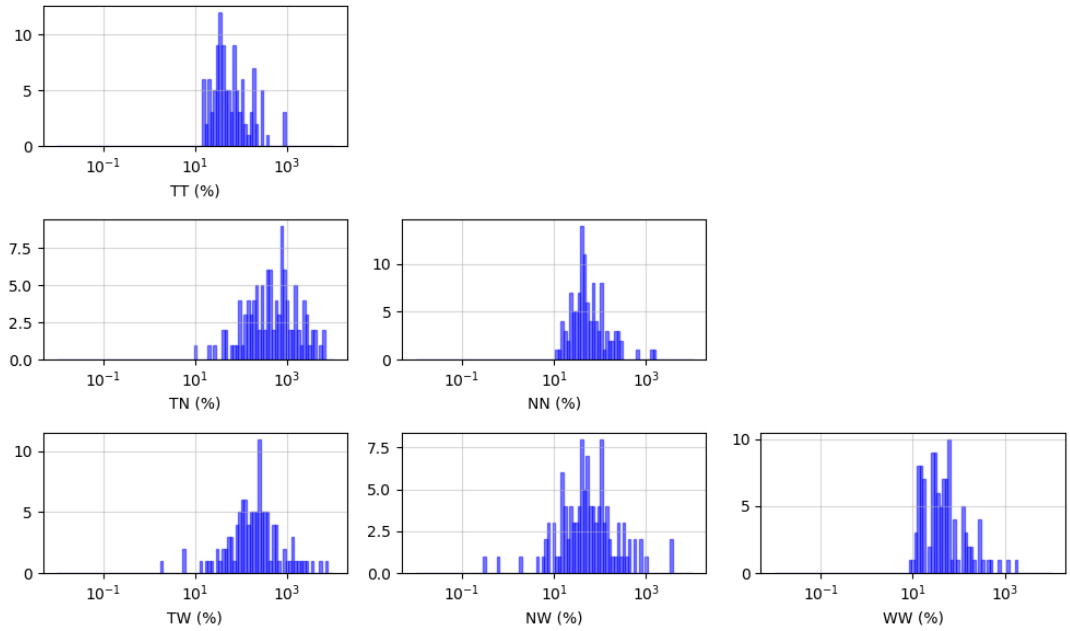

Figure 56 Relative differences of the estimated noise-only covariance matrices with respect to the average covariance matrix of the population for the Sentinel 3A tracking campaign

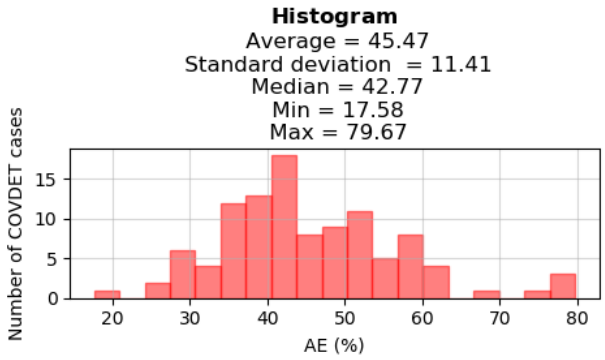

Figure 57 Histogram of the dynamic consider parameter estimations for the Sentinel 3A campaign

Table 32 Covariance containment test for the Sentinel 3A case for the noise-only covariance (left) and the consider covariance (right). Colour scale is applied to each column to compare the theoretical value against the measured, where a similar colour denotes proximity of both values. t_0 stands for estimation epoch and subsequent prediction times are expressed relative to it.

Time	Noise-only covariance			Consider covariance		
	1-σ	2-σ	3-σ	1-σ	2-σ	3-σ
t_0	20.00%	42.61%	56.52%	20.00%	42.61%	56.52%
t_0 + 1 day	13.91%	31.30%	42.61%	23.48%	36.52%	51.30%
t_0 + 2 days	9.57%	24.35%	36.52%	29.57%	58.26%	73.91%
t_0 + 3 day	12.17%	23.48%	34.78%	40.87%	68.70%	83.48%
t_0 + 4 days	10.43%	22.61%	31.30%	48.70%	79.13%	88.70%
t_0 + 5 days	8.70%	21.74%	26.09%	53.91%	79.13%	86.96%
t_0 + 6 days	11.30%	20.87%	26.09%	63.48%	88.70%	94.78%
t_0 + 7 days	8.70%	18.26%	25.22%	66.09%	85.22%	91.30%
t_0 + 8 days	5.22%	15.65%	23.48%	69.57%	89.57%	94.78%
Theoretical	66.70%	95.00%	99.70%	66.70%	95.00%	99.70%

Note that the orbital differences have been computed without considering an orbital averaging and this explains the two separate mean value observed in the out-of-plane direction. A slight divergence in the orbital plane will trigger orbital differences to appear negative or positive depending on the true anomaly of evaluation. Despite this fact, the author would have expected the distribution to be unbiased with 0 mean, displaying two peaks with a smaller variance of the overall distribution. Therefore, it has been thoroughly verified that only the along-track orbital differences can be assumed as normally distributed.

Figure 54 displays the evolution of the orbital differences for the T direction. As observed in the figure, all orbital differences are aggregated and time-tagged following the principles established in section 2.4, where the time of the last processed measurement of the OD batch is used as the estimation epoch and the reference start time for the prediction period of the orbit. This is especially important since the orbital batches were considered with fixed time spans, however batch periods do not coincide with the epoch of the last measurement. If unconsidered, the time tagging principle defined turn out to be useless as orbital differences from different relative prediction epochs are wrongly aggregated. Figure 54 allows for the analysis of the evolution of orbital differences with respect the prediction time, providing remarkable insight of the shape and magnitude of the observed covariance.

Finally, the analysis considered for the different test cases to check for covariance consistency will be reproduced, once that normality of the along-track distribution is ensured. The resulting WRMS of the different ODs is depicted Figure 55 and in Figure 56 the differences between the different estimated noise-only covariance matrices can be regarded. The differences among the different ODs and noise-only covariance matrices are remarkable due to the different conditions that influence the estimation process of an OD (i.e. measurement availability, number of measurements, geometry, etc.).

In order to provide a meaningful solution to the problem, a consider parameter estimation is processed per OD and propagation batch in which an atmospheric drag consider parameter is estimated. The final distribution of solutions leads to Figure 57 and a histogram has been used to represent the population of different estimated consider parameters. The results obtained depict a mean value of the consider parameter of 45.47 % error in the atmospheric drag model error with a standard deviation of 11.41%.

The results of the containment test (i.e. Mahalanobis distance computation as seen during the validation test cases) have no meaning when testing for a non-normal probability density function, as they are only representative when a multivariate normal distribution is tested. Thus, containment tests would yield to misleading results if used as orbital differences in the N and W direction are obviously not normal (as seen in Figure 54 and Figure 55). To express the performance of the Covariance Determination methodology, as the along-track direction is the single direction to have demonstrated a certain normality, a modified containment test with a similar statistical basis as that of the Mahalanobis test is listed in Table 32.

Note that the test reproduced in Table 32 is reduced to a simple univariate containment test, i.e. checking the percentage of orbital differences that lie within different sigma envelopes and compare with the theoretical values. From inspection of Table 32, it is clear that the Covariance Determination methodology provides a realism upgrade in the along-track direction, where the correction of the atmospheric drag consider parameter is more relevant.

In addition, Figure 58 is presented to graphically verify the realism upgrade introduced by the consider covariance. Looking at Figure 58 and Table 32 there is no doubt that the Covariance Determination methodology provides a remarkable upgrade in the covariance realism of the noise-only covariance, exclusive to the along-track direction. Inspecting Figure 58, there are clearly other effects playing non-negligible contributions to the covariance realism degradation as in the N and W directions the observed sigma diverges by an order of magnitude approximately from the noise-only sigma. The atmospheric drag consider parameter has only improved the covariance realism of the along-track, however correcting the remaining directions would lose a physical meaning since the distributions are far from normality.

An additional test is presented as the author deemed appropriate to correct for covariance unrealism estimating the uncertainty of the atmospheric drag force model and the uncertainty in the assumption of a range bias, as the results displayed in section 3.2.1.3 were indicative that radar measurements were inadequately corrected by the provider, hence probable covariance degradation might be caused by additional uncertainties in the measurement model. The results for the estimation of the dynamic and measurement model consider parameter are presented in Figure 59 and Figure 60. The graphical interpretation of the results is provided in Figure 61.

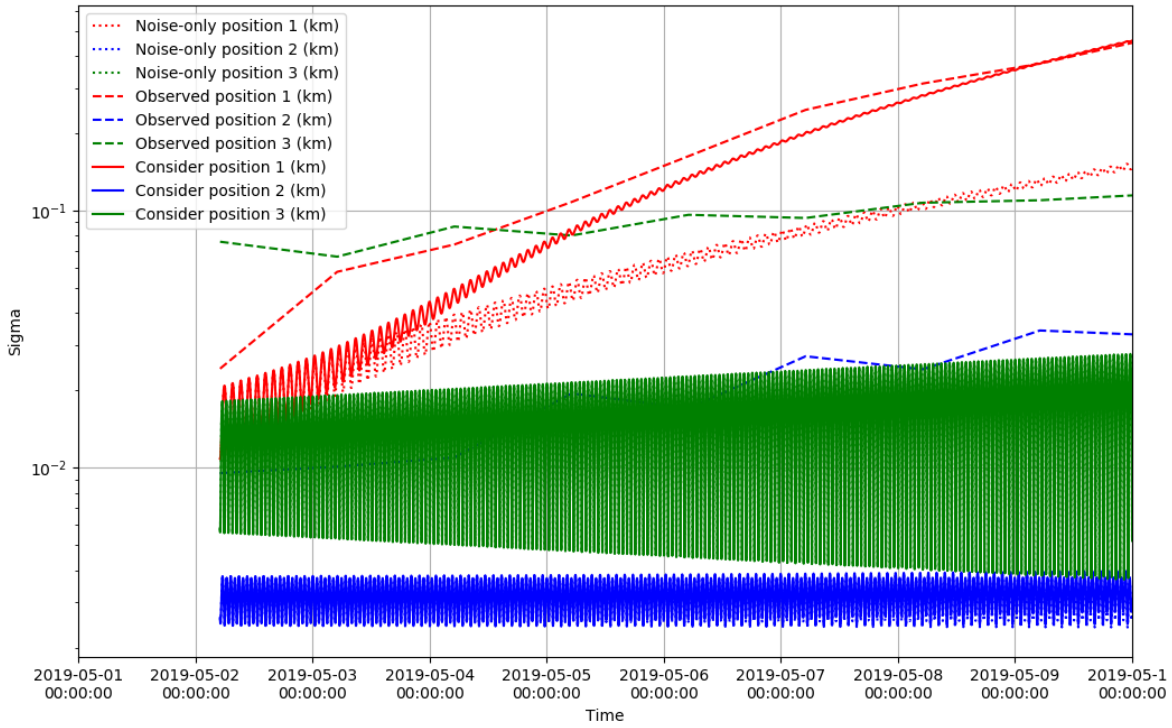

Figure 58 Evolution of the T, N and W position sigma of the noise-only, observed and consider covariance for the Sentinel 3A tracking campaign, fitting for a dynamic consider parameter

From Test Case C Figure 28, Figure 29, Figure 30 and Figure 32 it is observed that the uncertainty in the range bias affects both the along-track direction, cross-track and normal directions. For this reason and because there are non-modelled effects in the cross-track and normal direction, the present case is presented. The results represent an improvement in the containment metrics (comparing Table 32 and Table 33) as the along-track uncertainty is better characterized with the addition of a measurement model consider parameter. For the remaining directions, a certain improvement is observed as the range bias consider parameter also contributes scaling the uncertainty in all the directions.

The results for the atmospheric drag consider parameter (Figure 59) display slight changes when compared with Figure 57, as the estimation distribution gives a similar mean value and standard distribution. The results of the range bias consider parameter are far from normal (Figure 60), displaying a central tendency around the 35 m of range bias uncertainty although affected by heavy outliers. The covariance containment test for the same OD batch presented before is as follows:

Table 33 Covariance containment results using the consider covariance for the Sentinel 3A tracking campaign, correcting for a dynamic and measurement model consider parameter

Time	1-σ	2-σ	3-σ
t_0	49.57%	74.78%	80.87%
t_0 + 1 day	60.00%	79.13%	85.22%
t_0 + 2 days	67.83%	87.83%	89.57%
t_0 + 3 day	57.39%	82.61%	87.83%
t_0 + 4 days	54.78%	84.35%	90.43%
t_0 + 5 days	59.13%	84.35%	89.57%
t_0 + 6 days	66.09%	88.70%	94.78%
t_0 + 7 days	66.09%	85.22%	91.30%
t_0 + 8 days	67.83%	88.70%	94.78%
Theoretical	66.70%	95.50%	99.70%

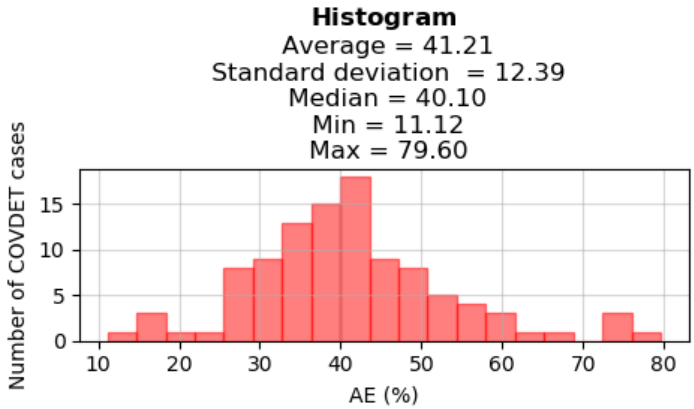

Figure 59 Histogram of the dynamic consider parameter estimations for the Sentinel 3A tracking campaign (2)

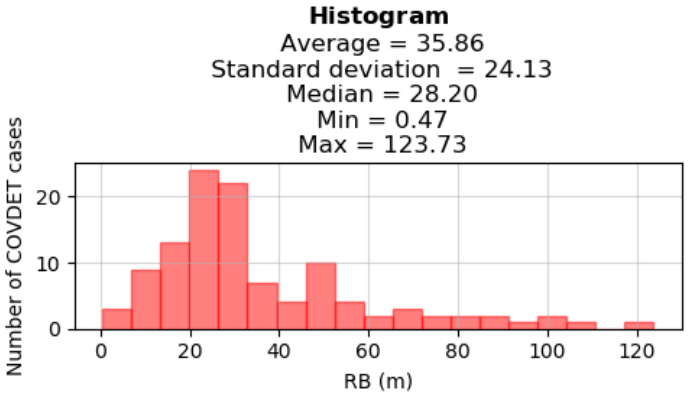

Figure 60 Histogram of the measurement consider parameter estimations for the Sentinel 3A tracking campaign

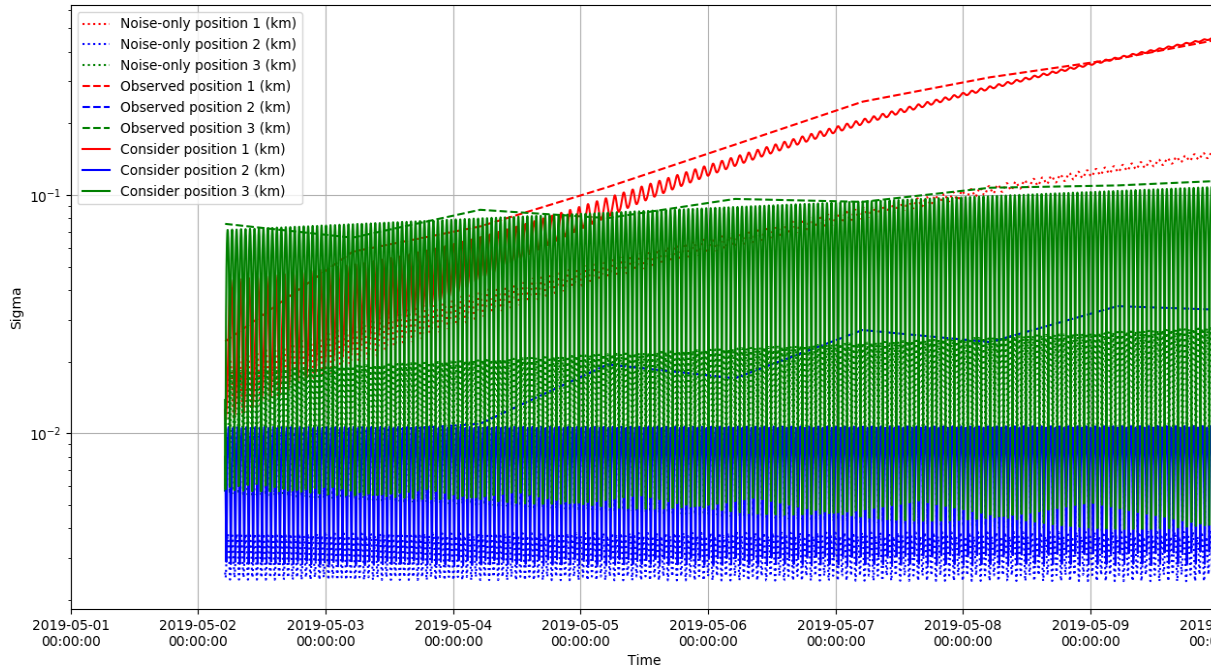

Figure 61 Evolution of the T, N and W position sigma of the noise-only, observed and consider covariance for the Sentinel 3A tracking campaign, fitting for a dynamic and measurement model consider parameter

This chapter represents the summary of the different test cases and the results obtained which are used to verify and validate the Covariance Determination methodology and the different consider parameters implemented. In addition, the different tests provided remarkable insights in the degradation of state prediction and covariance realism when dynamic and measurement model uncertainties are present and unconsidered in orbit determination processes. Finally, this chapter also presented the results of applying the Covariance Determination methodology to a real tracking campaign, processing measurements from LeoLabs radar network during an entire year. Important results concerning the improvement on covariance realism were obtained and next chapter will provide a thorough analysis on them.

4

DISCUSSION

The previous chapter gave a clear and factual exposition of the different results obtained from several validation test cases, aimed at verifying the fitness and performance of the novel Covariance Determination methodology. The present chapter provides the insights derived from the point of view of the author, aimed at answering the different question posed for the research from a scientific and engineering perspective. The discussion of the results will be subdivided into the validation cases and the real case of the Sentinel 3A satellite.

4.1 Discussion on validation and verification results

The present section has the aim to answer several of the research question posed during the development of this research project and analyse the different outcomes that the test cases have provided.

4.1.1 Test Case A

Test Case A is the first test case presented and has the aim to verify that in the absence of model errors, either in the dynamics or measurements, a regular orbit determination and propagation process provides an estimated covariance matrix (noise-only) that represents realistically the uncertainty of the state vector, provided that measurements are correctly weighted and the residuals are unbiased.

From Figure 15, an important conclusion can be drawn: that all covariance matrices are practically the same, as the relative differences among them come from the randomly generated measurements. From the containment tests, Table 11, the average noise-only covariance complies with the covariance containment metrics almost perfectly at different epochs even when propagated far from the estimation epoch. This is reinforced by the containment test of the observed covariance matrix, which indicates the same compliance with the theoretical results. The conclusions derived from the previous analysis suggest that the noise-only covariance matrix, obtained as product of an OD, represents to a high degree of accuracy the uncertainty of the state when only measurement noise is present (and properly weighted). Moreover, that the observed covariance and the noise-only covariance are statistically equal covariance matrices.

4.1.2 Test Case B

Test case B addressed the effect of errors in the modelling of the atmospheric drag force and its impact in the degradation of covariance realism. A similar analysis to test case A is presented with initial similar conclusions. Noise-only estimated covariance matrices show little differences between them (as seen in Figure 17) and it might lead to the wrong conclusion that the different orbit determinations are consistent among them and that the covariance matrix is a good measure of the orbital state uncertainty.

Although having introduced a perturbation in the models, a good fit of the orbit determinations is observed (inspecting Figure 16). The rationale is simple and described in section 2.1.3.1, as the estimation of the drag coefficient averages out dynamic model errors. This is clearly observed by looking at Figure 18, where a perfect correlation between the introduced perturbation and the error incurred in the estimation the drag coefficient is appreciated. At first, the introduction of a model error does not seem to modify the orbital state or the computed covariance, however the uncertainty realism degradation will come with the propagation of the noise-only covariance.

From Figure 19, Figure 20 and Figure 21 the effect of the perturbation in the atmospheric force model is observed to produce a strong drift in the along-track direction, observed to be quadratic with time as the orbital differences rapidly grow with propagation (see Figure 22). A perturbation in the atmospheric model of the drag force yields a divergence in the orbital differences with a strong dependence on the propagation time.

The analysis of containment for the noise-only covariance matrix (see Table 13) demonstrates that noise-only covariance is a poor representation of the state uncertainty when dynamic model errors are present, as its consistency and realism degrade with the propagation time. Note that only in the estimation epoch does the noise-only covariance comply with the containment theoretical metrics and as it is propagated further from the estimation epoch its metrics worsen. The very reason of the Covariance Determination methodology is to provide a correction to the unrealistic noise-only covariance, through the consider parameters, so that a consider covariance adjusts to a more realistic representation of the state uncertainty.

The results of the Covariance Determination for the estimation atmospheric drag consider parameter perfectly recovered the input model error uncertainty, as shown in Table 14. The containment metrics (Table 13) as well as Figure 23 and Figure 24 verify that the consider covariance is able to capture the true state uncertainty by means of the estimation of the consider parameter, while the noise-only matrix becomes a poor representation of the state vector uncertainty. Mainly, the uncertainty degradation is observed in the along-track direction where the consider parameter provided a remarkable improvement of covariance realism.

A relevant conclusion is obtained from inspection of Figure 25, where the contribution of a unitary consider parameter to the correction of the noise-only covariance matrix is represented. The effect of such consider parameter is to add uncertainty in the variance of the C_D component, as an error in the atmospheric model will yield perturbations in the estimation of the drag coefficient. The growth in the variance of the along-track position term comes as a result of the propagation mechanism of the covariance matrix, which translates the uncertainties of the drag coefficient to uncertainties in the along-track position. Hence, the atmospheric drag consider parameter will only have an impact in the covariance realism degradation of the along-track position.

The key conclusions of test Case B are:

- A successful validation of the atmospheric drag force model consider parameter and its effect on covariance unrealism, through extensive analysis of the results at display, is provided.
- The successful validation of the Covariance Determination methodology in its aim to correct for covariance unrealism when model errors are present, but unconsidered, in an orbit determination process.
- The study of the effect of atmospheric drag model errors in the computation and propagation of an orbital state and the derived consequences to the correct representation of state uncertainty. The effect of a perturbation in the atmospheric drag force model is appreciated in the along-track direction, degrading the realism of the noise-only covariance matrix, through an increased uncertainty of the estimated drag coefficient.

4.1.3 Test Case C

Test case C addressed the effect of errors in the modelling of the range bias and its impact in the degradation of covariance realism. Consistency between the different ODs is not observed anymore (Figure 26 and Figure 27) since the perturbation introduced in the range bias yields to an irregular measurement residual distribution, as the weights defined for the processed ODs only account for Gaussian modelled measurements with 0 mean. Hence, the first important conclusion is that distribution of WRMS of the different ODs is not unitary and normally spread around 1. The second important conclusion is that the differences among the different covariance matrices, although being small, are comparatively higher than those showed for the previous cases given the varied quality of the fittings obtained.

From Figure 28, Figure 29 and Figure 30 it can be appreciated that range bias model error translates into orbital differences for all principal directions (along-track, cross-track and radial) being the most noticeable effect observed in the along-track direction (with almost a 1:1 correlation, as at estimation epoch a range bias of 40 m leads to

almost 40 m drift in the along-track direction). Furthermore, for the along-track, normal and cross-track directions its effect in the orbital differences increases with time (Figure 28 to Figure 30). In addition, contrary to test Case B, the influence of the range bias perturbation is not entirely absorbed by any dynamical estimated parameter (i.e. C_D or C_r) of the OD, hence orbital differences among the computed distributions are appreciated at estimation epoch. Finally, from Figure 31 the effect of a perturbation in the range bias with respect propagation time is assessed yielding the following conclusion: analogous to Case B, a perturbation in the range bias leads to a quadratic increase of the along-track position error with respect propagation time. However, for the present case, the range bias introduces a constant and linear effect that are not negligible when compared to the quadratic term.

Orbital differences suggest that the noise-only covariance matrix will fail to capture the true state vector uncertainty, as verified in Table 17, where the containment metrics for the noise-only covariance are provided. To correct for covariance unrealism, the Covariance Determination methodology is applied giving an estimated range bias uncertainty nearly identical to the input perturbation. The containment metrics of the consider covariance are listed in Table 16, where the improvement of covariance realism is demonstrated comparing the obtained values for the different propagations periods to the theoretical values. Moreover, further verification is obtained from inspecting Figure 32, as the degradation of covariance realism for the noise-only covariance is appreciated whereas the consider covariance is found to perfectly fit the observed covariance. Note that not only the along-track direction is corrected estimating the range bias model uncertainty but noticeable contributions are observed in the cross-track and normal directions.

Analogous to the previous test case, the contribution of the range bias consider parameter has been analysed in Figure 34. The main conclusions derived are that its effects are mostly noticeable in the position components of the covariance matrix and in the variance of the estimated drag coefficient. Thus, at estimation epoch, inspecting Figure 32, the noise-only and consider covariance diverge in the variances of the position components. Since the range bias consider parameter also has a considerable effect in the correction of the variance of the drag coefficient, its contribution will be translated to an increased uncertainty of the along-track direction through propagation, similar to that shown for the atmospheric drag consider parameter although comparatively smaller.

The key conclusions of the present case are:

- A successful validation of measurement model consider parameters and its effect on covariance unrealism, through extensive proofing and analysis of the results at display, is provided.
- The study of the effect of range bias model errors in the computation and propagation of an orbital state and the derived consequences to the correct representation of state uncertainty. An uncertainty in the range bias is appreciated to act almost entirely in the along-track direction, with small contributions to the normal and cross-track directions as well. In addition, the variance of the drag coefficient is also affected by it.
- Further validation of the Covariance Determination methodology is provided.

4.1.4 Test Case D

Test Case D addressed the impact of the atmospheric drag force model consider parameter when processing operational orbits to compute an observed covariance using the observed covariance methodology. The difficulties of processing operational-like orbits lie in the scarce number of samples to process and the sensibility of the generated observed covariance to possible outliers.

Similar conclusions to case B are obtained in the processing of the different ODs, in the absorption of the model perturbation by the estimated drag coefficient and in the effect of the perturbation introduced to the propagated orbital differences. Also, covariance containment tests for the noise-only covariance lead to the same conclusion: in the presence of model errors, the noise-only covariance is unable to properly represent the uncertainty of the state estimation problem.

The most noticeable difference for the present test is the addition of normality tests. Normality is critical to ensure that a covariance matrix is realistic, as discussed in 1.2. Two normality tests are provided in which the null hypothesis of normality cannot be rejected, considering a significance level of 5%.

By ensuring that the distribution of orbital differences is normal, the fitting of the consider covariance to the observed covariance complies with the first two requirements of a realistic covariance matrix. The final requirement is verified inspecting the results displayed in Table 20 and Figure 43, where the containment metrics as well as the figure show the improvement in covariance realism of the consider covariance.

Note that comparing both case B and D, some differences are observed at estimation epoch between the observed covariance and the consider covariance. For case B, both covariance matrices appear with the same sigma values at estimation epoch (see Figure 23) whereas in case D, although having identical set up, some divergence is observed between the observed and consider covariance matrices. This is due to the fact that in case D, the estimation epoch does not coincide with the epoch of the last measurement and orbital differences appear to be somewhat bigger than they should be.

The key conclusions of the present case are:

- The Covariance Determination algorithm has been validated together with its use with operational like orbits in a close-to-reality simulation environment.
- The relevance of modelling atmospheric drag model errors in operational orbits is proved with the conclusions extracted from this test case, as containment and consistency metrics have demonstrated that the consider covariance provides a realistic representation of the true state uncertainty.

A meticulous validation methodology was presented in section 2.7 together with consistent metrics to test for covariance realism and asses the performance of the Covariance Determination methodology. The methodology has been systematically validated through different test case and important insights in the effect of model perturbations were derived. Next section will comment on the solutions obtained after the processing of the Sentinel 3A tracking campaign.

4.2 Discussion on Sentinel 3A results

The present section will provide the author analysis to the results obtained for the processing of the Sentinel 3A orbit determination and posterior Covariance Determination campaign.

First of all, to obtain accurate solutions for the different processed ODs, a high-fidelity dynamic model considering several relevant perturbations was employed. Because the Sentinel 3A satellite mission requires a specific set of orbital parameters, station-keeping manoeuvres are executed on a regular basis, approximately once per month. The orbit determination and subsequent propagated states affected by station-keeping manoeuvres were filtered and discarded as the state estimation and prediction they provided was poor.

Once filtered, inspecting Figure 49, a noticeable drift of some of the orbit estimations considered is appreciated. In order to perform a realistic aggregation of orbital differences a more stable period was finally selected (see Figure 48). Despite having carefully removed orbits affected by manoeuvres and unstable periods of radar measurement, the processing required further filtering as the aggregated population of orbital differences was found to be far from normal and affected by few outliers. The author considered a last filter by establishing a rejection criteria looking for the normality of the aggregated orbital differences, where the median of the distribution is used with a certain scaling factor to reject for outliers. The author deemed appropriate to select the median as a more robust metric to define the rejection intervals due to the increased performance in the presence of strong outliers and skewed data (from [Manikandan, 2011]). Several scaling factors were tried giving different results, however the most promising result turned out to be $k = 3$ (see Table 30). Any scaling factor below 3 would provide a normal distribution in the along-track direction although rejection rates would increase substantially, thus not providing a realistic representation of the distribution of orbital differences.

Normality is ensured in the along-track direction, however for the normal and cross-track direction the hypothesis of normality does not hold true. The first condition for covariance realism is violated as seen in Table 31, where the average of the orbital differences at different propagation epochs is seen to experience non-negligible biases. The second condition for covariance realism is not fulfilled as the multivariate PDF sampling of the state estimation displays a behaviour far from Gaussian. Normality is rejected for the N and W directions from inspection of Figure 51 and Figure 52 and from [Vallado & Seago, Covariance realism, 2009], multivariate normality cannot be assumed. Thus covariance realism cannot be achieved since the observed orbital differences cannot be approximated as a multivariate Gaussian distribution. From this point forward, only the covariance realism of the along-track direction is discussed as it has been demonstrated to be the single direction displaying unbiased normally distributed orbital differences.

The aggregation of the orbital differences in the along-track direction for the filtered orbits is displayed in Figure 54. The figure provides a first measure of the typical standard deviation of the orbital differences which are in the order of 30 metres. For the remaining two directions the standard deviation is around 70 metres for the W direction (out-of-plane) and 7 metres for the N direction Typical standard deviations for the noise-only covariance matrices estimated from the ODs are in the order of 10 m for the along-track direction, 10 m for the out-of-plane direction

and 3 m for the cross-track direction. Comparing both covariance matrices, it is clear that the noise-only covariance matrix fails to properly represent the real uncertainty of the state vector at estimation epoch and during propagation. Huge differences are appreciated and the author considers that the following phenomena might be the cause for them:

- Covariance matrix fails to represent the real uncertainty of the state vector if measurement or dynamic models errors are unconsidered, as seen during the validation and verification.
- Such huge differences were not appreciated during the verification and validation test cases, as a single fixed systematic error for the whole orbital arc was assumed. In reality, the error of the dynamic and measurement continuously varies. Moreover, real measurements and satellite dynamics are affected by numerous perturbations at the same time.
- The relevant non-normal orbital differences appreciated in the out-of-plane direction are a consequence of the poor performance exhibited by the radar station in terms of angular measurements. Due to highly variable and extremely large angle measurement biases and residuals of the LeoLabs MSR radar (see section 3.2.1.3), the use of range and range-rate measurements only is advised yielding a state estimation that lacks sensitivity in the out-of-plane component and is highly dependent on the problem geometry, as suggested by [Wiegel & Patyuchenko, 2011].

At this point, two conclusions are clear: that the distribution of orbital differences is not normally distributed, thus covariance realism is not achievable, and that different aspects influence the huge differences observed between noise-only and observed covariance that yield an unrealistic representation of uncertainty. As of this point, the Sentinel 3A case is analysed using the same methodology introduced during the validation cases. Inspecting the quality of the different ODs (from Figure 55) one may think that the processed measurements have been given a too pessimistic weight, due to the low average value of WRMS. However, the calibration process results (see Table 27) provided the true weights that the processed measurement should exhibit. Normally, OD processes fail to realistically represent measurement residuals, giving fairly optimistic values and averaging out measurement noise (regarding it as Gaussian) while unsuccessfully removing other effects such as biases.

In addition, the different processed ODs have delivered different covariance matrices, as the different epochs of estimation, number, quality and geometry of the measurements processed varies all over the year and influence the solution provided by the estimation process (see Figure 56). The Covariance Determination methodology is highly sensitive to variations in the assumed a-priori noise-only covariance and the OD batch selected to perform the fitting. Therefore to provide a feasible analysis of the estimated variance of the consider parameter, each covariance matrix is fitted to the observed covariance and a study of the distribution of consider parameters is done. As one may expect, none of the noise-only covariance matrices are able to capture the true uncertainty of the orbit estimation problem as demonstrated in test Case B, C and D.

Furthermore, it is no secret that the atmosphere is a highly variable stochastic environment and that the different parameters that are used in the modelling of the atmospheric drag force also exhibit a remarkable variation from OD solution to OD solution (i.e. atmospheric density, attitude of the satellite, drag coefficient, etc.). In the atmospheric drag consider parameter, the effect of the uncertainty of the different parameters is absorbed, however from OD to OD the uncertainty of the modelled parameters will vary. For this reason, it is more sensible to estimate a consider parameter per batch and study the behaviour of the whole distribution of values rather than assuming a fixed value for the complete year of predicted and estimated orbits.

Because bigger orbital differences are observed in the along-track direction and because this direction is the single one experiencing a normally distributed evolution of the orbital error (either in estimation and propagation) the covariance realism upgrade is sought in the along-track direction by means of estimating an atmospheric drag consider parameter. Processing the different batches using the Covariance Determination methodology gave a distribution of estimated consider parameter with a mean value of 45.47 % error in the atmospheric drag model error with a standard deviation of 11.41% (see Figure 57). The relevance of the computed value of 45.47% of error in the drag force model comprises the contribution of the different sources of uncertainty in the definition of the main relevant parameters, i.e. the ballistic coefficient and the atmospheric density. Recall that atmospheric density uncertainty is in the order of 15-20% (considering low to medium solar activity) and that the ballistic coefficient can vary up to an order of magnitude from its nominal value. Assuming that the computed value of the consider parameter is not only absorbing uncertainties of the atmospheric drag force model but other non-modelled effects, the computed value is considered by the author to be a representative approximate measure of the uncertainty of the drag force model.

Like a station calibration process, the Covariance Determination methodology averages out the differences between the consider covariance and the noise-only covariance estimating the variance of the consider parameter. However, as depicted in Figure 58, there are other relevant phenomena that are not modelled in the atmospheric drag consider parameter that affect the covariance realism in the along-track, cross-track and normal direction. It is highly possible that some of this phenomena are partially absorbed in the estimation of the atmospheric drag consider parameter. For this reason, the distribution of estimated values represents an approximate measure of the atmospheric model uncertainty but not a definitive value.

The selected containment metrics employed in the validation of this case intend to mimic the Mahalanobis distance metric used in the validation and verification cases. In this case, as only the orbital differences in the along-track direction can be considered Gaussian, a containment test is performed by considering the percentage of points of the distribution that fall inside of $k-\sigma$ envelopes and compared with theoretical value of a normal univariate Gaussian distribution. The containment metrics listed in Table 32 (right) display a solid improvement of covariance realism when compared with the metrics obtained for the noise-only covariance (see Table 32, left). A graphical interpretation of the result is found in Figure 58, where the consider covariance achieves a covariance realism improvement in the along-track direction with respect to the noise-only covariance.

A second case is provided where both a dynamic and measurement model consider parameter are estimated. The resulting distribution of values are presented in Figure 59 and Figure 60, where the mean value of the atmospheric model uncertainty has slightly decreased when compared to the previous case (as the range bias uncertainty also impacts the along-track direction) and the range bias uncertainty displays a central tendency around the 35 m and a far from normal distribution affected by heavy outliers.

The containment metrics for the second case are listed in Table 33, where an improvement on covariance realism is achieved, as the range bias uncertainty is able to reduce the differences between the consider covariance and the observed in the along-track direction, especially at epochs close to the estimation epoch. This is also appreciated by looking at Figure 61. The conclusion is that the atmospheric drag consider parameter affects the uncertainty in the along-track direction showing a stronger correlation with propagation (as expected) while the range bias consider parameter provides a scaling of the covariance matrix in the along-track direction already noticeable at estimation epoch (compare between Figure 61 and Figure 58, or Table 33 and Table 32). Furthermore, comparing Figure 61 and Figure 58 a clear covariance realism upgrade of the normal and cross-track directions is achieved, yielding to the conclusions that there are other relevant contributions to the covariance realism problem that are not modelled through the atmospheric drag consider parameter.

The author considers this case to be relevant as it indicates the need for a better understanding on the additional driving uncertainties affecting the realism of covariance for LEO objects, which may be modelled through the consideration of other dynamic and measurement model consider parameters. In addition, the author considers the computed value of the range bias to lack realism, due to the great dispersion of the solutions and because the estimated parameter is correcting the covariance of a non-Gaussian uncertainty.

4.3 Discussion on research questions

During the following section, the different research questions posed in this report will be answered with the results presented during Section 3 and the discussion presented in Section 4.

To the question *“To what extent do dynamic and measurement modelling inaccuracies impact the state estimation and prediction problem, i.e. the provision of an accurate state and a realistic covariance?”*

During the validation cases B and C, the effect of different dynamic and measurement model uncertainties has been assessed, more concretely inaccuracies in the modelling of the atmospheric drag force and the range bias.

From Case B, the effect of a perturbation in the drag force is found to affect the estimation of an accurate drag coefficient. In the estimation process, any perturbation of the dynamics can be averaged out by estimating the drag coefficient. This does not affect the provision of an accurate position and velocity in the estimation of the orbit but it does affect the prediction of the future state, as the inaccurate drag coefficient has a direct impact in the state during the propagation. In the end, an increasing along-track error is observed that depends quadratically on the propagation time. In the covariance field, all the aforementioned conclusions lead to a covariance realism degradation of the noise-only covariance dependent on the propagation time and exclusive to the along-track direction.

From Case C, the effect of a perturbation in the range bias is found to affect the estimation of an accurate state (being the most important contribution in the position components). Thus, contrary to the case presented before,

position and velocity errors are observed at estimation epoch and increase during the propagation in a quadratic fashion for the along-track direction (as it is the direction that is observed to be more affected by a perturbation of the range bias). This is also observed in the covariance, where the uncertainty is found unrealistic in all directions at estimation epoch and the covariance realism degradation grows with propagation.

To the question: *"How can dynamic and measurement modelling uncertainties be characterized in the theory of the consider parameters using a Weighted Batch Least-Squares estimator?"*

Dynamic and measurement model uncertainties need to be characterized by means of a zero mean and normally distributed random variable. The definition of an atmospheric drag and range bias consider parameter is described thoroughly in this report, together with the added formulation required for the adaptation of Weighted BLS algorithm to include these parameters and the consider parameter theory. An analogous process can be followed to define further consider parameters trying to model the uncertainties of different dynamic and measurement model uncertain parameters.

Consider parameters are included in a different space, namely the consider space, different from the estimation space, where state vector and desired dynamic parameters are to be determined by the least-squares algorithm. As detailed during the methodology section of this report, consider parameters do not affect the results of the estimation problem due to its formulation yet affect the covariance provided by the least-squares problem, adding the uncertainty of consider parameters to the noise-only covariance matrix.

To the question: *"To what extent does the Covariance Determination methodology improve the covariance realism of regular orbit determination and propagation products?"*

During the validation cases, the Covariance Determination algorithm has been tested displaying the performance to correct covariance unrealism of orbit determination and propagation products. During the validation cases, the covariance realism improvement is such that the resulting consider covariance is found to be identical to the empirical uncertainty of the state estimation and prediction problem. On the contrary, it is also demonstrated that the noise-only covariance, product of the OD, fails to properly represent the real uncertainty of the estimation and propagation process and that the unrealism depends on the magnitude of the unconsidered uncertainty.

Thus, through the different validation cases, the need for a covariance realism improvement methodology turned out to become essential in the presence of unconsidered uncertainty sources. In addition, the proposed methodology proved to be sufficiently powerful to treat for a sample of such unconsidered sources. For this reason, the author consider that the validation of the devised methodology is completed successfully and that its power and utility are broadly demonstrated.

However, when it came to dealing with real orbit determination and propagation processes, the methodology proved unfeasible. The processed orbits displayed inconsistent errors when compared to POD solutions yielding a non-Gaussian behaviour of the orbit estimation and propagation processes. Orbital errors and residuals were expected to behave as white noise (Gaussian) considering the lapses of propagation times, the accuracy of the used SST sensors and the scale of the treated uncertainties. However, this was not true for the considered orbits, reason for which the methodology could not be applied to its full extent. Normality is proved in the along-track direction, reason for which a variance realism improvement is carried out successfully leading to the estimation of a representative distribution of atmospheric drag consider parameters. The results show that the methodology achieves remarkable results as long as the hypothesis posed during its development are fulfilled.

To the question: *"To what extent does the proposed validation methodology reflect the fitness and power of the Covariance Determination methodology?"*

The proposed validation methodology tackles the different cases devised both from the orbit determination and covariance realism perspective. Because the validation of the methodology requires the processing of perturbed ODs it is mandatory to check the quality of the state estimation problem and verify that the numerical results comply with the theory.

First of all, from the OD perspective the simulated radar measurements and processed ODs are analysed qualitatively to ensure that enough tracks and low measurement rejection rates are achieved. By measuring the WRMS of the processed ODs it is ensured that the residuals are properly modelled considering and by measuring

the different noise-only covariance matrices of the ODs it is verified that the uncertainty for the complete set of estimation processes is nearly identical.

From the covariance realism perspective, several metrics are defined as suggested by numerous relevant references to test for uncertainty realism. First of all, normality of the orbit errors in both estimation and prediction is verified by inspecting the average value of the distribution and the shape of the spread through the use of the Michael's normality test. When normality of the different univariate distributions of position is ensured, containment of the whole multivariate distribution is checked using the Mahalanobis distance. The aforementioned metric determines the degree to which the uncertainty, characterized by means of a covariance matrix, represents the real uncertainty of the state estimation and prediction problem comparing the statistics obtained with the numerical results versus the theoretical statistics of containment.

Thus, the validation methodology is able to check the quality of the processed ODs and analyse the covariance realism of any covariance matrix allowing to obtain remarkable insight.

To the question: *"To what extent are the present results of the study on covariance realism improvement of a satellite tracking campaign of the Sentinel 3A satellite representative of the inaccuracies of real dynamic and measurement models?"*

The results obtained for the Sentinel 3A case in terms of covariance realism need a careful consideration. First of all, recall that the resulting orbital differences obtained between estimated/propagated orbits and POD solutions cannot be regarded as Gaussian distributions. Thus the Covariance Determination methodology could not be applied in its full extent.

The author considers the results obtained, i.e. the atmospheric drag consider parameter, to be an approximate representation of the real uncertainty of the atmospheric drag model. Given the different uncertainty sources to be regarded (atmospheric density defined from atmospheric models, cross-sectional area variation, drag coefficient definition, varying mass and velocity) the computed result provides a feasible approximation of the true uncertainty of the atmospheric drag force model. However, there are more contributions to the uncertainty unrealism rather than just the modelling of the atmospheric drag force and for this reason the author considers that the computed value is somehow compensating for them as well.

For future covariance realism corrections, the computed results can be used as a first approximation of the uncertainty of the atmospheric drag force model (taking into account that the value has a certain variability, expressed through the standard deviation of the distribution).

The author proposes a series of recommendations in the next chapter that seek to improve the usefulness of the devised methodology based on further developing of the research presented in this project or the study of the inconsistencies encountered during the processing of the real orbits of the Sentinel 3A satellite.

The novelty and uniqueness of the devised methodology is properly addressed and discussed during Section 1.2.3. The author considered that the reader would acquire a better interpretation of the differences of the conceived methodology with respect similar to techniques when these are presented.

This chapter concludes the discussion of the presented results and provides the point of view of the researcher in the matter and the conclusions at which the author arrived through careful examination of the data and literature available. Finally, next chapter will provide the main conclusions of this research project and the recommendations to continue the work presented here.

5

CONCLUSIONS AND RECOMMENDATIONS

This research project has presented a novel methodology, named Covariance Determination, to fulfill the scientific aim expressed in the following statement:

"Conceptualize, develop, implement and validate a novel methodology to achieve a covariance realism improvement during state estimation and orbit prediction using the theory of the consider parameters in batch least-squares estimators".

The Covariance Determination methodology intends to become an alternative technique for covariance unrealism mitigation, suitable for any type of object and SST sensor measurement considered during a regular OD and orbit propagation process. The very motivation for the development of this technique is the major relevance of the covariance in the provision of accurate SST and STM services. Covariance is key to many SST products that will become essential if a sustainable and feasible space exploitation is to be achieved and maintained in the near future.

The methodology presented in this work lays its foundations in the theory of the consider parameters and modifies a Batch Least-Squares OD algorithm to introduce physically meaningful corrections in the computation of the covariance matrix. The consider parameters theory corrects a noise-only covariance matrix by adding the uncertainty of several modelled consider parameters, accounting for measurement and dynamic model uncertainties. During the introduction and methodology section, the most relevant sources of uncertainty have been defined and discussed through an extensive review of existing literature. In a later section, several consider parameters are defined in order to account for the driving uncertainties of the covariance unrealism problem of a LEO object.

Several metrics of covariance realism are investigated and implemented, from relevant literature in the matter, to test for the fitness and performance of the Covariance Determination methodology. Namely, three main features of a distribution of orbital differences are tested: whether the average of the distribution lies near to the true value (i.e. unbiased estimation), whether the distribution of each element of the state vector can be considered as a univariate normal distribution and whether the dispersion of the distribution complies with the tested covariance matrix. A MC chain is presented to generate the required input for the validation of the methodology, in which a set of different orbit determinations are performed, affected by a systematic perturbation in either a dynamic or measurement model parameter. The aim of the methodology is to capture the underlying uncertainty of the models (expressed by means of the aforementioned perturbation) estimating the contribution of a physically meaningful consider parameter through the Covariance Determination methodology.

The results are of paramount relevance as they establish a clear conclusion that is common to different validation cases: the estimated covariance matrix of an orbit determination (i.e. a noise-only covariance matrix) is unable to provide a realistic characterisation of the state uncertainty when model errors are present but unconsidered, as usual in classical orbit determination, and its realism degrades with orbit propagation. Thus, the need for estimating certain consider parameters to characterise the uncertainty of the models involved becomes critical.

Inspecting the first three test cases many relevant insights can be derived:

- Considering unbiased measurements perturbed by Gaussian white noise, Case A showed that the covariance matrix derived from an orbit determination provides a proper definition of the state uncertainty, in the absence of model errors and provided that measurements are properly weighted.

- Case B reveals that the effect of a perturbation in the atmospheric drag model yields a drift on the along-track direction of the predicted state, whereas the perturbation at estimation epoch is absorbed on the estimated drag coefficient. The drift experienced in the along-track direction during the prediction of the orbit is quadratically related to the perturbation introduced, as one may expect from the acceleration of the atmospheric drag, as it acts through the tangential direction and is related to the along-track position by a double integration. The consider covariance, fitted to the observed covariance through the use of a dynamic consider parameter, has shown to provide a realistic representation of the state uncertainty. Hence the modelling of a dynamic consider parameter is validated from this test case. Note that the atmospheric drag force model consider parameter is only correcting for uncertainty unrealism in the along-track direction, as any perturbation of the model will be expressed in this direction through propagation.

- Case C reveals the effect of an error in the definition of the range measurement model, which yields a drift in all directions having a most noticeable effect in the along-track direction. An error in the range measurement model is shown at estimation epoch, having almost a 1:1 correlation with respect to the drift observed in the along-track direction. The consider covariance, fitted to the observed covariance through the estimation of a measurement model consider parameter has been proven to provide a realistic representation of the state uncertainty, hence the modelling of a measurement model consider parameter is validated from this test case. The range measurement model consider parameter will correct for uncertainty realism mainly in the along-track direction as well as having a minor impact in the cross-track and normal directions.

- Case D aimed to test the methodology in a realistic environment with simulated operational orbits. The results are analogous to test case B, successfully ending the validation process of the Covariance Determination methodology.

The practical application of the Covariance Methodology results in the processing of the Sentinel 3A satellite measurements provided by LeoLabs. SST radar measurements covering one year of measurements were processed, providing a set of estimated orbital states and predicted orbits. To characterize the evolution of the uncertainty during propagation, predicted orbits were compared against the true state of the satellite, assumed to be the state estimated via POD. The previous analysis yielded a set of orbital differences that, aggregated through prediction time, represent a sampling of the probability density function of the orbital state estimation and prediction. The first conclusion derived from the analysis of orbital differences is that the noise-only covariance matrix, as already verified in the validation cases, does not provide a trustworthy representation of the orbital state uncertainty.

The quality of the estimated ODs is observed to be highly time-varying due to the availability of the measurements, the geometry of the problem, the manoeuvres performed by the satellite and the quality of the measures for the batch considered. A priori, after filtering out batches affected by satellite manoeuvres, some estimated orbits displayed large dispersions with respect to the true state. To further remove outliers two different criteria were established: a certain period within the complete year of measurements is selected as orbital differences appear to be consistent and a rejection criteria for possible outliers is established to discard spurious states through the scaled median of the distribution. The resulting orbital differences are tested for normality and the following conclusions are drawn: only orbital differences in the along-track direction can be assumed as normal while cross-track and normal differences do not pass the normality test.

Covariance realism is no longer feasible in the orbit estimation and prediction of the Sentinel 3A tracking campaign using only LeoLabs measurements. In light of the events, the author showed the performance of the methodology by displaying univariate containment metrics of the along-track direction, where a covariance realism upgrade of the estimated consider parameter can be observed. The results yield unequivocal conclusions: a covariance realism improvement is achieved as containment metrics improve when a dynamic consider parameter is estimated, correcting for the uncertainty of the atmospheric drag model.

Not only does the methodology provide a covariance realism improvement but also a significant value for the uncertainty of the atmospheric drag model is obtained. Typical values for the uncertainty of the drag force model are found to be distributed around 45% of relative error with a standard deviation of 11 %. Note that these values are representative of the joint uncertainty of the different parameters that define the atmospheric drag, namely the atmospheric density model, the attitude of the spacecraft, solar and geomagnetic activity. Therefore, a variability

of the uncertainty of the atmospheric drag model from OD to OD is expected as the aforementioned parameters vary with time and space.

To conclude to work presented in this Master Thesis, the author presents several recommendation which intend to be the guideline for future research on covariance realism improvement of SST tracking campaigns:

- Further research is required to understand the cause of the non-Gaussian orbital differences obtained. The author advises collecting measurements from different well-characterized SST sensors (i.e. radar and optical telescope). In particular, the author suggests employing radar measurements with better angular accuracy and better characterised biases or additional optical telescope measurements, as the observability of the problem would improve. In particular, the author strongly advises to use angle measurements obtained from optical telescopes as the typical noise for right ascension and declination measurements of SST optical telescopes is of 0.7 arc-seconds (from [Siminski, Weigel, & Fiedler, 2014]), compared to the 0.2 to 10 degrees typical noise from LeoLabs angular measurements. The author considers that these implementations would yield to a normally distributed aggregation of orbital differences, and a covariance realism analysis would be feasible.

- The author considers that computing orbital differences averaged through an entire orbital period would increase the quality of the observed covariance matrices obtained, as a more stable evolution of the covariance matrix could be derived. Additionally, the author expects the resulting distributions of orbital differences to be more prone to normality, provided that other underlying causes for non-Gaussianty are treated and corrected.

- Objects orbiting in the LEO regime are exposed to a wide variety of orbital perturbations. From the literature review, the author deemed the uncertainty of the atmospheric drag force model to be the most relevant uncertainty contribution. However, other orbital perturbation uncertainties may play an important role depending on the circumstances of the case, hence these should be modelled by means of additional consider parameters in order to correct other relevant contributions that affect the uncertainty realism of the estimated and predicted state.

- From relevant literature, the uncertainty concerning the drag force model and particularly that of the atmospheric density model are considered to be highly correlated with time and space. During the present work, this uncertainty has been considered as a Gaussian white noise not correlated with time or space. Several studies suggest the characterisation of the atmospheric drag force model uncertainty by means of a Gaussian noise model dependent on time. Different models can be considered and are available such as the random walk model, the Brownian motion model or the Ornstein-Uhlenbeck process (see [Schiemenz, Utzmann, & Kayal, 2019], [Siminski J. , 2016] and [Sagnieres & Sharf, 2017]). For future work, the author considers that the definition of a Gaussian time dependent atmospheric drag consider parameter would improve the results displayed so far.

- The implementation and the cases discussed consider objects orbiting in the LEO regime, where the atmospheric force is usually the most relevant contribution to the uncertainty realism problem. As mentioned, the methodology is devised to work for all types of objects and measurements, thus for future work the author suggests the implementation of the modelled solar radiation pressure consider parameter, as well as the validation and verification of the implementation through a test case considering a simulated GEO orbiting object. Ultimately, a covariance realism improvement could also be achieved for GEO or even Geostationary Transfer Orbit (GTO) objects, where the solar radiation pressure is the main perturbing force.

The results of this research project have led to the publication and presentation of a peer-reviewed conference paper in the 70th International Astronautical Congress (IAC) held in Washington, on October 2019, and a conference paper to be defended in the 2nd IAA Conference on Space Situational Awareness (ICSSA), to be held in Washington on January 2020. Both papers are attached to this document as an Appendix.

Bibliography

Akella, M. R., Junkins, J. L., & Alfriend, K. T. (1996). Non-gaussian error propagation in orbital mechanics. *Journal of Astronautical Sciences, 44*.

Alfano, S. (2005). A numerical implementation of spherical object collision probability. *Journal of the Astronautical Sciences, 53*, 103-109.

Anderson, R., Born, G., & Forbes, J. (2009, 8). Sensitivity of Orbit Predictions to Density Variability. *J. Spacecraft and Rockets*. doi:10.2514/6.2008-6443

Argenteiro, P., & Lynn, J. J. (1974). *Estimation strategies for orbit determination of applications satellites.* techreport, GSFC (Goddard Space Flight Center), NASA. Retrieved from https://ntrs.nasa.gov/archive/nasa/casi.ntrs.nasa.gov/19740011388.pdf

Aristoff, H., & Poore, S. (2014). Error estimation and control for efficient and reliable orbit (and uncertainty) propagation. *24th AAS/AIAA Space Flight Mechanics Meeting.*

Aristoff, H., & Poore, S. (2014). Non-linear uncertainty propagation in orbital elements and transformation to Cartesian space without loss of realism. *2014 AAS/AIAA Astrodynamics Specialist Conference.*

Aristoff, P. (2012). Implicit Runge-Kutta methods for uncertainty propagation. *2012 Advanced Maui Optical and Space Surveillance Technologies Conference.*

Aristoff, P. (2014). Orbit and uncertainty propagation: a comparison of Gauss-Legendre-, Dormand-Prince-, and Chebyshev-Picard-based approaches. *Celestial Mechanics and Dynamical Astronomy*.

Aristoff, P. (2014). Realistic state and measurement error uncertainty computation. *Scientific and Technical Report FA9550-12-C-0034, Numerica Corporation.*

Bastida, B. (2019). The Future of the Environment (ESA/ESOC Space Debris Office).

Bowman, B., Tobiska, W. K., Marcos, F., Huang, C., Lin, C., & Burke, W. (2008, 8). A New Empirical Thermospheric Density Model JB2008 using New Solar and Geomagnetic Indices. *AIAA/AAS Astrodynamics Specialist Conference and Exhibit.* American Institute of Aeronautics and Astronautics. doi:10.2514/6.2008-6438

Bruinsma, S. L., Sanchez-Ortiz, N., Olmedo, E., & Guijarro, N. (2012). Evaluation of the DTM-2009 thermosphere model for benchmarking purposes. *Journal of Space Weather and Space Climate, 2*, A04. doi:10.1051/swsc/2012005

C. Sabol, K. H., & Schumacher, P. (2010). Linearized orbit covariance generation and propagation analysis via simple Monte Carlo simulations. *20th AAS/AIAA Space Flight Mechanics Meeting.*

CCSDS. (2009, 11). Orbit data messages (blue book). (CCSDS, Ed.) Retrieved from https://public.ccsds.org/Pubs/502x0b2c1.pdf

CCSDS. (2010, 5). Navigation data: definitions and conventions (green book). Retrieved from https://public.ccsds.org/Pubs/502x0b2c1.pdf

Cefola, P. (1972, 9). Equinoctial orbit elements - Application to artificial satellite orbits. *Astrodynamics Conference.* American Institute of Aeronautics and Astronautics. doi:10.2514/6.1972-937

Cerven, W. T. (2011). Covariance error assessment, correction, and impact on probability of collision. *2011 AAS/AIAA Space Flight Mechanics Meeting.*

Chan, F. K. (2008, 3). Spacecraft Collision Probability. *Aerospace Press*. doi:10.2514/4.989186

Chris Sabol, e. a. (2010). Linearized orbit covariance generation and propagation analysis via simple Monte Carlo simulations. *Texas Engineering Experiment Station 334 Wisenbaker Engineering Research Center.*

Craychee, T. A., Carrico, J. P., & Hujsak, R. (2009, 8). Correlating spacecraft debris from various tracking measurements. *AAS/AIAA Astrodynamics Specialist Conference.*

DeMars, K. J. (2010). Nonlinear orbit uncertainty prediction and rectification for space situational awareness. Retrieved from https://repositories.lib.utexas.edu/handle/2152/ETD-UT-2010-12-2596

DeMars, K. J., Bishop, R. H., & Jah, M. K. (2013, 7). An entropy-based approach for uncertainty propagation of non-linear dynamical systems. *Journal of Guidance, Control, and Dynamics, 36*, 1047-1057. doi:10.2514/1.58987

Díez, A., Pastor, A., López-Jiménez, S., Souto, A., García, P., & Escobar, D. (2019, 4). Covariance determination from operational orbits and sensor data. *4th International Workshop on Key Topics in Orbit Propagation Applied to Space Situational Awareness.*

Drummond, O. E., Jr., A. J., & Waugh, S. (2006). On target track covariance consistency. *SPIE Conference on Signal and Data Processing of Small Targets.*

Drummond, O. E., Ogle, T. L., & Waugh, S. (2007, 9). Metrics for Evaluating Track Covariance Consistency. (O. E. Drummond, & R. D. Teichgraeber, Eds.) *Signal and Data Processing of Small Targets 2007, Proc. of SPIE Vol. 6699, 669916, (2007*. doi:doi:10.1117/12.740303

Duncan, M., & Long, A. (2006, 8). Realistic Covariance Prediction for the Earth Science Constellation. *AIAA/AAS Astrodynamics Specialist Conference and Exhibit.* American Institute of Aeronautics and Astronautics. doi:10.2514/6.2006-6293

Emmert, J. T. (2015, 9). Thermospheric mass density: A review. *Advances in Space Research, 56*, 773-824. doi:10.1016/j.asr.2015.05.038

Emmert, J. T., Warren, H. P., Segerman, A. M., Byers, J. M., & Picone, J. M. (2017, 1). Propagation of atmospheric density errors to satellite orbits. *Advances in Space Research, 59*, 147-165. doi:10.1016/j.asr.2016.07.036

ESA. (2009). Mathematical Models and Algorithms. *NAPEOS.* Retrieved from http://hpiers.obspm.fr/combinaison/documentation/articles/NAPEOS_MathModels_Algorithms.pdf

ESA. (2017). Space Situational Awareness - Detecting Space Hazards (brochure). Retrieved from https://www.esa.int/Safety_Security/SSA_Programme_overview

ESA-Sentinel. (2019). *Satellite Parameters for POD of the SENTINEL 3A mission*. (ESA, Editor) Retrieved from https://sentinels.copernicus.eu/web/sentinel/technical-guides/sentinel-3-altimetry/pod/satellite-parameters;jsessionid=A97AC4F0ADF56FD99D388CFFF985483F.jvm1

ESA-SSA. (2011). Space Situational Awareness - Space Weather Customer Requirements Document. Retrieved from http://swe.ssa.esa.int/DOCS/SSA-SWE/SSA-SWE-CRD-1001_i4r5a.pdf

ESOC-(ESA). (2019). ESA's Annual Space Environment Report. Retrieved from https://www.sdo.esoc.esa.int/environment_report/Space_Environment_Report_latest.pdf

European-Comission. (2018). Proposal for a regulation of the european parliament and of the council : establishing the space programme of the Union and the European Union Agency for the Space Programme and repealing Regulations (EU) No912/2010, (EU) No 1285/2013, (EU) No377/2014 and Decision541/2014/EU.

Flegel, S. K., & Bennett, J. (2018). Normality in State Uncertainties from Orbit Determination results fitting Optical Measurements. *The Advanced Maui Optical and Space Surveillance Technologies Conference.*

Folcik, Z., Lue, A., & Vatsky, J. (2011, 9). Reconciling covariances with reliable orbital uncertainty. *Advanced Maui Optical and Space Surveillance Technologies Conference*, (p. E34). Retrieved from http://adsabs.harvard.edu/abs/2011amos.confE..34F

Foster, J. L., & Frisbee, J. H. (1998). *Position error covariance matrix scaling factors for early operational ISS debris avoidance.* Tech. rep., Johnson Space Center.

Ghrist, R. W., & Plakalovic, D. (2012). Impact of non-Gaussian error volumes on conjunction assessment risk analysis. *2012 AAS/AIAA Astrodynamics Specialist Conference.*

Griffith, N., Nicolls, M., Lu, E., & Park, I.-K. (2017). Orbit determination perfomance of the LEOLABS radar network. *1st IAA Conference on Space Situational Awareness, Orlando, FL, USA.*

Gronchi, G. F., Baù, G., & Milani, A. (2016, 9). Keplerian integrals, elimination theory and identification of very short arcs in a large database of optical observations. *Celestial Mechanics and Dynamical Astronomy, 127*, 211-232. doi:10.1007/s10569-016-9725-9

Heiner Klinkard, B. F. (1998). Orbit and Attitude Perturbations due to Aerodynamics and radiation pressure. *ESA Workshop on Space Weather*. doi:10.1.1.621.4598

Hill, K., Alfriend, K., & Sabol, C. (2008, 8). Covariance-Based Uncorrelated Track Association. *AIAA/AAS Astrodynamics Specialist Conference and Exhibit.* American Institute of Aeronautics and Astronautics. doi:10.2514/6.2008-7211

Horwood, J. T., & Poore, A. B. (2012). Orbital state uncertainty realism. *2012 Advanced Maui Optical and Space Surveillance Technologies Conference.*

Horwood, J. T., Aristoff, J. M., Singh, N., Poore, A. B., & Hejduk, M. D. (2014, 6). Beyond covariance realism: a new metric for uncertainty realism. In O. E. Drummond (Ed.), *SPIE Proceedings: Signal and Data Processing of Small Targets.* SPIE. doi:10.1117/12.2054268

Horwood, J., & Poore, A. B. (2012, 9). Orbital State Uncertainty Realism. *Advanced Maui Optical and Space Surveillance Technologies Conference*, (p. 48). Retrieved from http://adsabs.harvard.edu/abs/2012amos.confE..48H

John Emmert, H. W., & Segerman, A. (2014). Propagation of forecast errors from the Sun to LEO trajectories: How does drag uncertainty affect conjunction frequency? *2014 Advanced Maui Optical and Space Surveillance Technologies Conference.*

JSpOC. (2019). *Space-Track webpage*. Retrieved from https://www.space-track.org

Julier, S. J., & Uhlmann, J. K. (2004, 3). Unscented Filtering and Nonlinear Estimation. *Proceedings of the IEEE, 92*, 401-422. doi:10.1109/jproc.2003.823141

K. DeMars, & Jah, M. K. (2013). An entropy-based approach for uncertainty propagation of non-linear dynamical systems. *Journal of Guidance, Control, and Dynamics*.

K. Hill, K. H., & Jah, M. K. (2010). Covariance based scheduling of a network of sensors. *2010 AAS Astrodynamics Symposium.*

Kelso, T. S. (2019). Analysis of the Iridium 33-Cosmos 2251 collision. *Amercian Astronautical Society, AAS 09-368*. Retrieved from https://amostech.com/TechnicalPapers/2009/Iridium_Cosmos_Collision/Kelso.pdf

King-Hele, D. (1987). Satellite orbits in an atmosphere. Theory and applications. *Satellite orbits in an atmosphere. Theory and applications.. D. King-Hele. Blackie and Son Ltd., Glasgow, UK. 11+ 291 pp. Price£ 49.00 (1987). ISBN 0-216-92252-6.*

Klinkard, H. (2006). *Space Debris: Models and Risk Analysis* (1 ed.). Springer and Praxis Publishing.

Krag, H. (2019). The Space Debris Environment (ESA/ESOC Space Debris Office).

Kuang, D., Desai, S., Sibthorpe, A., & Pi, X. (2014, 1). Measuring atmospheric density using GPS–LEO tracking data. *Advances in Space Research, 53*, 243-256. doi:10.1016/j.asr.2013.11.022

Lafontaine, J., & Hughes, P. (1982, 1). A modified Jacchia 1977 Model Atmopshere and its Aplications to Orbit Determination. *Celestial Mechanics, 29*, 3-26. doi:10.1007/bf01358595

Laurens, S., Seimandi, P., Couetdic, J., & Dolado, J. C. (2017). Covariance matrix uncertainty analysis and correction. In F. S. T. Flohrer (Ed.), *7th European Conference on Space Debris. 7*. ESA Space Debris Office. Retrieved from https://conference.sdo.esoc.esa.int/proceedings/sdc7/paper/338/

Lerch, F. J. (1991, 3). Optimum data weighting and error calibration for estimation of gravitational parameters. *Bulletin Geodesiqu, 65*, 44-52. doi:10.1007/bf00806341

Lopez-Jimenez, S. (2019). Literature Study for MSc Thesis - TU Delft.

Lopez-Jimenez, S., Pastor, A., Escobar, D., Setty, S., & Agueda, A. (2019). Towards Covariance Realism in Batch Least-Squares Orbit Determination. *70th International Astronautical Congress (IAC), Washington D.C., United States, 21-25 October 2019*.

M.D. Hejduk, L. C. (2016). *Evaluating Probability of Collision Uncertainty*. Retrieved from https://ntrs.nasa.gov/search.jsp?R=20160005313

Mahalanobis, P. C. (1936). On the generalised distance in statistics. *Proceedings of the National Institute of Sciences of India*, *2*, pp. 49-55.

Manikandan, S. (2011). Measures of central tendency: Median and mode. *Journal of Pharmacology and Pharmacotherapeutics, 2*, 214. doi:10.4103/0976-500x.83300

Marc Fernandez, J. F. (2018). *COPERNICUS POD REGULAR SERVICE REVIEW FEB - MAY 2019.* techreport, GMV, TU Delft.

Michael, J. R. (1983). The stabilized probability plot. *Biometrika, 70*, 11-17. doi:10.1093/biomet/70.1.11

O. Rodriguez Fernandez, J. U., F. Bonaventure, D. G., & M. Nicolls, N. (2018). Evaluation of a Commercial Radar Network to Support Conjunction Assessment. *69th International Astronautical Congress (IAC), Bremen, Germany, 1-5 October 2018.*

Oliver Montenbruck, E. G. (2000). *Satellite Orbits: Models, Methods and Applications* (1 ed.). Springer.

Pastor, A. (2017). Orbit determination methods for track-to-track association.

Pastor-Rodríguez, A., Antón, D. E., Sanjurjo, M., & Maté, A. Á. (2018, 10). Object Detection Methods for Radar Survey Measurements. *69th International Astronautical Congress.* Retrieved from https://iafastro.directory/iac/paper/id/44403/summary/

Pastor-Rodríguez, A., Escobar, D., Sanjurjo-Rivo, M., & Águeda, A. (2018). Correlation Techniques to Build-up and Maintain Space Objects Catalogues. *7th International Conference on Astrodynamics Tools and Techniques.* Retrieved from https://indico.esa.int/event/224/contributions/3861/

Peterson, G. E., Sorgeb, M. E., McVeyc, J. P., Gegenheimerd, S., & Henninge, G. A. (2018). Tracking requirements in LEO for space traffic management in the presence of proposed small satellites. *69th International Astronautical Congress, Bremen, Germany.*

Poore, A. B., Aristoff, J. M., Horwood, J. T., Armellin, R., Cerven, W. T., Cheng, Y., . . . Weisman, R. M. (2016, 6). *Covariance and Uncertainty Realism in Space Surveillance and Tracking.* Tech. rep., Numerica Corporation Fort Collins United States. Retrieved from https://apps.dtic.mil/docs/citations/AD1020892

Rossi, A. (2005). The earth orbiting space debris. *Serb. Astron. no. 170*, 1-12. doi:10.2298/saj0570001r

Royston, P. (1993). Graphical Detection of Non-Normality by Using Michaels Statistic. *Applied Statistics, 42*, 153. doi:10.2307/2347417

Sabol, C., Hill, K., Alfriend, K., & Sukut, T. (2013, 3). Nonlinear effects in the correlation of tracks and covariance propagation. *Acta Astronautica, 84*, 69-80. doi:10.1016/j.actaastro.2012.08.023

Sáez-Bo, D., Pastor-Rodríguez, D. E., & Ayuga-García, F. (2018). Cataloguing Performance Assessment Method of SST Sensor Networks. *7th International Conference on Astrodynamics Tools and Techniques.* Retrieved from https://indico.esa.int/event/224/contributions/3862/

Sagnieres, L., & Sharf, I. (2017). Uncertainty characterization of atmospheric density models for orbit prediction of space debris. *Proceedings of the 7th European Conference on Space Debris, Darmstadt, Germany, publishe by the ESA Space Debris Ofice.*

Scheeres, D. J. (1993). *Failure Modes of Reduced-Order Orbit Determination Filters and their remedies.* Technical Report, NASA, Navigation Systems Section. Retrieved from https://ntrs.nasa.gov/archive/nasa/casi.ntrs.nasa.gov/19940009900.pdf

Schiemenz, F., Utzmann, J., & Kayal, H. (2019, 6). Least squares orbit estimation including atmospheric density uncertainty consideration. *Advances in Space Research, 63*, 3916-3935. doi:10.1016/j.asr.2019.02.039

Schrama, E. J. (2018, 8 27). Lecture notes on Planetary sciences and Satellite Orbit Determination.

Shapiro, S. S., & Wilk, M. B. (1965, 12). An Analysis of Variance Test for Normality (Complete Samples). *Biometrika, 52*, 591. doi:10.2307/2333709

Siminski, J. (2016, 3). Techniques for assessing space object cataloguing performance during design of surveillance systems. *6th International Conference on Astrodynamics Tools and Techniques (ICATT).*

Siminski, J., Weigel, M., & Fiedler, H. (2014, 9). Catalog build-up for geostationary orbit using simulated short-arc tracklets. *Advanced Maui Optical and Space Surveillance Technologies (AMOS) Conference*, (p. E21). Retrieved from http://adsabs.harvard.edu/abs/2014amos.confE..21S

Snow, D. (2016). JSpOC SP Catalog Covariance Realism. Retrieved from https://ntrs.nasa.gov/archive/nasa/casi.ntrs.nasa.gov/20160005313.pdf

Space (JFCC SPACE), J. F. (2018). Space-Track. Retrieved from https://space-track.org

T Horwood, J., & Poore, A. (2012, 1). Orbital state uncertainty realism. *Proceedings of the Advanced Maui Optical and Space Surveillance Technologies Conference, held in Wailea, Maui, Hawaii, September 11-14, 2012*.

Tapley, B. D., Schutz, B. E., & Born, G. H. (2004). *Statistical Orbit Determination* (1 ed.). (Elsevier, Ed.) Academic Press.

Thode, H. C. (2011). Normality Tests. In *International Encyclopedia of Statistical Science* (pp. 999-1000). Springer Berlin Heidelberg. doi:10.1007/978-3-642-04898-2_423

Vallado, D. (2010). *Orbital Mechanics Fundamentals, Encyclopedia of Aerospace Engineering.* Wiley. doi:10.1002/9780470686652.eae285

Vallado, D. A. (1997). *Fundamentals of astrodynamics and applications.* (M. A. Hollander, Ed.) Mc Graw Hill.

Vallado, D. A. (2005). An analysis of state vector propagation using differing flight dynamics programs. *AAS/AIAA Astrodynamics Specialist Conference.*

Vallado, D. A., & Finkleman, D. (2014, 2). A critical assessment of satellite drag and atmospheric density modeling. *Acta Astronautica, 95*, 141-165. doi:10.1016/j.actaastro.2013.10.005

Vallado, D. A., & Seago, J. H. (2009). Covariance realism. *AAS/AIAA Astrodynamics Specialist Conference.*

Wakker, K. (2015). *Fundamentals of Astrodynamics.* (T. U., Ed.) TU Delft.

Wiegel, M., & Patyuchenko, A. (2011). Orbit Determination Error Analysis for a future Space Debris Tracking Radar. *European Space Surveillance Conference.* Retrieved from https://elib.dlr.de/70242/1/ESSC2011_weigel.pdf

Wilkins, M., & Alfriend, K. (2000, 8). Characterizing orbit uncertainty due to atmospheric uncertainty. *Astrodynamics Specialist Conference.* American Institute of Aeronautics and Astronautics. doi:10.2514/6.2000-3931

Yanez, C., Gupta, M., Morand, V., & Dolado, J. C. (2019). On the Gaussianity validity time for orbital uncertainty propagation. *Proc. 1st NEO and Debris Detection Conference, Darmstadt, Germany, 22-24 January 2019, published by the ESA Space Safety Programme Office.*

Yang, Y., Yue, X., & Dempster, A. G. (2016, 4). GPS-based onboard real-time orbit determination for leo satellites using consider Kalman filter. *IEEE Transactions on Aerospace and Electronic Systems, 52*, 769-777. doi:10.1109/taes.2015.140758

Zhang, Y., Wu, H., & Cheng, L. (2012, 6). Some new deformation formulas about variance and covariance. *2012 Proceedings of International Conference on Modelling, Identification and Control*, (pp. 987-992).

Appendices

A

NLRMSISE-00 ATMOSPHERIC MODEL

In the following section the dynamic models used in the orbit determination process and in the propagation will be detailed. It is important to define such models as they represent the source of error and uncertainty that is not considered, most of the times, in an orbit determination process. Particularly, the solution of an OD will depend on the models implemented, as models for the atmospheric density and prediction of geomagnetic indices are constantly updated and improved, derived from different data sources and using different techniques. Some of them will be better at describing low atmospheric density variations while others will prove more valuable at high altitudes, where density variations are driven by other physical phenomena. Hence, to understand the solutions and the values of the consider parameters variances obtained, the models employed to generate predictions for the geomagnetic index, the solar flux and the density will be explained.

The density model implemented in the orbit propagator employed by GMV's software is the MSISE-90 model (Mass Spectometer and Incoherent Scatter). This model gives predictions of the neutral temperature and density in Earth's atmosphere, from ground to thermospheric altitudes. From 72.5 km upwards, the MSISe-90 model is based on the MSISE-86 model with some corrections applied thanks to the information produced by the Space Shuttle flights and updated incoherent scatter results. As the orbits considered during this work are at LEO regions, the model to be considered does not differ much from the MSISe-86 model. A good reference of the termospheric models employed in the space industry can be found in [Klinkard, 2006] section B.

MSIS models were first derived from Earth and atmospheric monitoring mission in the early stages of space exploration. Some of the mission which took part in the retrieval of significant data for the creation of such models are AE-B, OGO 6, San Marco 3, Aeros and AE-C. The MSIS models differ from drag-based models as they rely on mass-spectometer data to characterize the atmospheric behaviour. They implement a specific species analytical method based on temperature and concentration profiles to compute total densities. In contrast, drag-based models integrate diffusion equations using empirical temperature profiles. The parameters that have the greatest impact on the state of the termosphere and that are relevant to the MSISE-86/90 model are:

- z or geodetic altitude of the satellite
- t_{LST} local solar time
- t_d day of the year
- ϕ geodetic latitude
- t_{UT} universal time
- $\bar{F}_{10.7}$ mean solar activity
- $F_{10.7}$ current solar activity
- A_p geomagnetic activity index or six-hourly k_p index.

Hence, MSISE-90 model tries to capture diurnal, seasonal and annual variations of the density of the atmosphere and its compositions (because of its species-wise approach). Its main contributions are the altitude and solar and magnetosphere activity, modelled as a function of the satellite with respect to Earth's surface.

From [Klinkard, 2006] p. 335, model's accuracy is expected to be $\Delta\rho_{1\sigma} \approx 15\%$ although using exact and updated input parameters. The situation worsens when extreme solar and geomagnetic phenomena occur, as the variation of these contributions can lead to density errors of more than 100%. Because of the nature of the measures, the MSISE models provide a good fit for high termospheric regions, where vast amounts of data could be retrieved. However, the fit is worse at low altitudes as available data is scarcer. It is advisable to use drag-based models for low altitudes as their accuracy is far better than mass-spectometer based models.

Variations in atmospheric conditions (temperature, density and composition) are driven by solar activity. The energy emitted by the Sun in the form of photons and solar wind reaches the Earth atmosphere in the form of extreme ultraviolet and X-ray frequency bands. Such energy bands are absorbed by the atmosphere, mainly the termosphere, leading to heavy changes of temperature and density. There are 3 main effects of Sun's radiation to Earth's atmosphere, first the diurnal effect due to the Sun's ultraviolet radiation heating of the atmosphere, having its impact on a 24 h base and that produces also spatial variations with respect to time. The second effect is related to Sun's extreme ultraviolet radiation, which shows dependencies on the Sun rotation cycle (27 days) and Sun's solar activity (11 years). The last effect is due to solar wind, which has an effect on atmospheric density as it interacts with Earth's magnetosphere.

As commented on this section, a proxy to measure the solar activity is the $F_{10.7}$. However, all models use an averaged solar activity index $\bar{F}_{10.7}$ formed by the average of the preceding $F_{10.7}$ values from the last 3 solar rotations (or 81 days). It is important to remark that the atmosphere does not react instantly to solar activity but the models use $F_{10.7}$ from the past day to model density changes. For long term forecasts, actual prediction models can compute accurately up to 2 solar cycles (22 years) of averaged solar activity data.

As commented above, solar wind and ejected charged particles of the Sun do have an impact on our atmosphere, as they react with the magnetosphere and change the value of the magnetic field in those regions. Because of the random behavior of the geomagnetic activity, no long term forecast can be produced (only up to 27 days).

It is clear that orbit determination processes and orbit forecasts will have to rely on predictions and available information retrieved from different sources. The degree of accuracy of the density is difficult to assess and for this reason its uncertainty has a great impact in the overall uncertainty of the drag acceleration (as shown in section 2.1.3.1). There are several sources from which solar radiation parameters and geomagnetic indices can be obtained, some of them are:

- National Oceanic and Atmosphere Administration (NOAA): This organism delivers a daily report with the values for the past day, once processed, and a prediction for the coming two days, together with the mean solar flux index.
- Celestrack: The following webpage publishes relevant information about Space Weather data every 3 hours, giving updates on observed solar flux indexes and predictions for the next 44 days.
- GMV software (RSGAconv): Software tool developed by GMV to compute predictions for the solar flux index using historical data. The software is able to ingest historic data (from NOAA) from large periods, up to several solar cycles, to compute estimations of the indexes ranging from 1 day to several years.

The sole fact of using proxies as a representation of the interactions between solar radiation, magnetosphere and the atmosphere in the definition of our models is introducing a certain uncertainty. Moreover, if this indexes are not observed but predicted the uncertainty is greater. It is clear that the modelling of the drag acceleration is difficult and continuous research is being done. The scope of this work will not focus on computing the dependencies of drag model uncertainties, however, it is important to understand where they come from.

B

CONFERENCE PAPERS

In the present section the conference paper presented in the IAC 2019 and ICSSA 2020 are attached.

70th International Astronautical Congress (IAC), Washington D.C., United States, 21-25 October 2019.

IAC-19-A.6.9.3

Towards Covariance Realism in Batch Least-Squares Orbit Determination

Sergi López-Jiménez[a]*, Alejandro Pastor[a], Srinivas Setty[b], Diego Escobar[a], Ernst Schrama[c], Alberto Águeda[a]

[a] *GMV, Calle Isaac Newton 11, Tres Cantos, 28670, Spain, serlopez@gmv.com, apastor@gmv.com, descobar@gmv.com, aagueda@gmv.com*
[b] GMV Insyen, Münchener Str. 20, Weßling, 82234, Germany, *harsha.shresty@gmail.com*
[c] *Delft University of Technology, The Netherlands, e.j.o.schrama@tudelft.nl*
* Corresponding Author

Abstract

Regular products within the field of Space Surveillance and Tracking (SST) and Space Traffic Management (STM), such as high-risk collisions, upcoming re-entries or fragmentations, rely both on the estimated state and associated uncertainty of detectable resident space objects (RSOs). Classical orbit determination (OD) algorithms provide the required estimations, assuming that the uncertainty in the state of the object is properly characterized by its state vector covariance and assuming Gaussian processes.

However, a common problem of classical orbit determination processes is the misrepresentation of the RSOs uncertainty through the estimated covariance. Ultimately, this causes a great impact in the quality and accuracy of SST products as the estimated covariance is overly optimistic (too small) and the true uncertainty of the object is not captured. One of the causes for the **unrealism of the estimated covariance** is found in the classical OD approaches, as they fail to consider, or properly characterize, the uncertainty of the dynamical models used to describe the motion of the objects, such as the atmospheric drag force or the solar radiation pressure acting on the orbiting RSOs. Because these models provide a deterministic solution to a stochastic phenomenon, an inherent associated uncertainty should be regarded when used during an orbit determination.

The aim of this work is to devise a methodology to improve the covariance realism of common OD processes through the classical theory of **consider parameters** of batch least squares methods. The methodology uses the classical theory of consider parameter to add to the estimated covariance the contribution coming from the uncertainty of the consider parameters. To do so, the variances of the consider parameters are estimated through another least squares process, with which the propagated covariance best fits a so-called observed covariance, previously derived, in a process named **covariance determination**. The influence of the main sources of dynamic model uncertainty can be evaluated by examining the resulting covariance correction for each uncertainty source (e.g. atmospheric drag force modelling, sensor calibration parameters or solar radiation prediction).

This publication focus on studying the effect of the atmospheric drag force and range bias modelling uncertainty in the correction of an estimated covariance. The proposed methodology has been applied to a simulated realistic scenario of measurements and objects to evaluate the consistency of the corrected covariance via Monte Carlo analysis. Thorough analyses are presented to illustrate the effect of dynamic model errors on covariance realism.

Keywords: *space surveillance and tracking, space traffic management, uncertainty realism, covariance realism, orbit determination*

1. Introduction

The provision of most of the Space Surveillance and Tracking (SST) services depends on how well modelled is the uncertainty on the resident space objects (RSOs), i.e. **uncertainty realism**. Assuming Gaussian processes, the uncertainty in the state of the objects can be represented by their **covariance**, which can be directly obtained via classical orbit determination (OD) given that the measurements are available.

These services comprise conjunction analysis, sensor tasking and scheduling, catalogue build-up and maintenance or manoeuvre and anomaly analysis among others. All of them rely on covariance as a means of approximating the orbit uncertainty of RSOs, as Gaussian statistics provide a feasible and preliminary approximation of the probability density function of the state estimation problem (considering small orbital errors and linear dynamics). Covariance unrealism not only depends on the dimension of the main directions of uncertainty but also on the orientation of these directions with respect to the true uncertainty of the orbit [1]. For instance, covariance misrepresentation (either in

orientation or dimension) can lead to differences of more than an order of magnitude in the computation of the probability of collision [2]. It is clear that covariance realism is desired in conjunction analysis but proper representation of orbit uncertainty is of the utmost importance to all the aforementioned services (see [3] and [2] for further examples on the relevance of covariance in SST products).

It is an extended practice among SST service providers to artificially increase the covariance using non-physical scaling factors, acting as a safety margin in order to compensate for uncertainty misrepresentation [1]. However, most of them do not rely on a physical approach but an statistical approach is used to generate these correction coefficients.

Forecasts predict that the increasing number of RSOs may require better state uncertainty characterisation. For future Space Traffic Management (STM) systems, it is desirable to identify high probability collisions and avoid false alarms [4]. The need of a robust technique to correct covariance, considering both statistics and dynamics, to include a complete set of uncertainty sources, becomes the central motivation of this work.

This paper presents a new methodology to improve covariance realism in OD processes, within the field of SST and STM. The main goal is to properly account for the uncertainty of the main dynamical models to improve covariance unrealism.

This methodology is based on the consider parameters theory [5] [6]. The classical theory is revisited and an estimation of the variances of these consider parameters proposed.

Such additional estimation process relies on a least-squares problem in the covariance space, where a parallelism is established with a classical OD algorithm. Starting from an initially estimated a-posteriori covariance, a least-squares process is performed through a complete batch of observations (observed covariances obtained from an statistical comparison of past orbital solution) so as to correct the initial state (estimated a posteriori covariance without consider parameters contribution) and obtain a best-fitting solution. In our case, the estimated parameters that will lead to the sought correction are the variances of the consider parameters contemplated, which will then be used to correct future orbit determination a posteriori covariance solutions. The method described allows for a physical solution of the scaling parameters that would be implemented otherwise using empirical safety factors.

The application as well as the software used to generate the different solutions and run the simulations is within GMV's SST software suite.

2. Background

Some of the terms that are used along this paper are now defined for clarification:

- **Observation:** set of measurements related to a certain epoch, belonging to a given object and obtained by certain sensor, e.g. range, range-rate, azimuth, elevation, right ascension, declination.
- **Orbit determination (OD)**: process with which the orbital state (position and velocity at the estimation epoch, as well as dynamical parameters such as drag coefficient or solar radiation pressure coefficient) of an object are estimated based on observations obtained from sensors, typically telescopes and/or radars in SST.
- **Estimated parameters/orbital state**: set of orbital parameters (position, velocity and dynamical parameters) obtained through an orbit determination process.
- **Estimated/determined orbit**: evolution over time of an object's state obtained through an orbit determination process over a time interval with available observations.
- **Predicted/propagated orbit**: evolution over time of an object's state obtained through an orbit propagation process of a previously estimated orbital state over a time interval without available observations
- **A-posteriori covariance**: covariance of the estimated orbital state resulting from an orbit determination process. Depending on whether consider parameters have been consider or not:
    - **Noise-only covariance**, if no consider parameters have been included in the orbit determination. Therefore, it only accounts for measurement noise.
    - **Consider covariance**, if consider parameters have been included in the orbit determination. This covariance matrix is larger than the noise-only one.
- **Propagated covariance**: uncertainty characterization over time of the orbit (position and velocity) of the object obtained through propagation of the a-posteriori covariance
- **Consider parameters**: parameters that are not estimated in the orbit determination process but whose uncertainty is added to the a-posteriori covariance in order to improve covariance realism.
- **Variance of consider parameters**: uncertainty of the consider parameters.
- **Observed covariance**: uncertainty characterization over time of the object's orbit generated from an statistical analysis of estimated and propagated orbits, covering the propagation time interval and relative to the start time of the propagation
- **Observed covariance generation**: process in which different orbits, including estimated (obtained through orbit determination processes) and

propagated ones, are compared among them in order to derive the observed covariance.

- **Covariance determination**: process in which the variance of consider parameters is estimated in order to fit the propagated covariance to the observed covariance.

The theory used in this work lays its foundations on the classical theory of batch least-squares OD, with the addition of the so-called consider parameters directly into the residuals equation [5]:

$$\Delta \boldsymbol{z} = \boldsymbol{H}_y\left(\boldsymbol{y}_0 - \boldsymbol{y}_0^{ref}\right) + \boldsymbol{H}_c\boldsymbol{c} + \boldsymbol{\varepsilon} \quad (1)$$

where $\boldsymbol{H}_y$ and $\boldsymbol{H}_c$ are partials of the measurements with respect to the state vector, $\boldsymbol{y}_0$ and consider parameters, $\boldsymbol{c}$, respectively, while $\boldsymbol{\varepsilon}$ denotes the measurement errors.

The consider parameters are assumed to be random Gaussian variables with zero mean and a certain standard deviation, i.e.:

$$c \sim \mathrm{N}(0, \sigma_c) \quad (2)$$

As a consequence of the previous assumption, the solution of the estimated parameters does not change with respect to a classical batch least-squares without consider parameters, as the expected value of the consider parameter is zero. However, the resulting a-posteriori covariance of the estimated parameters now takes into account the consider parameters, leading to the following expression for the so-called consider covariance matrix [5]:

$$\boldsymbol{P}_c = \boldsymbol{P} + \left(\boldsymbol{P}\boldsymbol{H}_y^T\boldsymbol{W}\right)\left(\boldsymbol{H}_c\boldsymbol{C}\boldsymbol{H}_c^T\right)\left(\boldsymbol{P}\boldsymbol{H}_y^T\boldsymbol{W}\right)^T \quad (3)$$

being $\boldsymbol{P}$ the estimated a-posteriori covariance from a regular OD (also known as noise-only covariance), without consider parameters, **W** the weighting matrix, and **C** a diagonal matrix containing the variance of the estimated parameters. The dimensions of the involved matrices are gathered below for clarification:

- $\boldsymbol{P}$, $\boldsymbol{P_c} \in \mathbb{R}^{n_y} \times \mathbb{R}^{n_y}$
- $\boldsymbol{H_y} \in \mathbb{R}^{n_z} \times \mathbb{R}^{n_y}$
- $\boldsymbol{H_c} \in \mathbb{R}^{n_z} \times \mathbb{R}^{n_c}$
- $\boldsymbol{W} \in \mathbb{R}^{n_z} \times \mathbb{R}^{n_z}$
- $\boldsymbol{C} \in \mathbb{R}^{n_c} \times \mathbb{R}^{n_c}$

Where n_y is the number of estimated parameters, n_z is the number of measurements and n_c the number of consider parameters

This theory enables a covariance correction (estimation uncertainty) without degrading the integrity of the orbit solution (estimation expectation). However, it is important to note that the variance of the consider parameters is not usually known and this explains why the contribution from consider parameters is not typically added to the a-posteriori covariance.

In our methodology, the variance of consider parameters is obtained through an additional estimation process in the covariance space. The variance of the consider parameters is estimated by minimizing the residuals between the observed and consider covariance. The latter is computed by adding the contribution of the consider parameters to the noise-only covariance using Equation (3).

3. Error modelling

The main sources of un-modelled uncertainties in typical OD processes in the SST and STM frameworks are:

- **Errors in atmospheric drag force model**, coming either from errors in the estimation of atmospheric density, errors in the computation of the cross-section of the object, errors in the estimation or prediction of solar and geomagnetic proxies, etc.
- **Errors in measurement reconstruction models**, coming from errors in the range biases estimated during the calibration of a given radar sensor
- **Errors in solar radiation force models**, coming errors in the solar radiation pressure acting on the satellite or errors in the computation of the cross-section of the object.

The first two sources affect mainly Low Earth Orbit (LEO) objects, where the atmospheric drag is the main driver of uncertainty and observations are normal from radar sensors. The third source of uncertainty is more relevant in Geosynchronous Earth Orbit (GEO) regime, and not further analyzed in this paper. However, the methodology proposed in this work is intended to be applied in the future to this third case.

3.1 Atmospheric drag force model error

The modelling of atmospheric drag forces is one of the greatest contributions to an unrealistic uncertainty. The use of deterministic models to predict stochastic phenomena like atmospheric density, and ballistic parameters, among others, is not sufficient and an uncertainty correction should be applied to an estimated covariance to account for these random phenomena.

The atmospheric drag force model error has been included in the typical model:

$$\boldsymbol{D} = -\frac{\alpha}{2B}(1 + c_{AE})|\boldsymbol{v}|\boldsymbol{v} \quad (4)$$

where α is the atmospheric density, B the ballistic coefficient, $\boldsymbol{v}$ the orbital velocity and c_{AE} the corresponding atmospheric drag force model error consider parameter.

The consider parameter, c_{AE}, intends to account for both spacecraft model and atmospheric density errors that do not depend on time. It is expected to have zero mean, as required by the consider parameters theory, and an associated standard deviation to account for errors in the modelling of the different atmospheric drag parameters.

3.2 Range bias model error

Radar calibration errors are another contributor to the un-modelled uncertainty. Systematic errors in the calibration of a radar sensor and the inherent uncertainty in the calibration procedure may lead to an unconsidered source of noise. Therefore, to account for such effects the range bias consider parameter has been included into the range measurement equation as it follows:

$$\rho = \rho^* + c_{RBE} \tag{5}$$

where ρ^* is the former range and c_{RBE} the consider parameter.

4. Covariance determination

The covariance determination algorithm has been conceptualized with great parallelism to a classical OD. The initially defined solution, or the estimated a-posteriori covariance from an OD, is corrected through a fitting process using the variance of consider parameters as the parameters to fit.

The observations are represented by batches of observed covariance matrices that characterize the evolution of the uncertainty as it is propagated far from the initial state.

The estimated parameters are the variances of the consider parameters, $\boldsymbol{c}$. The residuals, to be minimized, in this covariance determination problem are:

$$\boldsymbol{P}_{obs}(t_i) - \boldsymbol{P}_c(\boldsymbol{c}, t_i) \tag{6}$$

where $\boldsymbol{P}_{obs}$ is the observed covariance matrix (measurements in the covariance space and obtained as described below) and $\boldsymbol{P}_c$ is the consider covariance matrix, given by Equation (3).

The consider matrix depends on the estimated variance of consider parameters.

4.1 Covariance propagation

The involved covariance matrices are propagated via the complete transition matrix, $\Phi(t, t_0) \in \mathbb{R}^{n_y} \times \mathbb{R}^{n_y}$, i.e.:

$$\boldsymbol{P}_c(t, \boldsymbol{y}_0) = \boldsymbol{\Phi}(t, t_0)\boldsymbol{P}_c(t_0, \boldsymbol{y}_0)\boldsymbol{\Phi}^{\mathrm{T}}(t, t_0) \tag{7}$$

being $\boldsymbol{\Phi}(t_i, t_0)$ the state transition matrix that allows to propagate the covariance matrix from t_0 to t. It is a square matrix of dimension 6 (position and velocity) plus the number of dynamical parameters (usually drag and solar radiation coefficients). Not only the position and velocity covariance are propagated but the complete covariance matrix is, as dynamical parameters covariance elements (such as the drag coefficient element) increase the covariance of the other covariance elements (position/velocity) thanks to the pre and post-multiplication of the complete transition matrix. Alternative covariance propagation techniques could be considered instead, if required.

4.2 Observed covariance generation

The covariance matrix is mathematically defined as:

$$\boldsymbol{cov}(\boldsymbol{x}, \boldsymbol{x}) = \frac{1}{N}\sum_{i=0}^{N}[\boldsymbol{x}_i - E(\boldsymbol{x})][\boldsymbol{x}_i - E(\boldsymbol{x})]^{\boldsymbol{T}} \tag{8}$$

It can be shown that the covariance of the state vector is the same as the covariance of the difference between state vectors if Gaussian independent and identically distributed random variables are assumed [7]. These orbital differences are computed in the TNW local frame. The observed covariance is obtained by comparing the determined orbits against predicted ones, as shown in Fig. 2. This is based on a purely statistical consistency analysis of orbital differences between predicted and determined orbits from independent and uncorrelated ODs. This procedure is depicted in Fig. 1, where both estimated/determined and propagated/predicted orbits from independent OD processes are represented as horizontal lines. Each orbital comparison is assembled in the corresponding prediction time bin. They are representative of the error of the propagated orbits and therefore, of the uncertainty evolution. This method has been successfully applied to covariance derivation from operational orbits [8].

Therefore, by aggregating orbital differences between pairs of predicted and determined orbits from independent and uncorrelated ODs, it is possible to obtain the evolution of the covariance matrix along the prediction time. To do so, each pair is evaluated and statistics along certain prediction time window obtained. The prediction time is referred to as the relative time with respect to the epoch of the last observation.

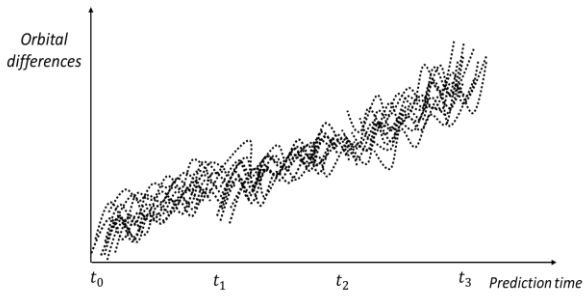

Fig. 1. Aggregation of the orbital differences along the prediction time for the generation of observed covariance.

By considering a sufficient amount of independent orbits, a statistical trend of the evolution of the differences along time arises and a covariance evolution can be generated. However, it is important to detect and filter outliers to avoid polluting the statistical analysis. They come from two different sources: manoeuvre modelling mismatch and correlated OD processes. The

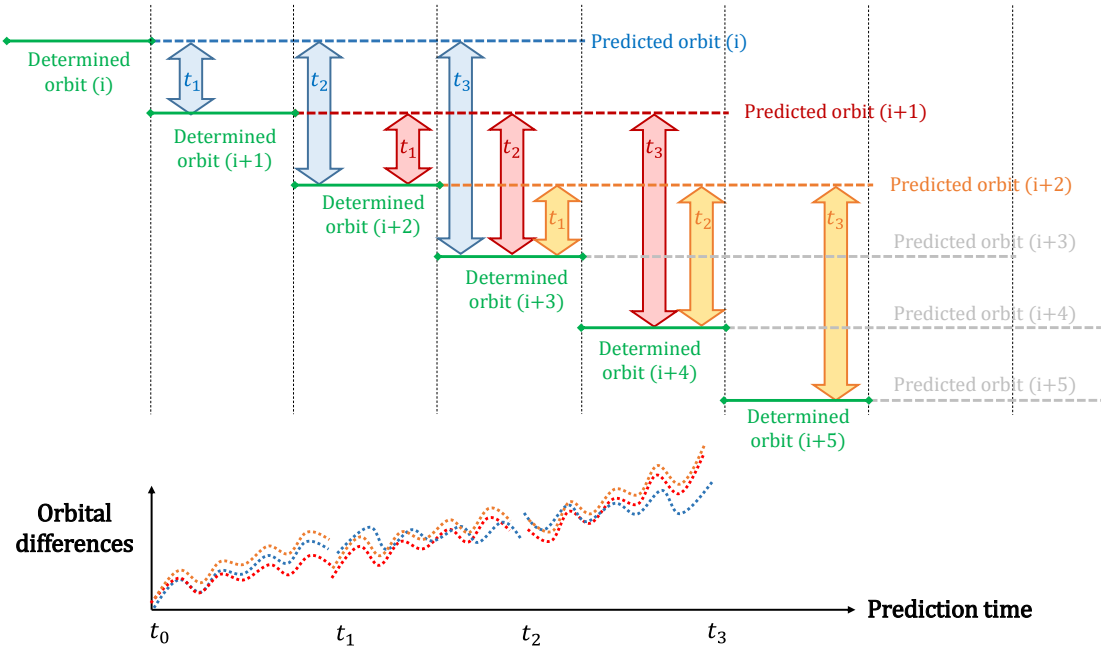

Fig. 2. Sketch of the orbital differences assembly for the generation of observed covariance

first implies operational satellite manoeuvres not properly captured during one orbital update and can be tackled with an upper-bound threshold on the orbital differences, while the second is related to the fact that common measurements may have been considered on two orbital updates and entails lower-bound thresholds.

After computing the orbital differences of each orbit pair, three additional steps are performed:

- Outlier rejection, band pass filter to detect both manoeuvre modelling mismatch and correlated OD processes.
- Root Mean Square (RMS) computation, corresponding to the different elements of the observed covariance matrices.
- RMS fitting, to obtain the final continuous observed covariance evolution.

5. Validation

Although the ultimate objective is to use the presented covariance determination methodology with real data, a validation chain has been prepared to understand the role of the different model errors and prove the performance of the covariance determination algorithm. A simulation environment has been setup with the capability of simulating realistic orbits, radar measurements and ultimately enable the execution of different OD processes including the different effects at hand: impact of atmospheric drag force and range bias models errors. For this purpose, several cases have been defined. First, a case with only measurement noise. Second, a case where an atmospheric drag force error is simulated, together with measurement noise. And third, a case where a range bias is simulated, together with measurement noise.

In all cases, a Monte-Carlo (MC) based approach is used, where each sample represents a different perturbation on the parameters being modelled (range bias and/or atmospheric drag force), and measurements are generated with representative noise matching typical accuracy of radar sensors. Each sample represents an estimated orbit affected by measurement noise, and the value of the consider parameter being simulated, which is constant in a particular sample. This sequence is depicted in Fig. 3.

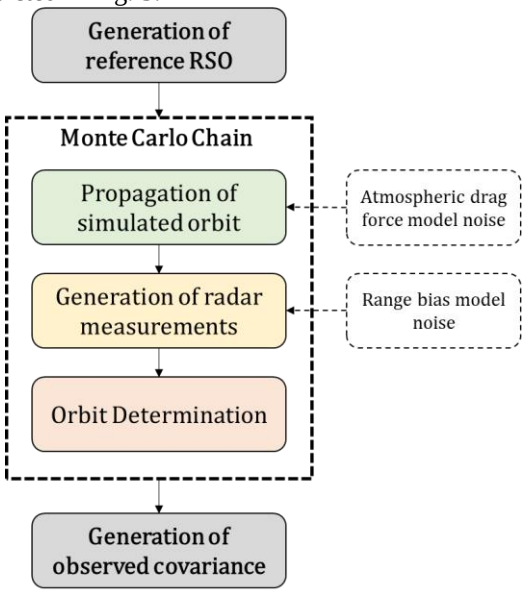

Fig. 3. Validation sequence schematic

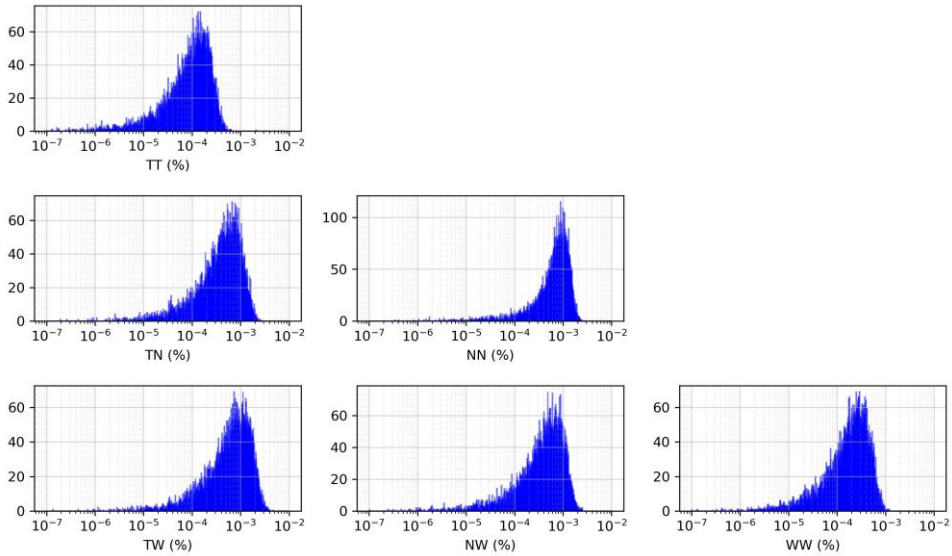

Fig. 4. Histogram of the relative differences between covariance TNW position elements (from the OD of each MC point) in *Case 1*

The test cases aim at producing a reasonable population of orbits so that an observed covariance matrix can be derived as a product. The observed covariance matrix is to be fed to the covariance determination algorithm, with the purpose of estimating the variance of the consider parameter so that consider covariance matrix is best fitted to the observed ones.

In order to generate such populations, a processing scheme has been defined with the following steps for each MC point:

- Propagation of the reference orbit of an RSO with a high-fidelity propagator. The resulting ephemeris are required for the simulated radar observations generation, as well as for further validation. Dynamical model errors, such as atmospheric drag force ones, can be included here, thus resulting in a cloud of simulated orbits.
- Generation of radar measurements using the previously simulated orbits. During the measurement computation, typical measurement noise and range bias model error are considered.
- Using the simulated measurements, ODs are performed, leading to a cloud of estimated orbits. This cloud is intended to sample the probability density function characterizing the uncertainty of the orbit determination.

By definition, the consider parameter is a systematic error affecting a whole orbital arc, for this reason each MC trial will be affected by a different value of a consider parameter, either dynamic or sensor calibration. Its value will be determined as sample of a Gaussian distribution. The purpose of the validation is for the covariance determination algorithm to recover the standard deviation of the input consider parameter error, given a proper sampling of the probability density function associated to the state estimation problem.

It is worth mentioning that the error in the model noise affecting each sample of the population is generated considering a certain value for the parameter, therefore it becomes a systematic error during the generation of measurements and estimation of the state vector. However, as each sample is affected by a unique value, it will generate a different orbital estimation.

For the results presented in this paper, the observed covariance is directly computed with Equation (8), considering the cloud of MC orbital estimations. However, on an operational environment this is not feasible and therefore the aforementioned methodology, presented in Section 4.2, is proposed to generate the so-called observed covariance.

6. Results

In this section, results of several tests of the validation sequence are presented.

The orbit and physical properties of the reference RSO are compiled in Table 1. The orbit has been taken from a public TLE of SENTINEL-3A (41335) [9].

Table 1. Simulated RSO orbit and physical properties

Reference RSO	
Semi-major axis	7186.877 km
Eccentricity	0.001113
Inclination	98.72 deg
RAAN	77.03 deg
Mass	100 kg
Area	10 m^2
Drag coefficient	0.4

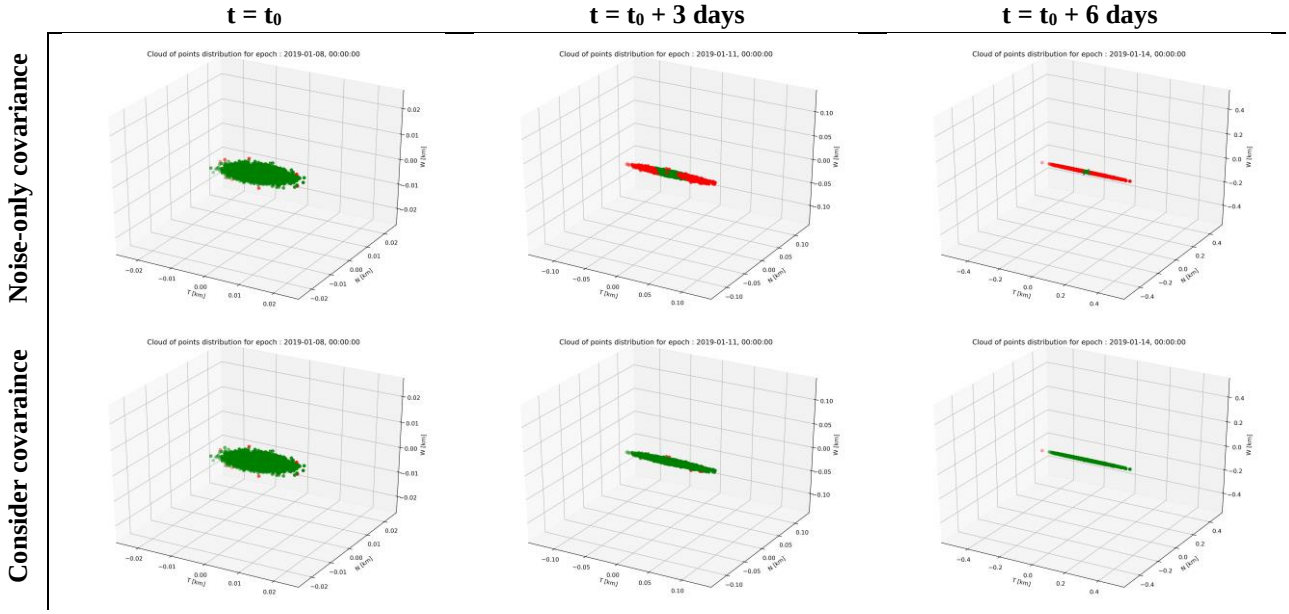

Fig. 5. Position covariance containment considering a 4-σ ellipsoid for *Case 2*

The dynamical model used is a complete one: 16x16 gravity field, third body perturbation of the Moon and MSIS-90 atmospheric density model.

The estimation time span of the involved ODs is of 1 week and the estimation is propagated one week after the last observation available.

Three cases are presented in this section:

- *Case 1*: Measurement noise only
- *Case 2*: Measurement noise and atmospheric drag force model error
- *Case 3*: Measurement noise and range bias model error

The considered period of time for measurement generation and orbit determination is of one week (from 01-01-2019 to 01-08-2019). The estimation epoch, t_0, is set at the end of this time interval (i.e. 01-08-2019). Finally, the estimated orbits and covariance matrices are propagated one week ahead.

The results of the analyses performed can be grouped in three main categories:

- **Covariance consistency:** to evaluate the quality of the ODs, as well as the differences between covariance matrices considering all estimated orbits. For instance, in the atmospheric drag force model error, the estimated drag coefficient during the MC ODs is compared against each MC perturbation to check if it captures the model error.
- **Covariance containment:** to ensure the observed covariance is able to capture the position dispersion of the cloud of MC points. To do so, an approach similar to [10] is followed: computation of the Mahalanobis distance [11] to get the percentage of points lying inside a k-sigma ellipsoid at different epochs. Additional results, supporting this containment are provided, such as position residuals distributions.
- **Covariance realism:** to investigate the differences between the consider covariance (output from the proposed covariance determination procedure) and the noise-only covariance. By observing the evolution of the different covariance matrices, the use of consider parameters (as well as their estimated sigma values) can be justified.

For each case a sample of 10,000 MC points have been processed following the MC chain introduced in section 5.

6.1 Case 1: Measurement noise only

This initial case is the simplest one, since the only noise inputted to the MC chain is the measurement noise. Therefore, the measurements used for each OD are different, but since a zero-mean Gaussian noise model is considered, it is expected to be well-captured during the estimation process. The considered sigmas are presented in Table 2.

Table 2. Simulated measurement noise sigma

Measurement	Sigma
Two-way range	10 m
Azimuth and elevation	300 mdeg
Two-way range-rate	1000 mm/s

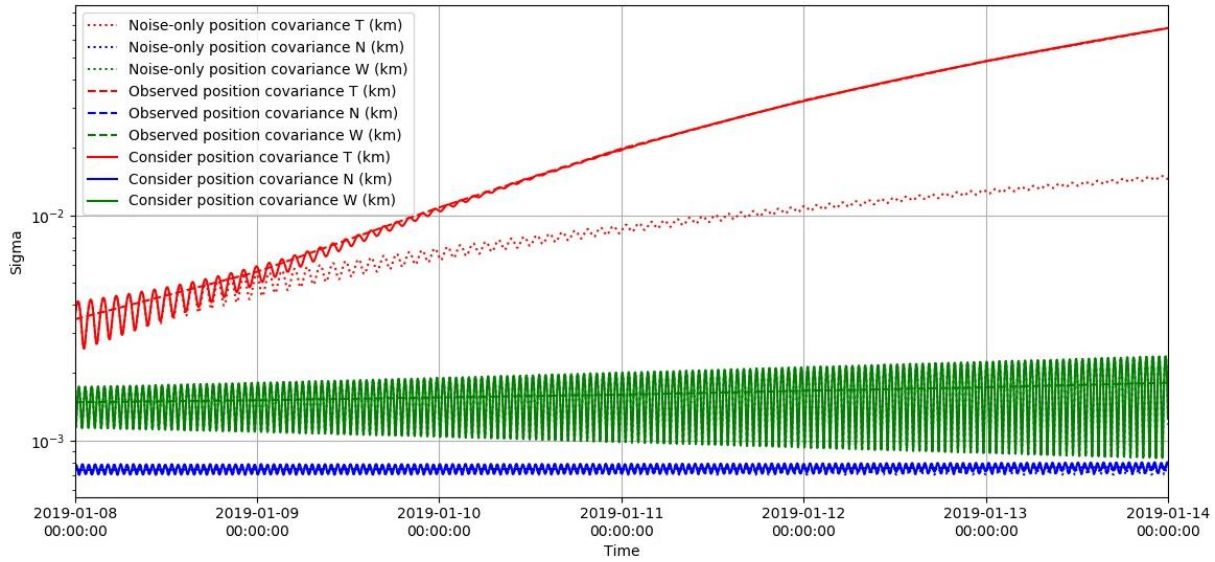

Fig. 6. Evolution of the T, N and W position sigma of the noise-only, observed and consider covariance in *Case 2*

Regarding covariance consistency, Fig. 4 shows the histogram of the relative differences between the 10,000 covariance matrices estimated via classical OD (for each MC point). The differences are computed by using the average covariance as reference. The relative differences for all the position elements are below 0.01%, i.e. they are essencially the same. The quality of the ODs has also been assessed by checking the weighted RMS, whose histogram is shown in Fig. 7. The distribution is centered at 1.0 (meaning that the residuals match the expected values, i.e. measurement weights) with an standard deviation lower than 0.03.

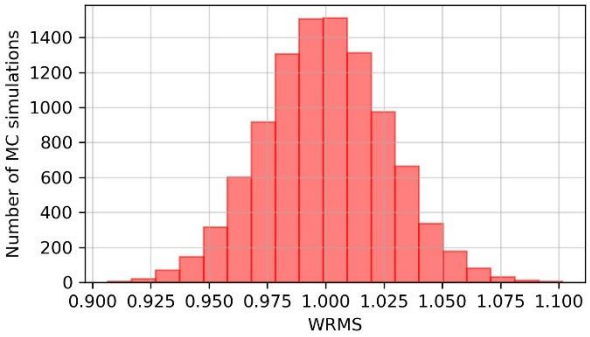

Fig. 7. Histogram of the weighted RMS of the OD for each MC point in *Case 1*

In terms of covariance containment, Table 3 proves that the so-called noise-only covariance is able to properly capture the measurement noise as expected. Besides, the theoretical containment probabilities of k-σ shells given a 3-dimensional Gaussian distributions are also included at the bottom of each table [12].

Table 3. Covariance containment results for *Case 0*

Time	1-σ	2-σ	3-σ	4-σ
t_0	19.72%	73.68%	97.26%	99.87%
t_0 + 1 day	20.20%	74.04%	97.23%	99.89%
t_0 + 2 days	19.62%	74.06%	97.07%	99.86%
t_0 + 3 day	19.91%	73.79%	97.08%	99.87%
t_0 + 4 days	19.42%	73.87%	97.13%	99.87%
t_0 + 5 days	19.79%	73.94%	97.24%	99.86%
t_0 + 6 days	19.35%	74.05%	97.05%	99.87%
Theor.	19.90%	73.90%	97.10%	99.87%

6.2 Case 2: Measurement noise and atmospheric drag force model error

This case includes the previous measurement noise model and the following additional gaussian atmospheric drag force model error:

$$c_{AE} \sim N(0, \sigma_{AE} = 5\%\, C_D) \tag{9}$$

being C_D the reference drag coefficient.

In terms of covariance consistency, the weighted RMS and the differences among the estimated (MC) covariance matrices have been analysed, obtaining similar results as those presented for *Case 1*.

As expected, the estimated drag coefficient absorbs the atmospheric drag force error. This is shown in Fig. 9, where the blue points, corresponding each to a MC point, stick to the red dotted line (1:1 slope, with certain dispersion due to measurement noise).

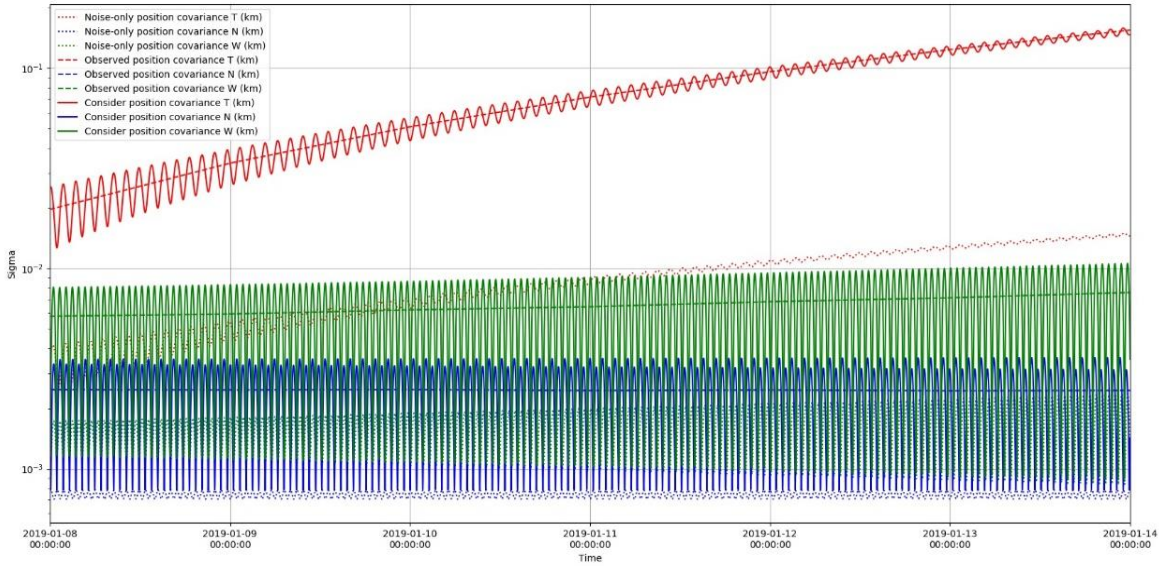

Fig. 8. Evolution of the T, N and W position sigma of the noise-only, observed and consider covariance in *Case 3*

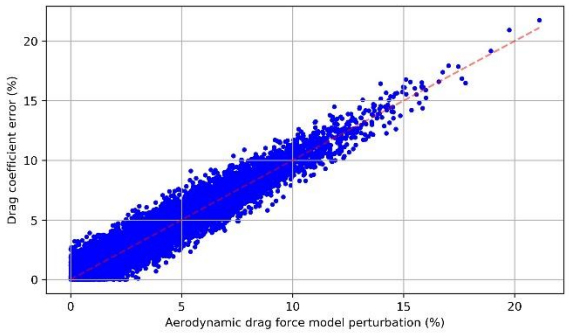

Fig. 9. Drag coefficient error as a function of the atmospheric drag force model perturbation in *Case 2*

The main effect of the atmospheric drag force model error is observed in the T-position, as shown in Fig. 10. There is a strong dependence with time, as depicted by the increasing slope as time moves away from the estimation epoch. The reason why the RMS is not zero at t_0 is the effect of the measurement error (recall range measurement noise sigma of 10m).

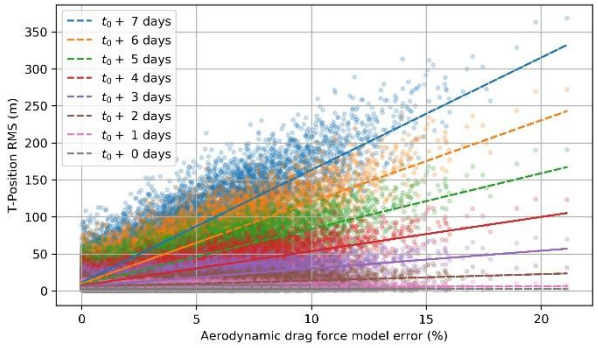

Fig. 10. T-Position RMS as a function of the atmospheric drag force model error at different epochs in *Case 2*

Regarding covariance containment, Table 4 and Table 5 gather the results in terms of percentage of MC points inside the k-σ position ellipsoid several days after the last measurement for the noise-only (average estimated covariance from all MC ODs) and consider covariance, respectively.

Table 4. Noise-only covariance containment of *Case 2*

Time	1-σ	2-σ	3-σ	4-σ
t_0	19.61%	74.03%	97.06%	99.89%
t_0 + 1 day	18.56%	70.66%	96.48%	99.83%
t_0 + 2 days	12.54%	55.92%	86.31%	97.17%
t_0 + 3 day	9.28%	42.58%	72.89%	88.93%
t_0 + 4 days	7.20%	34.77%	62.24%	79.96%
t_0 + 5 days	5.47%	26.70%	49.64%	66.14%
t_0 + 6 days	4.66%	21.98%	42.08%	57.49%
Theor.	19.90%	73.90%	97.10%	99.87%

Table 5. Consider covariance containment of *Case 3*

Time	1-σ	2-σ	3-σ	4-σ
t_0	19.64%	73.97%	97.05%	99.88%
t_0 + 1 day	19.84%	73.64%	97.28%	99.91%
t_0 + 2 days	19.88%	74.00%	97.11%	99.91%
t_0 + 3 day	19.71%	73.87%	97.16%	99.91%
t_0 + 4 days	19.37%	74.44%	97.20%	99.89%
t_0 + 5 days	19.49%	73.86%	97.18%	99.89%
t_0 + 6 days	19.51%	74.11%	97.28%	99.89%
Theor.	19.90%	73.90%	97.10%	99.87%

Moreover, Fig. 5 shows the TNW position of each MC point, taking as reference the average state of the whole population. Green points are those laying inside the 4-σ covariance ellipsoid and red points those laying outside. It is clear how the noise-only covariance fails containing the points, while the consider covariance is able to retain most of them. Looking both at Table 4 and Table *5* as well as Fig. 6, noise-only covariance degrades and becomes more unrealistic as time goes by while consider covariance is able to capture state uncertainty through time.

Finally, Fig. 6 shows the evolution of the T, N and W position sigma of the noise-only, observed and consider covariance matrices along time. The first insight is that noise-only covariance is far from the observed one, and the second is that the consider covariance has been properly fitted to the observed covariance. The consider covariance matrix has been obtained after a covariance determination process that provided a value for the estimated variance of the atmospheric drag force model error of $24.27(\%)^2$, i.e. a standard deviation of 4.93%, almost the 5% of the input noise model.

The residuals after the fitting were found to be several orders of magnitude below the covariance correction and the covariance components itself.

Hence, the covariance determination algorithm has been validated, together with the implementation of a dynamic consider parameter to account for atmospheric drag force modelling uncertainty.

6.3 *Case 3: Measurement noise and range bias model error*

This case includes the former measurement noise model and the following additional gaussian range bias model error:

$$c_{RBE} \sim N(0, \sigma_{RBE} = 20m) \quad (10)$$

This value has been chosen to be greater than the range measurement noise so that the impact is clear.

The first impact of the range bias model error can be observed in the weighted RMS of the ODs, as presented in Fig. 11. The shape is not similar to the *Case 1* (Fig. 7) since now the measurement noise does not match the measurement weight, leading always to a weighted RMS greater than the unity.

Furthermore, differences between the estimated covariance matrices from the MC ODs have been inspected and, as in *Case 2*, no significant differences are observed, i.e. all MC ODs are consistent.

Regarding covariance containment, *Table 6* and Table 7 gather the results in terms of percentage of MC points inside the k-σ position ellipsoid after several days after the end of the measurement time interval for the noise-only and consider covariance, respectively.

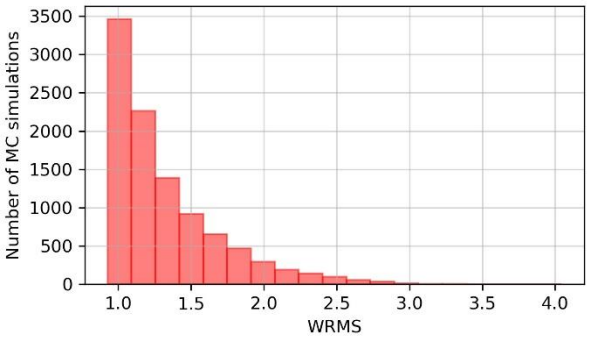

Fig. 11. Histogram of the weighted RMS of the OD for each MC point in *Case 3*

Table 6. Noise-only covariance containment of *Case 3*

Time	1-σ	2-σ	3-σ	4-σ
t_0	2.94%	14.12%	26.81%	37.24%
t_0 + 1 day	2.49%	12.33%	23.30%	33.19%
t_0 + 2 days	2.83%	15.41%	29.04%	40.89%
t_0 + 3 day	1.96%	10.17%	20.24%	29.37%
t_0 + 4 days	2.07%	11.14%	21.51%	30.29%
t_0 + 5 days	1.76%	8.78%	18.16%	26.53%
t_0 + 6 days	1.82%	10.34%	19.40%	27.75%
Theor.	19.90%	73.90%	97.10%	99.87%

Table 7. Consider covariance containment of *Case 3*

Time	1-σ	2-σ	3-σ	4-σ
t_0	20.36%	73.84%	96.98%	99.92%
t_0 + 1 day	19.84%	73.61%	97.23%	99.90%
t_0 + 2 days	20.53%	73.88%	96.85%	99.91%
t_0 + 3 day	19.19%	74.02%	97.10%	99.88%
t_0 + 4 days	19.85%	74.14%	96.95%	99.89%
t_0 + 5 days	19.33%	74.20%	97.09%	99.90%
t_0 + 6 days	19.85%	74.07%	96.97%	99.92%
Theor.	19.90%	73.90%	97.10%	99.87%

It can be seen by inspecting Table 6 that covariance degrades as time goes by, having an unrealistic covariance yet at the initial estimation epoch. Again, this leads to the conclusion that the estimated covariance is unable to account for systematic errors and that the consider covariance complies with the covariance containment all along the orbital evolution.

The main effect of the range bias model error is observed in the T-position, as shown in Fig. 12. The t_0 lines approximately sticks to a 1:1 slope straight line, meaning that this position RMS is mainly due to the range bias model error.

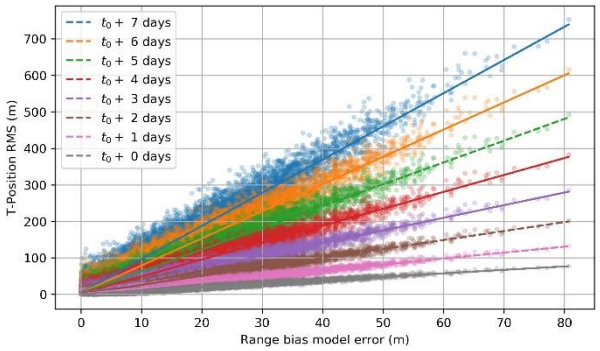

Fig. 12. T-Position RMS as a function of the range bias model error at different epochs in *Case 3*

Fig. 8 shows the evolution of the T, N and W position sigma of the noise-only, observed and consider covariance matrices along time. The same conclusions pointed out for *Case 2*, apply to this *Case 3*: noise-only is far from the observed one and again the consider covariance has been properly fitted to the observed covariance. The estimated variance of the range bias model error of 399.85m^2, i.e. a standard deviation of 19.996m, very close to the 20m of the noise model.

Again, the residuals after the fitting were found to be several orders of magnitude below the covariance correction and the covariance components itself. Thus, the implementation of a dynamic consider parameter to account for measurement modelling uncertainty is justified.

7. Conclusions

The paper has presented the foundations of a methodology to improve covariance realism. The motivation is endorsed by the main conflicts that arise as a consequence of an unrealistic covariance. Future SST and STM products are intended to rely on robust techniques for uncertainty characterization to face the challenges of the next generation of space constellations and the increasing number of RSOs.

A review of the OD and consider parameters theory has been presented together with an algorithm to estimate the variance of the consider parameters so that an estimated covariance can be best fitted to an observed covariance. Different consider parameters have been included, concerning the errors incurred when modelling the motion of RSOs and when performing sensing campaigns with ground based radar stations. Furthermore, a validation scheme has been detailed to assess the benefits of this novel technique, defining different test cases. It has been shown that the estimated state covariance, product of an OD, cannot characterize the uncertainty of the state estimation when model errors are present over an arc. These errors play a crucial role in the uncertainty characterization, as seen in the covariance containment analysis made during the previous section.

Interesting results regarding the effect of the model errors on the covariance realism and on the OD related products, such as state vector estimation and covariance have been discussed. The proposed validation chain has provided powerful and exhaustive results in terms of covariance consistency, containment and realism.

The work presented in this paper is preliminary, as only simulated data has been considered. The covariance determination methodology has been partially validated, achieving a remarkable covariance realism improvement and properly weighting the effect of model uncertainties. Further studies will consider the estimation of several consider parameters at once, together with the validation of the methodology in other orbital regimes and with different environmental conditions.

In addition, the methodology is going to be applied to a real operational environment, starting with SENTINEL-3A satellite, since GPS measurements, required to generated POD orbits are publicly available, and for which there are radar measurements available from LeoLabs. The covariance determination algorithm is the same as presented in this paper, being the only change the use of the observed covariance methodology for operational purposes, introduced in section 4.2.

Acknowledgements

The authors would like to acknowledge the contributions from Alfredo Miguel Antón Sánchez and Adrián Díez Martín from GMV for their support, review and advice.

References

[1] L. C. J. M.D. Hejduk, "Evaluating Probability of Collision Uncertainty," 2016. [Online]. Available: https://ntrs.nasa.gov/search.jsp?R=20160005313.

[2] A. B. Poore, J. M. Aristoff, J. T. Horwood, R. Armellin, W. T. Cerven, Y. Cheng, C. M. Cox, R. S. Erwin, J. H. Frisbee, M. D. Hejduk, B. A. Jones, P. Di Lizia, D. J. Scheeres, D. A. Vallado and R. M. Weisman, "Covariance and Uncertainty Realism in Space Surveillance and Tracking," 2016.

[3] A. Pastor-Rodríguez, D. Escobar, M. Sanjurjo-Rivo and A. Águeda, "Correlation Techniques to Build-up and Maintain Space Objects Catalogues," in *7th International Conference on Astrodynamics Tools and Techniques*, 2018.

[4] G. E. Peterson, M. E. Sorgeb, J. P. McVeyc, S. Gegenheimerd and G. A. Henninge, "Tracking requirements in LEO for space traffic management in the presence of proposed small satellites," in *69th International Astronautical Congress, Bremen, Germany*, 2018.

[5] E. G. Oliver Montenbruck, Satellite Orbits: Models, Methods and Applications, Springer, 2000.

[6] B. D. Tapley, B. E. Schutz and G. H. Born, Statistical Orbit Determination, Elsevier Academic Press, 2004.

[7] Y. Zhang, H. Wu and L. Cheng, "Some new deformation formulas about variance and covariance," in *2012 Proceedings of International Conference on Modelling, Identification and Control*, 2012.

[8] A. Díez, A. Pastor, S. López, A. Souto, P. García and D. Escobar, "Covariance determination from operational orbits and sensor data," in *4th International Workshop on Key Topics in Orbit Propagation Applied to Space Situational Awareness*, 2019.

[9] J. F. C. C. Space (JFCC SPACE), *Space-Track*, 2018.

[10] Z. Folcik, A. Lue and J. Vatsky, "Reconciling covariances with reliable orbital uncertainty," in *Advanced Maui Optical and Space Surveillance Technologies Conference*, 2011.

[11] P. C. Mahalanobis, "On the generalised distance in statistics," in *Proceedings of the National Institute of Sciences of India*, 1936.

[12] W. E. Wiesel, Modern Orbit Determination, Aphelion Press, 2003.

[13] D. Snow, "JSpOC SP Catalog Covariance Realism," 2016.

2nd IAA Conference on Space Situational Awareness (ICSSA)

Washington D.C., USA

IAA-ICSSA-20-0X-XX

DO YOU KNOW WHERE YOU ARE IN SPACE? IMPROVING ORBITAL UNCERTAINTY REALISM THROUGH COVARIANCE DETERMINATION

S. López-Jiménez[1], A. Pastor[1], D. Escobar[1] and A. Águeda[1]

[1] *GMV, Calle Isaac Newton 11, Tres Cantos, 28670, Spain, serlopez@gmv.com, apastor@gmv.com, descobar@gmv.com, aagueda@gmv.com*

Keywords: *space debris, space surveillance and tracking, uncertainty realism, covariance realism, orbit determination*

ABSTRACT

The problem of characterizing the uncertainty in the estimated state of resident space objects (RSOs) is of major importance in the framework of Space Surveillance and Tracking (SST) and Space Traffic Management (STM) activities and particularly for product provision (e.g. high-risk collisions, upcoming re-entries, fragmentations). Most of these products rely not only on the estimated orbits but also on their associated uncertainty, which are estimated during the catalogue build-up and updated through maintenance as more measurements are available.

The proposed methodology extends the classical batch least squares estimation with the consider analysis. The goal of the methodology is to estimate the consider parameters variance with which a consider covariance is best fitted to a so-called observed covariance. The influence of the main sources of dynamic model uncertainty (atmospheric modelling, object geometry, geomagnetic and solar radiation indexes prediction, sensor calibration parameters, among others) can be investigated by evaluating their contribution to the covariance realism improvement.

The methodology has been applied to a simulated realistic scenario of measurements to evaluate the consistency of the corrected covariance via Monte Carlo analysis. Furthermore, an interesting case involving real measurements from radars is analyzed and investigated through comparisons against precise orbit determination solutions for the Sentinel 3A satellite.

1 INTRODUCTION

The uncertainty of the object's state is usually represented by the covariance obtained from the estimation process, provided that the assumptions of Gaussianity and linearity hold true. The covariance matrix is a feasible approximation of the true uncertainty of the Resident Space Object (RSOs) if Gaussian statistics deliver a proper characterization of the true Probability Density Function (PDF) of the object (i.e. small orbital differences, linear regime and short propagation times). Covariance is obtained via orbit determination (OD) algorithms given that measurements are available.

However, the quality of final Space Surveillance and Tracking (SST) products will depend on how well the covariance characterizes the true uncertainty, i.e. uncertainty realism. Covariance unrealism is affected both by the scaling and orientation of the covariance matrix with respect the true PDF [1]. For instance, covariance

misrepresentation (either in orientation or dimension) can lead to differences of more than an order of magnitude in the computation of the probability of collision [2]. Not only is covariance realism desired in conjunction analysis but also for other products (see [3] and [2] for further examples on the relevance of covariance in SST products). The accessibility and exploitation of the future space environment will greatly depend on the realistic provision of SST products. For future Space Traffic Management (STM) systems, a basic operational requirement is to be able to identify high probability collisions while discarding false alarms effectively [4].

It is a common practice among SST product providers to artificially increase the covariance matrix by means of a scaling factor, acting as a safety factor [1]. The principal drawback of these techniques is the definition of a scaling factor that lacks physical insight in the covariance realism problem and is only based on statistical consistency techniques and processing of empirical data.

The novel methodology introduced in the present is based on the consider analysis (or consider parameters) theory presented in [5] and [6]. The novelty of the technique proposed is the definition of a methodology to estimate the variances of the consider parameters to mitigate covariance unrealism. Hence, the central motivation of this paper becomes the definition of a novel technique that considers both dynamics and statistics when treating for covariance unrealism, targeting the most relevant causes for covariance realism degradation.

An additional estimation process is conceived to compute the variances of certain modelled consider parameters. The estimation is done by means of a least-squares estimator algorithm in the covariance space, where a parallelism is established with a classical OD algorithm. A noise-only covariance (i.e. a covariance matrix derived from an OD) is fitted to a time evolving observed covariance (obtained from an statistical comparison of past orbital solutions) where the variances of certain consider parameters are estimated. In the covariance determination methodology, the estimated parameters will lead to the sought correction and consequent improvement of covariance realism. This novel method entails the definition of physically derived weights that give empirical insight on the expected uncertainty of certain dynamic and measurement models, applicable for posterior propagations.

In Section 1 the motivation, as well as the relevant terminology and the covariance realism metrics will be discussed, laying the theoretical foundations of the methodology. In Section 2, the validation chain used for the verification of the conceived methodology and its implementation is introduced together with previous conclusion obtained from [7]. In Section 3, the results of the validation case plus the operational case of the Sentinel 3A satellite are displayed and discussed. Finally, Section 4 summarizes the conclusions and future work.

1.1 *Relevant terminology*

Some of the terms that are used along this paper are now defined for clarification:

- **Observation:** set of measurements related to a certain epoch, belonging to a given object and obtained by certain sensor, e.g. range, range-rate, azimuth, elevation, right ascension, declination.
- **Orbit determination (OD)**: process with which the orbital state (position and velocity at the estimation epoch, as well as dynamical parameters such as drag coefficient or solar radiation pressure coefficient) of an object are estimated based on observations obtained from sensors, typically telescopes and/or radars in SST.

- **Estimated parameters/orbital state**: set of orbital parameters (position, velocity and dynamical parameters) obtained through an orbit determination process.
- **Estimated/determined orbit**: evolution over time of an object's state obtained through an orbit determination process over a time interval with available observations.
- **Predicted/propagated orbit**: evolution over time of an object's state obtained through an orbit propagation process of a previously estimated orbital state over a time interval without available observations
- **A-posteriori covariance**: covariance of the estimated orbital state resulting from an orbit determination process. Depending on whether consider parameters have been consider or not:
    - **Noise-only covariance**, if no consider parameters have been included in the orbit determination. Therefore, it only accounts for measurement noise.
    - **Consider covariance**, if consider parameters have been included in the orbit determination. This covariance matrix is larger than the noise-only one.
- **Propagated covariance**: uncertainty characterization over time of the orbit (position and velocity) of the object obtained through propagation of the a-posteriori covariance
- **Consider parameters**: parameters that are not estimated in the orbit determination process but whose uncertainty is added to the a-posteriori covariance in order to improve covariance realism.
- **Variance of consider parameters**: uncertainty of the consider parameters.
- **Observed covariance**: uncertainty characterization over time of the object's orbit generated from an statistical analysis of estimated and propagated orbits, covering the propagation time interval and relative to the start time of the propagation
- **Observed covariance generation**: process in which different orbits, including estimated (obtained through orbit determination processes) and propagated ones, are compared among them in order to derive the observed covariance.
- **Covariance determination**: process in which the variance of consider parameters is estimated in order to fit the propagated covariance to the observed covariance.

1.2 Covariance realism metrics

From [8], several metrics for testing covariance realism are defined, giving especial emphasis in the analysis of the Gaussianity of the population of samples derived from successive ODs, either for the validation and processing of real orbits. The following conditions should be fulfilled if covariance realism is sought:

- The distribution of the satellite's predicted position is normal.
- The mean error of the predicted satellite's location is approximately 0.
- The dispersion of the error in the predicted states is consistent with the predicted covariance (i.e. covariance containment is achieved).

It is assumed that if a multivariate normal distribution is normal in all its directions (i.e. univariate distributions are proven to be normal) the complete multivariate distribution can be regarded as normal. From [8], different normality tests are compared and one empirical test is regarded as the best option: Michael's statistical (see [9] and [10] for further reference on the implementation). This test provides a powerful graphical statistical test to reject normality based on the definition of confidence boundary regions dependent on a significance level of the test (defined by the author).

The mean error of the predicted state will be computed for a set of predicted epochs by measuring the bias between the true reference state and the dispersion of computed states.

Finally, the containment condition will be measured as introduced in [7], by measuring the Mahalanobis distance (see [11]) of each MC sample and check whether the conditions for a normally distributed 3 degrees of freedom multivariate distribution are fulfilled (from [12]).

Note that in the previous paper, no tests for normality were introduced as the population of orbitals states were derived using a sufficient sampling (10000 samples) and by considering Gaussian processes in the addition of the perturbations. For the cases considered hereafter these conditions do not hold and thus normality must be ensured. If normality is rejected, deriving an observed covariance is still feasible however lacks statistical and physical consistency, as no Gaussian distribution will characterize a non-Gaussian PDF and covariance realism will not achievable.

2 VALIDATION CHAIN

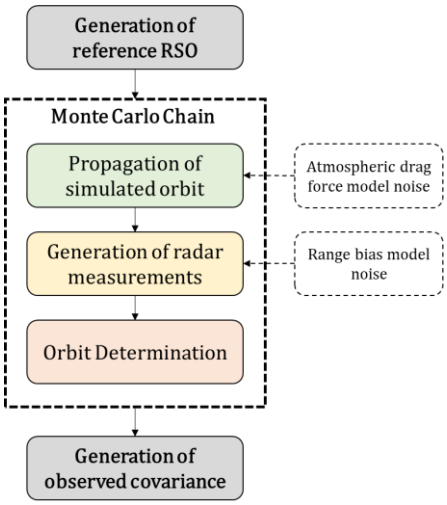

Figure 1 Validation chain of the Covariance Determination

A Monte Carlo (MC) based approach is followed to sample the PDF characterizing the orbital state estimation uncertainty. Full insight in the validation chain, depicted in Figure 1, can be found in [7]. From the previous figure, there are important remarks about the validation chain worth mentioning:

- All the simulated orbits are generated considering the same reference RSO
- The MC chain yields a different orbital solution by considering two noise sources: a random Gaussian noise for the measurement generation process and a constant perturbation through a complete orbital arc.
- The aggregation of the MC samples will yield a population that fairly characterizes the PDF of the orbital estimation.

The previous validation chain provides insight on the effect of the different model errors in the estimation of the state and also in the covariance realism problem. In [7], several conclusions were derived:

- A perturbation in the atmospheric drag force model is compensated by the estimation of the drag coefficient, during the OD. However, the propagation of the state entails an accumulation of orbital error when comparing the estimated MC orbits vs. the reference one. This translates into a loss of realism of the noise-only covariance in the along-track direction, appreciated during the prediction/propagation of the associated uncertainty. A correction using a consider parameter for the atmospheric drag force model is required and its variance is estimated using the methodology. The computed consider parameter variance delivers a realistic consider covariance and the perturbation in the atmospheric drag force model is successfully recovered, validating the methodology and its implementation.

- A perturbation in the range bias has a direct impact in the orbital estimation of the OD. At estimation epoch, the different orbital solutions yield a dispersion of the orbital state that is appreciated mainly in the along-track direction (with non-negligible contributions to the cross-track and radial directions). At the same time, this yields a degradation of covariance realism not only during the propagation of the noise-only covariance matrix but also at estimation epoch. The modelled consider parameter effectively upgrades the covariance realism and recovers the input perturbation.

This paper discusses the performance of the methodology considering a set of realistic orbits. For this, the same validation chain as depicted in Figure 1 applies. Later on, a real case will be treated using the Precise Orbit Determination (POD) solutions and measurements of the Sentinel 3A satellite. Next section will introduce the extended metrics conceived for the analysis of the covariance realism of both noise-only and consider covariance, providing robust techniques to test for the performance of the devised methodology.

3 RESULTS

In the present section two different cases are presented. In order to conclude the validation process of the Covariance Determination methodology, *Case A* is presented aiming to prove the performance of the methodology when faced with a realistic set of simulated orbits affected by atmospheric model errors.

Furthermore, once concluded the verification of the methodology, a real scenario, *Case B*, is analyzed by performing a covariance realism improvement of the Sentinel 3A satellite orbit propagation, considering an entire year of measures.

3.1 Case A*: Validation case with realistic orbits and dynamic perturbation*

The orbit and physical properties of the reference RSO are listed in Table 1. The orbit has been taken from a public TLE of Sentinel-3A (41335) [13].

Table 1 Simulated RSO orbit and physical properties for Case A

Reference RSO	
Semi-major axis	7186.877 km
Eccentricity	0.001113
Inclination	98.72 deg
RAAN	77.03 deg
Mass	100 kg
Area	10 m^2
Drag coefficient	0.4

The dynamical model used is a complete one: 16x16 gravity field, third body perturbation of the Moon and MSIS-90 atmospheric density model. The features of this test case are displayed in the following table:

The aim of this test case is to validate the performance of the methodology when faced with a small sampling of the PDF associated to the uncertainty of the state estimation and prediction (yielding the observed covariance) considering subsequent batches of ODs. This case aims to mimic the process that would be considered when analyzing real measurements and orbits of a satellite, where the availability of measurements conditions the accuracy of the results. This case includes a Gaussian atmospheric drag force model error (AE) regarded as:

$$c_{AE} \sim N(0, \sigma_{AE} = 5\%) \quad (1)$$

In terms of covariance consistency among the different ODs, the weighted Root Mean Squared (RMS) and the differences among the estimated (MC) covariance matrices have been analyzed, obtaining similar results as those presented for *Case 1* displayed in [7]. Additional figures describing the results obtained for the present test case can be found in the Appendix (Figure 8, Figure 9, Figure 10, Figure 11 and Figure 12). As expected, the estimated drag coefficient absorbs the atmospheric drag force error.

Before testing covariance containment, it is of the utmost relevance to ensure that the distribution of orbital errors obtained from the comparison of predicted orbits against the reference one (following the method introduced in [7] and [14]) is normal and unbiased. The averaged error of the distribution is listed in Table 3 together with its relative magnitude with respect the standard deviation of the distribution.

Table 2 Features of Case A

Test case A	
Consider parameter	Atmospheric Drag Model Error
Observed covariance	Realistic simulated
Reference orbit	01-01-2018 to 01-07-2018
Measurement generation	5 days batch
Estimation epoch for OD	End of measurement period
Predicted orbit	Estimation epoch + 7 days

Table 3 Averaged and relative error of the distribution in the T, N and W directions, where t_0 stands for estimation epoch and subsequent prediction times are expressed relative to it, Case A

$\boldsymbol{Epoch}$	$\Delta T\ (m)$	$\Delta N\ (m)$	$\Delta W\ (m)$	$\Delta T/\sigma_T(\%)$	$\Delta N/\sigma_N(\%)$	$\Delta W/\sigma_W(\%)$
$\boldsymbol{t_0}$	0.326	0.132	0.188	7.06	8.48	11.24
$\boldsymbol{t_0 + 1day}$	0.505	-0.054	-0.184	6.94	-7.27	-11.15
$\boldsymbol{t_0 + 2days}$	0.047	-0.120	-0.209	0.37	-7.22	-11.78
$\boldsymbol{t_0 + 3days}$	-0.192	0.076	0.183	-0.90	10.08	10.31
$\boldsymbol{t_0 + 4days}$	-0.023	0.099	0.233	-0.07	13.94	12.19
$\boldsymbol{t_0 + 5days}$	-0.341	-0.101	-0.190	-0.67	-13.10	-9.82
$\boldsymbol{t_0 + 6days}$	-1.152	-0.083	-0.258	-1.63	-12.04	-12.40

Inspecting the previous table, the bias of the distribution is not found significant as in most of the cases, even during propagation, the relative value of the bias when compared with the standard deviation of the distribution is found to be 10 times smaller.

Furthermore, tests for univariate normality of the distribution are included for the T, N and W distributions. A 5% of significance level is defined by the author, selected as a common metric for statistical tests:

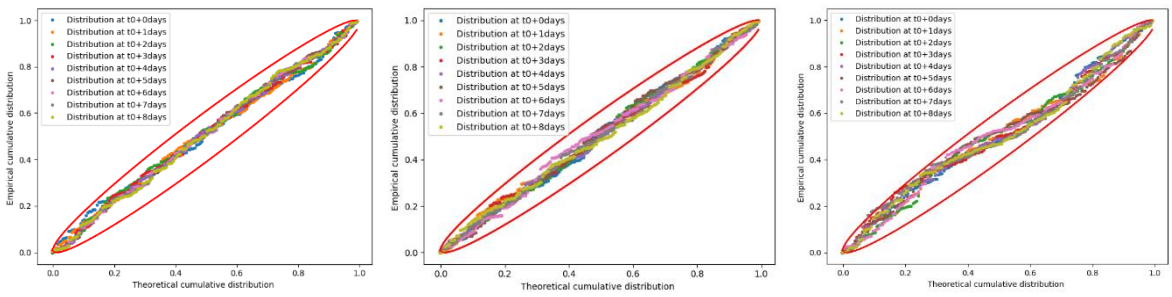

Figure 2 Michael's normality test for case A for the along-track (left), radial (center) and cross-track (right) directions at different propagation epochs, Case A

From inspection of the tests, the distributions are found to be normal. As none of the distributions is found to infringe the boundaries of the defined confidence regions, the univariate distribution are assumed normal because the null hypothesis of normality cannot be rejected. Note that in Figure 2 new points infringe the confidence regions, this is only indicative that at estimation epoch the normality of the W direction is rejected but as propagation occurs a normal distribution can be safely assumed.

Finally, the containment metrics are listed in the following tables to depict the performance of the methodology when correcting for covariance unrealism:

Table 4 Covariance containment analysis for the noise-only (left) and consider (right) position covariance of Case A, where t_0 stands for estimation epoch and subsequent prediction times are expressed relative to it, Case A

Time	Noise-only covariance				Consider covariance			
	1-σ	2-σ	3-σ	4-σ	1-σ	2-σ	3-σ	4-σ
t_0	20.93%	72.67%	96.51%	99.42%	9.88%	44.77%	75.00%	88.95%
t_0 + 1 day	18.23%	70.12%	95.87 %	99.25%	20.93%	64.53%	87.79%	97.67%
t_0 + 2 days	12.10%	55.01%	86.47%	96.35 %	19.77%	71.51%	96.51%	99.42%
t_0 + 3 day	8.74%	41.79%	72.05%	88.01%	24.42%	72.67%	94.77%	99.42%
t_0 + 4 days	6.67%	32.41%	61.42%	78.88%	19.77%	68.02%	96.51%	100.00%
t_0 + 5 days	5.23%	26.48%	49.00%	64.49%	23.84%	72.67%	94.77%	99.42%
t_0 + 6 days	4.01%	21.98%	41.67%	57.11%	20.35%	70.93%	96.51%	100.00%
Theor.	19.90%	73.90%	97.10%	99.87%	19.90%	73.90%	97.10%	99.87%

From inspection of the previous tables, the noise-only covariance matrix (Table 4, left) fails to realistically represent the uncertainty of the object during the prediction of its orbit. The containment metrics show a degradation of the realism that is not observed during the propagation of the consider covariance (Table 4, right). The solution provided by the Covariance Determination algorithm has estimated a variance of the atmospheric drag force model error of 26.49%^{2}, i.e. a standard deviation of 5.147%, almost the 5% of the input noise model. In addition, Figure 13 in Appendix shows graphically the degradation of the covariance realism of the noise-only covariance matrix compared to the increased realism that the consider covariance provides.

3.2 Case B: Sentinel 3A case

Table 5 summarizes the most relevant features of the Sentinel 3A Case B. The dynamical model used in the processing of the ODs and propagation of the orbits is a high-fidelity dynamic model considering high degree and order gravitational model with third body perturbations. Only range and range-rate measurements are considered. The data sources used for the processing of the different ODs of the Sentinel are summarized in Table 6.

The resulting weighted RMS of the different ODs is depicted in Figure 3. Weights seem to be wrongly defined for the processed measurements, however, a calibration procedure preceded the processing of ODs where weights and biases were accurately defined based on the comparison of measurements with respect to the Precise Orbit Determination (POD) solution.

Table 5 Features of Sentinel 3A case, Case B

Case of Sentinel 3A satellite	
Consider parameter	Atmospheric Drag Model Error
Observed covariance	Operational
Reference orbit	01-05-2018 to 01-06-2019
OD period	7 days batch
Shift between ODs	1 day
Estimation epoch	End of measurement period
Predicted orbit	Estimation epoch + 8 days

Table 6 Data sources for the Sentinel 3A tracking campaign, Case B

Sentinel 3A	
Orbits	POD orbits for Sentinel 3A
Manoeuvres	Publicly available [15]
Measurements	LeoLabs' PFISR & MSR radars

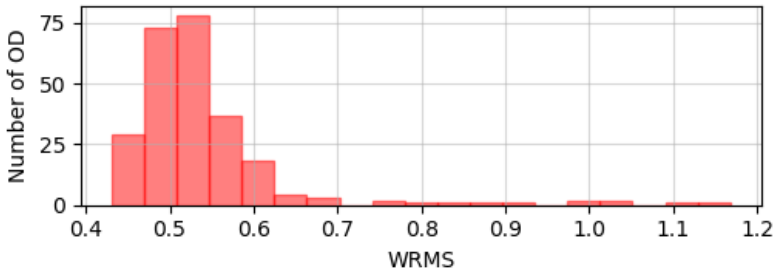

Figure 3 Weighted RMS of the ODs for the tracking campaign of the Sentinel 3A, Case B

The differences between the different estimated noise-only covariance matrices can be regarded in Figure 4. The differences among the different noise-only covariance matrix vary greatly due to the different conditions that influence the estimation process of an OD (i.e. measurement availability, number of measurements, geometry, etc.).

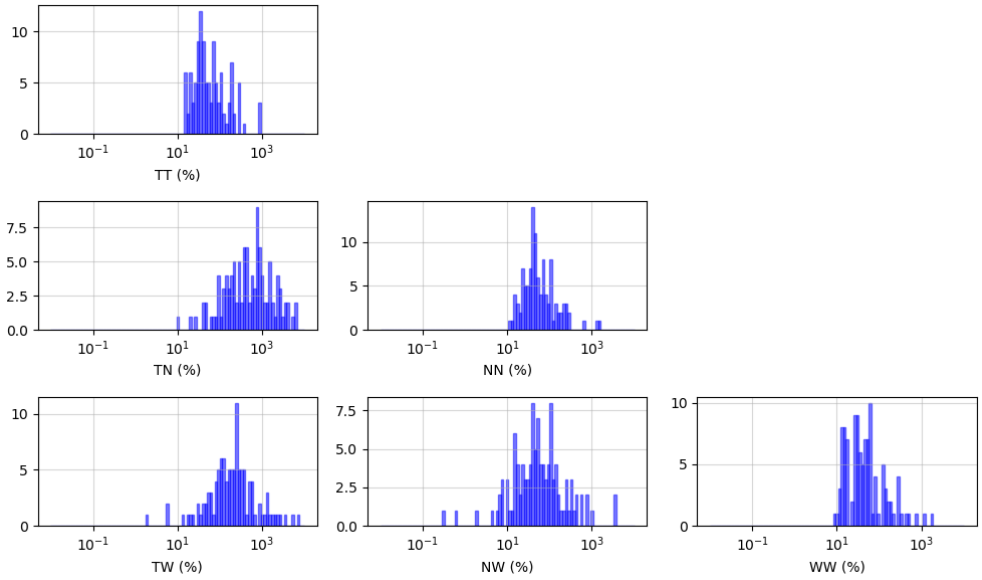

Figure 4 Relative differences of the estimated noise-only covariance matrices with respect to the average covariance matrix of the population for the Sentinel 3A tracking campaign, Case B

After all ODs were processed, the covariance realism metrics are used to analyze the complete distribution of orbital differences. Table 7 lists the results of the average orbital error.

Table 7 Averaged and relative error of the distribution in the T, N and W directions, where t_0 stands for estimation epoch and subsequent prediction times are expressed relative to it, Case B

Prediction epoch	$\Delta T\ (m)$	$\Delta N\ (m)$	$\Delta W\ (m)$	$\Delta T/\sigma_T(\%)$	$\Delta N/\sigma_N(\%)$	$\Delta W/\sigma_W(\%)$
$\boldsymbol{t_0}$	-11.71	-0.20	2.12	-45.27	-16.98	21.43
$\boldsymbol{t_0+1}$	-10.84	0.69	3.14	-22.67	49.34	34.03
$\boldsymbol{t_0+2}$	-9.69	-0.25	-6.37	-12.55	-14.75	-70.64
$\boldsymbol{t_0+3}$	-14.17	-0.55	-2.77	-12.32	-25.15	-25.49
$\boldsymbol{t_0+4}$	-21.58	0.22	7.88	-13.07	9.69	77.87
$\boldsymbol{t_0+5}$	-20.69	0.56	2.46	-9.07	18.61	19.21
$\boldsymbol{t_0+6}$	-30.97	-0.36	-9.14	-10.16	-10.35	-82.84
$\boldsymbol{t_0+7}$	-41.66	-0.45	-1.43	-10.96	-12.44	-9.71
$\boldsymbol{t_0+8}$	-50.43	0.20	10.71	-11.00	4.41	88.49

Next, the normality tests for orbital differences in the TNW frame distributions are shown in Figure 6. The only direction where normality can be assumed is the T direction while the N and W directions clearly reject the null hypothesis of normality.

Neither an unbiased orbital distribution can be assumed (inspecting Table 3) nor a univariate normal distribution is found in the radial and normal direction (see Figure 6). For this reason, as the only direction that shows a behavior close to normal is the along-track direction and because the effect of an atmospheric drag consider parameter is mostly noticeable in such direction, a realism upgrade in the along-track direction is sought using the Covariance Determination methodology.

Due to the fact that noise-only covariance matrices depend on the conditions of the OD (as shown in Figure 4), and since the solution of the Covariance Determination method depends on the considered noise-only covariance, a Covariance Determination processing was executed per OD. The final solutions are summarized in Figure 5, were a central tendency for the atmospheric drag consider parameter is observed with an average value close to the median. The average value of the consider parameter may be taken as a reference of the accumulated error introduced by the atmospheric drag force model.

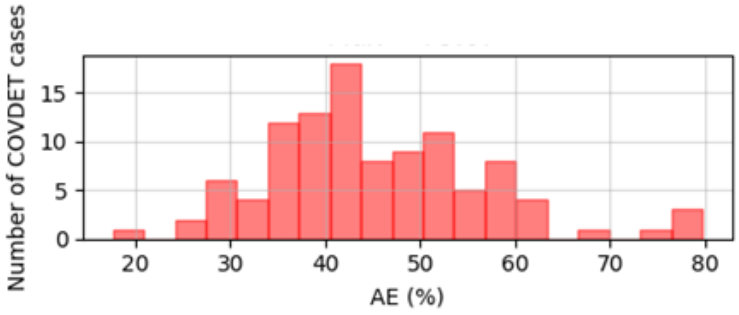

Figure 5 Histogram of the dynamic consider parameter estimations, Case B

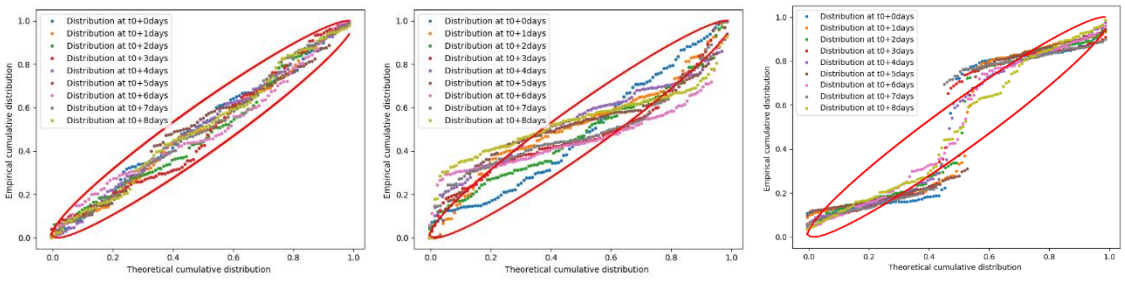

Figure 6 Michael's normality test for the Sentinel case and along-track (left), radial (center) and cross-track (right) directions at different propagation epochs, Case B

Finally, to test the methodology performance in the correction of covariance realism in the along-track direction a univariate containment test is employed (which is analogous to using the Mahalanobis distance on the position space). Since the only direction displaying a Gaussian behavior is the along-track, only containment will be analyzed in this direction, as covariance realism has no sense when the PDF sampling indicates a non-normal distribution of error. For this, the number of points contained in several sigma bounds are compared against the theoretical metrics of a normal univariate distribution. In Table 8 the results for both noise-only covariance and consider covariance are listed, where a significant improvement in covariance realism is achieved using the correction introduced by the atmospheric drag consider parameter estimated.

Table 8 Covariance containment results considering the for the noise-only (left) and consider (right) position covariance estimated from the OD for the Sentinel 3A tracking campaign, Case B

Time	Noise-only covariance			Consider covariance		
	1-σ	2-σ	3-σ	1-σ	2-σ	3-σ
t_0	20.00%	42.61%	56.52%	20.00%	42.61%	56.52%
t_0 + 1 day	13.91%	31.30%	42.61%	23.48%	36.52%	51.30%
t_0 + 2 days	9.57%	24.35%	36.52%	29.57%	58.26%	73.91%
t_0 + 3 day	12.17%	23.48%	34.78%	40.87%	68.70%	83.48%
t_0 + 4 days	10.43%	22.61%	31.30%	48.70%	79.13%	88.70%
t_0 + 5 days	8.70%	21.74%	26.09%	53.91%	79.13%	86.96%
t_0 + 6 days	11.30%	20.87%	26.09%	63.48%	88.70%	94.78%
t_0 + 7 days	8.70%	18.26%	25.22%	66.09%	85.22%	91.30%
t_0 + 8 days	5.22%	15.65%	23.48%	69.57%	89.57%	94.78%
Theor.	66.70%	95.00%	99.70%	66.70%	95.00%	99.70%

The graphical representation of the correction introduced by the Covariance Determination methodology is depicted in Figure 7. Inspecting the previous picture, it is clear that the noise-only covariance realism in the along-track direction is degraded while the consider covariance achieves remarkable improvements. However, as the atmospheric drag consider parameter only corrects for uncertainty unrealism in the along-track direction, the radial and normal directions display great divergences when comparing the observed covariance against the noise-only and consider covariance matrices.

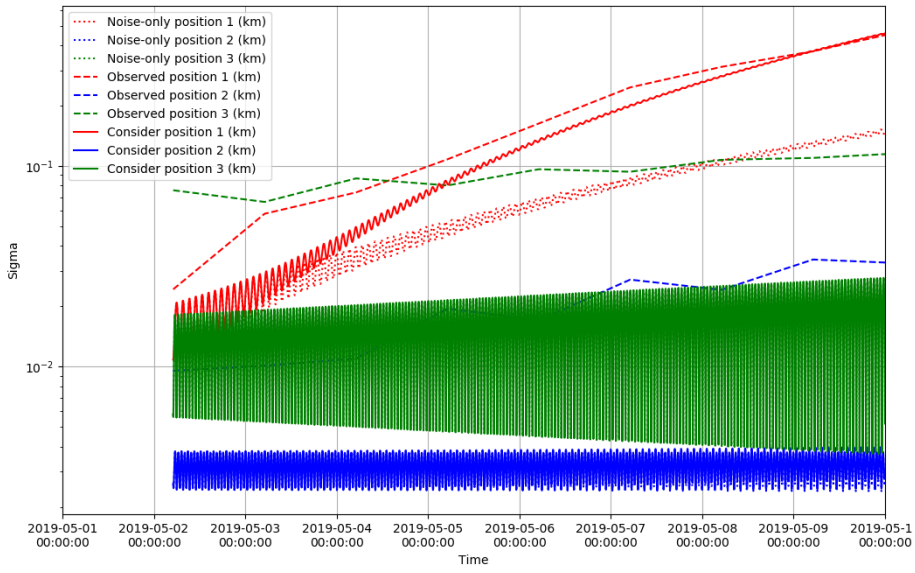

Figure 7 Evolution of the T, N and W position sigma of the noise-only, observed and consider covariance for the Sentinel 3A tracking campaign, fitting for a dynamic consider parameter, Case B

4 CONCLUSIONS

This paper has concluded the work initiated by a previous paper ending the validation campaign of the presented methodology to improve covariance realism. The motivation of the conceived methodology is endorsed by the requirements of current and future STM and SST providers, whose product critically depend on the quality and realism of the processed states and associated covariance matrices.

It has been shown how Covariance Determination methodology can effectively improve covariance realism in a simulated scenario considering realistic orbits. When uncertain values of the atmospheric drag force model are present but its uncertainty not considered during the propagation of the covariance matrix, a degradation of covariance realism is observed. However, the Covariance Determination methodology can effectively improve the covariance realism by providing a first estimation of the the uncertainties of physically meaningful consider parameters.

Additional metrics for covariance realism have been evaluated to ensure that the orbital distribution of errors around the reference state is normal and unbiased, as suggested in [8]. For *Case A*, these conditions were ensured whereas in *Case B*, the one of the Sentinel 3A satellite, the distributions were found to be neither unbiased nor Gaussian (with the single exception of the along-track direction).

Following from the previous conclusions, a Covariance Determination was carried out estimating the error of the atmospheric drag force model. Thanks to the investigated consider parameter, which has its main influence in the along-track direction, a covariance realism improvement can be still achieved.

A representative value of the error of the atmospheric drag force model is derived from the previous analysis, where a central tendency of the model's uncertainty of over 45% is observed. Taking into account that this value is the result of the aggregation of many uncertainty sources (i.e. atmospheric density model, drag coefficient, cross-sectional area variability, among others), the authors deemed to be representative the computed value.

Recommendations for future work will explore the reasons for the non-Gaussianity of the computed orbital distributions, the modelling of additional consider parameters that treat the uncertainty unrealism of the radial and normal direction and the implementation of a time-correlated consider parameters for the atmospheric drag force that follows a random-walk, Brownian motion or comparable noise model. Finally, linearity of the covariance propagation should be investigated and the use of non-linear uncertainty propagation techniques assessed.

5 ACKNOWLEDGMENTS

This work is part of an on-going Master thesis in "*New techniques for uncertainty realism improvement in Surveillance and Tracking orbit determination processes*" as part of the study program MSc. Aerospace Engineering at TU Delft in collaboration with GMV, expected to be presented in January 2020.

Besides, the authors would like to acknowledge the contributions from Ernst Schrama and Wim Simmons from TU Delft, as well as Adrián Díez Martín from GMV for their support, review and advice.

6 REFERENCES

[1] L. C. J. M.D. Hejduk, "Evaluating Probability of Collision Uncertainty," 2016. [Online]. Available: https://ntrs.nasa.gov/search.jsp?R=20160005313.

[2] A. B. Poore, J. M. Aristoff, J. T. Horwood, R. Armellin, W. T. Cerven, Y. Cheng, C. M. Cox, R. S. Erwin, J. H. Frisbee, M. D. Hejduk, B. A. Jones, P. Di Lizia, D. J. Scheeres, D. A. Vallado and R. M. Weisman, "Covariance and Uncertainty Realism in Space Surveillance and Tracking," 2016.

[3] A. Pastor-Rodríguez, D. Escobar, M. Sanjurjo-Rivo and A. Águeda, "Correlation Techniques to Build-up and Maintain Space Objects Catalogues," in *7th International Conference on Astrodynamics Tools and Techniques*, 2018.

[4] G. E. Peterson, M. E. Sorgeb, J. P. McVeyc, S. Gegenheimerd and G. A. Henninge, "Tracking requirements in LEO for space traffic management in the presence of proposed small satellites," in *69th International Astronautical Congress, Bremen, Germany*, 2018.

[5] E. G. Oliver Montenbruck, Satellite Orbits: Models, Methods and Applications, Springer, 2000.

[6] B. D. Tapley, B. E. Schutz and G. H. Born, Statistical Orbit Determination, Elsevier Academic Press, 2004.

[7] S. Lopez-Jimenez, A. Pastor, D. Escobar, S. Setty and A. Agueda, "Towards Covariance Realism in Batch Least-Squares Orbit Determination," *70th International Astronautical Congress (IAC), Washington D.C., United States, 21-25 October 2019,* 2019.

[8] D. A. Vallado and J. H. Seago, "Covariance realism," in *AAS/AIAA Astrodynamics Specialist Conference*, 2009.

[9] P. Royston, "Graphical Detection of Non-Normality by Using Michaels Statistic," *Applied Statistics,* vol. 42, p. 153, 1993.

[10] J. R. Michael, "The stabilized probability plot," *Biometrika,* vol. 70, pp. 11-17, 1983.

[11] P. C. Mahalanobis, "On the generalised distance in statistics," in *Proceedings of the National Institute of Sciences of India*, 1936.

[12] Z. Folcik, A. Lue and J. Vatsky, "Reconciling covariances with reliable orbital uncertainty," in *Advanced Maui Optical and Space Surveillance Technologies Conference*, 2011.

[13] J. F. C. C. Space (JFCC SPACE), *Space-Track,* 2018.

[14] A. Díez, A. Pastor, S. López-Jiménez, A. Souto, P. García and D. Escobar, "Covariance determination from operational orbits and sensor data," in *4th International Workshop on Key Topics in Orbit Propagation Applied to Space Situational Awareness*, 2019.

[15] ESA-Sentinel, "Satellite Parameters for POD of the SENTINEL 3A mission," 2019. [Online]. Available: https://sentinels.copernicus.eu/web/sentinel/technical-guides/sentinel-3-altimetry/pod/satellite-parameters;jsessionid=A97AC4F0ADF56FD99D388CFFF985483F.jvm1.

[16] Y. Zhang, H. Wu and L. Cheng, "Some new deformation formulas about variance and covariance," in *2012 Proceedings of International Conference on Modelling, Identification and Control*, 2012.

[17] W. E. Wiesel, Modern Orbit Determination, Aphelion Press, 2003.

[18] B. D. Tapley, B. E. Schutz and G. H. Born, Statistical Orbit Determination, Elsevier, Ed., 2004.

[19] D. Snow, "JSpOC SP Catalog Covariance Realism," 2016.

[20] A. B. Poore, J. M. Aristoff, J. T. Horwood, R. Armellin, W. T. Cerven, Y. Cheng, C. M. Cox, R. S. Erwin, J. H. Frisbee, M. D. Hejduk, B. A. Jones, P. Di Lizia, D. J. Scheeres, D. A. Vallado and R. M. Weisman, "Covariance and Uncertainty Realism in Space Surveillance and Tracking," 2016.

APPENDIX

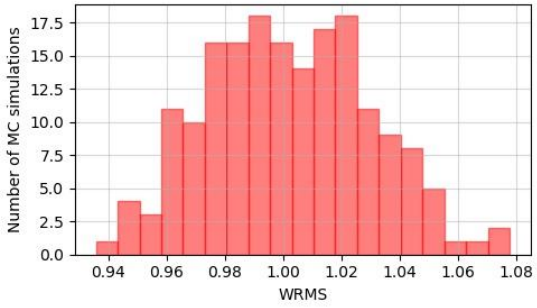

Figure 8 Weighted RMS of the ODs for test Case A

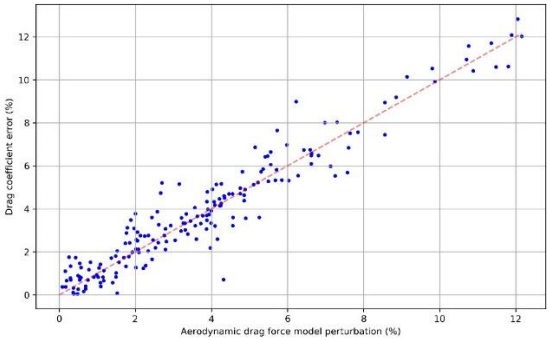

Figure 9 Drag coefficient error vs. atmospheric drag force model perturbation for test Case A

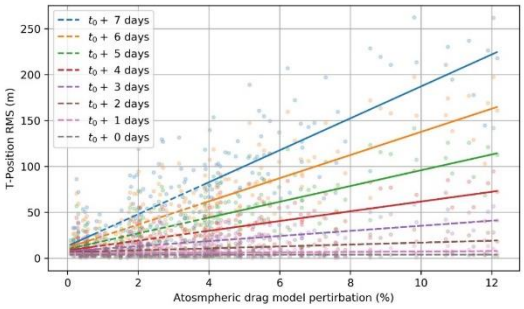

Figure 10 Atmospheric drag force model error vs. T-position RMS, Case A

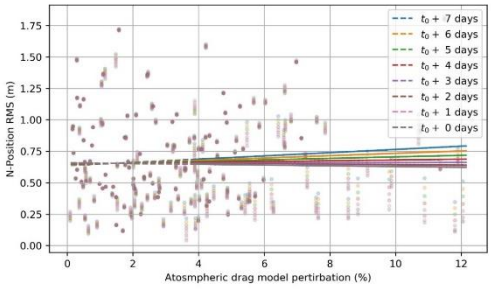

Figure 11 Atmospheric drag force model error vs. N-position RMS, Case A

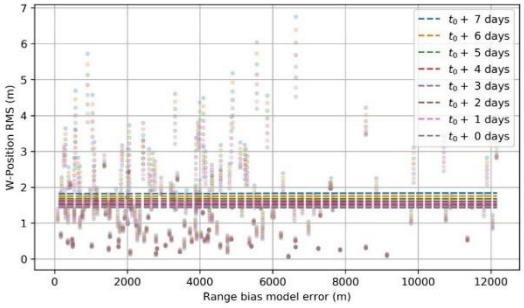

Figure 12 Atmospheric drag force model error vs. W-position RMS, Case A

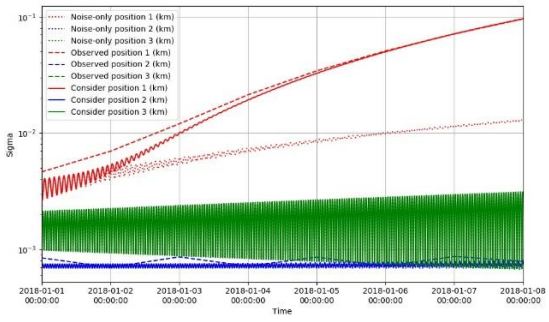

Figure 13 Evolution of the T, N and W position sigma of the noise-only, observed and consider covariance for test Case A